Slovak Biophysical Society

Proceedings of the

III. Slovak Biophysical Symposium

III. Slovak Biophysical Symposium

Comenius University
Faculty of Mathematics, Physics and Informatics
Bratislava
18. - 20. 4. 2008

The Slovak Biophysical Symposium is already a well-established biannual meeting of biophysicists. The III. Slovak Biophysical Symposium held on April 18-20, 2008, was organized by The Slovak Biophysical Society (SKBS) in collaboration with Department of Nuclear Physics and Biophysics, Faculty of Mathematics, Physics and Informatics, Comenius University (FMFI UK) in the year, when the FMFI UK celebrates the 30 anniversary of establishment of the Department of Biophysics. This Department was the first in Slovakia focused on education of students in biophysics on the base of the application of fundamental knowledge in physics for understanding of the mechanisms of the processes in living systems. The Department of Biophysics was established in 1978 at the Faculty of Natural Science of the Comenius University. The first head of this Department was Prof. Dr. Dušan Chorvát, D.Sc. After establishment of the Faculty of Mathematics and Physics, this Department was among the basic departments of the Faculty. In 1990 the Department of Biophysics was renamed on Department of Biophysics and Chemical Physics (DBCP). This underlined focus in education also on chemical physics. Until now more than 120 master and 50 PhD students have been graduated mostly in biophysics. In 2004 the DBPC was merged with Department of Nuclear Physics and is now known as Department of Nuclear Physics and Biophysics.

The Slovak Biophysical Society was established in 2001 and nowadays has almost one hundred active members. The members of SKBS include not only teachers and researchers working in the field of biophysics but also those working in other interdisciplinary areas.

The III. Slovak Biophysical Symposium was focused on following topics

- membrane systems and transport processes
- photobiophysics, modern microscopy and spectroscopy techniques
- protein structure and stability, interactions of ligands with biomacromolecules
- biosensors and nanobiotechnology
- applications of biophysics in medicine
- molecular modeling

Scientific Committee

Tibor Hianik (FMFI UK Bratislava)
Dušan Chorvát (ILC Bratislava)
Ján Jakuš (JLF UK Martin)
Pavol Miškovský (PF UPJŠ Košice)
Ivan Zahradník (UMFG SAV, Bratislava)

Organizing committee

Tibor Hianik - chairman
Igor Grman
Alžbeta Holubeková
Zuzana Kaderjáková
Jana Kirchnerová
Miroskav Krajčí
Slavomíra Poníková
Peter Rybár
Peter Topor

Sponsored by
H TEST a.s., Prague, Czech Republic
Shimadzu Slovakia, Bratislava

Table of Contents

Program

Friday, April 18, 2008

11.00-14.00 **Registration** (Lecture Room F2)

13.00-14.00 P**oster installation** (Ground Floor F1)

14.00-14.30 **Opening ceremony** (Lecture Room F1)

1. Membrane systems and transport processes
Chairs: **K. Ondriaš, I. Zahradník**

14.30-15.15
Tutorial Lecture
T1 **P. Balgavý.** Effects of lipids on the activity of sarcoplasmic reticulum calcium pump

15.15-15.35
O1 **K. Ondriaš**, Ľ. Máleková, Effect of H_2S on intracellular chloride channels

15.35-16.30 **Coffee break, posters and scientific exhibition**

16.30-18.10
O2 I. Valent, I. Zahradník, **A. Zahradníková,** The effect of altered ryanodine receptor gating on generation of calcium sparks and propagation of calcium waves in a cardiac myocyte model
O3 J. Gaburjáková, **M. Gaburjáková**, Effect of luminal Ca^{2+} on the stability of coupled gating between ryanodine receptors from the rat heart
O4 **B. Tencerová**, J. Gaburjáková, A. Zahradníková, M. Gaburjáková, Sensitivity of the cardiac ryanodine receptor to ATP and its impact on kinetics with different luminal Ca^{2+}
O5 **Z. Tomášková**, M. Gaburjáková, New permeation properties of cardiac ryanodine receptor in conflict with single-ion channel model predictions
O6 **R. Krivánek,** C.G. Jeworrek, L. Okoro, C. Czeslik, R. Winter, Volume and compositional fluctuations in phospholipid/sterol vesicles

18.30 **Welcome Dinner**

Saturday, April 19, 2008

2. Molecular interactions, thermodynamics, spectroscopy
Chairs: **D. Chorvát, jr, D. Jancura**

09.30-10.15
Tutorial Lecture
T2 **M. Antalík,** Thermodynamics of protein conformational transitions

10.15-11.00
O7 **Ľ. Lacinová**, M. Pavlovičová, M. Kurejová, N. Klugbauer, Participation of the

outermost basic residues in the S4 segments of the $Ca_V3.1$ T-type calcium channel in channel closing

O8 P. Gbúr, R. Dedic, D. Chorvát jr., J. Hála, P. Miškovský, **D. Jancura,** Time resolved luminescence and singlet oxygen formation after illumination of hypericin in complex with low-density lipoproteins

11.00-11.30 **Coffee break and posters**

11.30-12.30

O9 **D. Chorvát, Jr.**, A. Mateašik, A. Chorvátová, Sequential spectral unmixing of spectrally-resolved time-correlated single photon counting data

O10 **P. Jasem,** Interaction of Mn^{2+} ions with DNA studied by microcalorimetry

O11 **M. Kopáni**, M. Weis, J. Dekan, J. Jakubovský, M. Miglierini, Analysis of iron forms in the human spleen

12.45-14.15 **Lunch**

3. Novel trends

Chair: **M. Antalík**

14.15-15.00

Tutorial Lecture

T3 **T. Hianik,** DNA/RNA aptamers – structure and applications

15.00-15.45 **Meeting of the Slovak Biophysical Society**

16.00 **Visit of Devin Castle**

18.30 **Symposium Dinner**

Sunday, April 20, 2008

4. Biosensors and nanobiotechnology

Chairs: **M. Fojta, J. Labuda**.

09.30-10.15

Tutorial Lecture

T4 **M. Fojta,** Possibilities of application of electrochemical techniques in DNA damage studies

10.15-11.00

O12 **J. Labuda,** J. Galandová, A. Ferancová, Detection of dsDNA degradation using impedimetric DNA-based biosensor

O13 **F. Kienberger**, G. Kada, Atomic force microscopy in bio-nanotechnology

11.00-11.30 **Coffee break**

5. Molecular modeling. Application of biophysics in medicine

Chairs: **T. Bleha, J. Jakuš.**

11.30-13.10

O14 P. Cifra, Z. Benková, **T. Bleha**, Modeling DNA chain dimensions in nanochannels

O15 **J. Suchánek,** What is revealed about the evolution of the genetic code by similarities between tRNA genes

O16 **I. Kinclová**, G. Ruttkay-Nedecký, I. K. Haverlík, Phylogenetic analysis of influenza A virus neuraminidase

O17 **I. Poliaček**, J. Jakuš, What is known (and what is not) about neuronal mechanisms controlling the cough reflex

O18 **P. Jasem**, P. Jasem Jr., Ľ. Horovčák, Review of medical imaging methods

13.10 Closing ceremony

13.30 Lunch

Proceedings

TUTORIAL LECTURES

T1 **P. Balgavý**, Effects of lipids on the activity of sarcoplasmic reticulum calcium pump
T2 **M. Antalík**, Thermodynamics of protein conformational transitions
T3 **T. Hianik,** DNA/RNA aptamers – structure and applications
T4 **M. Fojta**, Possibilities of application of electrochemical techniques in DNA damage studies

SHORT ORAL PRESENTATIONS

O1 **K. Ondriaš**, Ľ. Máleková, Effect of H_2S on intracellular chloride channels
O2 I. Valent, I. Zahradník, **A. Zahradníková,** The Effect of Altered Ryanodine Receptor Gating on Generation of Calcium Sparks and Propagation of Calcium Waves in a Cardiac Myocyte Model
O3 J. Gaburjáková, **M. Gaburjáková**, Effect of luminal Ca^{2+} on the stability of coupled gating between ryanodine receptors from the rat heart
O4 **B.Tencerová**, J.Gaburjáková, A.Zahradníková, M.Gaburjáková, Sensitivity of the cardiac ryanodine receptor to ATP and its impact on kinetics with different luminal Ca^{2+}
O5 **Z. Tomášková**, M. Gaburjáková, New permeation properties of cardiac ryanodine receptor in conflict with single-ion channel model predictions
O6 **R. Krivánek** C.G. Jeworrek, L. Okoro, C. Czeslik, R. Winter, Volume and compositional fluctuations in phospholipid/sterol vesicles
O7 **L. Lacinová**, M. Pavlovicova, M. Kurejova, N. Klugbauer, Participation of the outermost basic residues in the S4 segments of the $Ca_V3.1$ T-type calcium channel in channel closing
O8 P. Gbúr, R. Dedic, D. Chorvát jr., J. Hála, P. Miškovský, **D. Jancura,** Time resolved luminescence and singlet oxygen formation after illumination of hypericin in complex with low-density lipoproteins
O9 **D. Chorvat, Jr.**, A. Mateasik, A. Chorvatova, Sequential spectral unmixing of spectrally-resolved time-correlated single photon counting data
O10 **P. Jasem,** Interaction of Mn^{2+} ions with DNA studied by microcalorimetry
O11 **M. Kopáni**, M. Weis, J. Dekan, J. Jakubovský, M. Miglierini, Analysis of iron forms in the human spleen
O12 **J. Labuda,** J. Galandová, A. Ferancová, Detection of dsDNA degradation using impedimetric DNA-based biosensor.
O13 **F. Kienberger**, G. Kada, Atomic force microscopy in bio-nanotechnology
O14 P. Cifra, Z. Benková, **T. Bleha**, Modeling DNA chain dimensions in nanochannels
O15 **J. Suchánek,** What is revealed about the evolution of the genetic code by similarities between tRNA genes
O16 **I. Kinclová**, G. Ruttkay-Nedecký, I. K. Haverlík, Phylogenetic analysis of influenza A virus neuraminidase
O17 **I. Poliaček**, J. Jakuš, What is known (and what is not) about neuronal mechanisms controlling the cough reflex
O18 **P. Jasem**, P. Jasem Jr., Ľ. Horovčák, Review of medical imaging methods

POSTERS

P1: **J. Gallová**, M. Svorková, D. Uhríková, S.S. Funari, P. Balgavý, Influence of sterols on the egg yolk phosphatidylcholine bilayer: a small-angle synchrotron X-ray diffraction study

P2: **M. Kotalová**, D. Uhríková, J. Teixeira, P. Balgavý, SANS study on extruded unilamellar DOPC+DOPS liposomes containing long-chain aliphatic 1-alcohols

P3: **A. Caro**, M. Zana, Ľ. Lacinová, Voltage-dependent Channels in Native and NGF-Differentiated Rat PC12 Cells

P4: **M.Zvarík**, L. Šikurová, Monitoring possibilities of the mitochondrial membrane potential by a thiadicarbocyanine tribromide fluorescent probe

P5: **E. Cocherová**, J. Parulek, A. Zahradníková, Effects of changes of ryanodine receptor gating on the susceptibility to arrhythmias in heart myocytes: a modeling study

P6:I. Zahradník, A. Zahradníková, Jr., Z. Kubalová, E. Poláková, J. Pavelková, A. Zahradníková Calcium channels and calcium signaling in cardiac excitation-contraction coupling

P7: **Zs. Kohuš**, Ľ. Lacinová, Inhibition of the $Ca_v3.1$ T-type calcium channel by silver ions

P8: **P. Pullmannová**, D. Uhríková, S. S. Funari, I. Lacko, F. Devínsky, P. Balgavý, SAX diffraction study of DNA-phospholipid-gemini surfactants aggregates

P9: **M. Drígeľová**, M. Pavlovičová, Ľ. Lacinová, The use of trivalent cations for a measurement of gating current from the $Ca_v3.1$ channel

P10: **M. Šimera**, V. Foltin, M. Morvová, E. Neu, J. Foltinová, Interdisciplinary proof of lead in placenta – contribution for diagnostic practice

P11: **P. Slezák**, L. Šikurová, Influence of storage of insulated erythrocytes membranes on membrane fluidity

P12: **J. Kirchnerová**, P. Topor, M. Uherek, V. Štrbák, D. Chorvát jr., NAD(P)H/flavin autofluorescence imaging of INS-1E insulinoma cell metabolism

P13: G. Lajoš, S. Sánchez-Cortés, **G. Fabriciová**, P. Miškovský, J. V. García-Ramos, D. Jancura, Study of the interaction of hypericin with phospholipids and low-density lipoproteins by a surface-enhanced Raman and fluorescence spectroscopy

P14 E. Jacobsen, **J. Staničová**, P. Gbur, P. Miškovský, D. Jancura, Determination of binding constants and kinetics of hypericin incorporation into serum albumins

P15: **L. Bryndzová**, M. Andrášová, V. Huntošová, Z. Naďová, P. Miškovský, Investigation of hypericin fluorescence in isolated mitochondriaand U-87MMG cells

P16: **P. Topor**,. M. Šrámek, A. Mateašík, Iterative deconvolution algorithms in confocal data reconstruction

P17: **S. Poniková**, M. Antalík, T. Hianik, A CD spectroscopy study of the formation of guanine quadruplexes by DNA aptamers that selectively bind thrombin at different exosites

P18: **M. Fojta**, L. Havran, P. Horáková, H. Pivoňková, S. Hasoň, P. Kostečka, J. Vacek, K. Němcová, E. Paleček, Magnetic beads-based electrochemical nucleic acids and protein sensing strategies

P19: **M. Karabaliev**, Formation of thin lipid films on glassy carbon, gold and Si/SiO_2 wafers by the method of electrostriction

P20: **M. Šnejdárková**, L. Bábelová, V. Polohová, T. Hianik, Development of biosensor with aptamer as bio-recognition element for QCM detection of IgE

P21: T. Hianik, A. Porfireva, **I. Grman**, G. Evtugyn, Biosensor based on aptabodies and carbon nanotubes – new tool for detection proteins

P22: **Z. Kaderjáková**, P.Grešner, C.Watala, L. Šikurová, I. Waczulíková, Effect of acetylsalicylic acid on platelet aggregation in condition of in vitro induced hypercholesterolemia

P23: **M. Kardošová**, O. Uličná, O. Vančová, B. Klajnert, L. Šikurová, I. Waczulíková, Spectroscopic method in the testing of pharmacologically active compounds on mitochondrial function

P24: **Z. Garaiová**, O. Uličná, O. Vančová, M. Labieniec, C.Watala, I.Waczulíková, Polarographic method in the testing of the effect of pharmacologically active compounds on mitochondrial function

P25: I. K. Haverlik, G. Ruttkay-Nedecký, **I. Kinclová**, Phylogenetic analysis of influenza A virus – neuraminidase active site

P26: **A. Holúbeková**, P. Mach, J. Urban, Spectra calculation of β-cyclodextrin - coumarine complexes

P27: **P. Palenčár**, P. Cifra, T. Bleha, Simulations of unfolding of polypeptide chains in confinement

P28: **M. Krajčí**, J. Urban, P. Mach, Theoretical study of structural changes caused by applying mechanical strain on peptide L_{24}

P29: **D. Fedunová**, M. Bánó, A. Bellová, J.Bágeľová, Z. Gažová, M. Antalík, Vicsometric detection of lysozyme and poly-L-lysine amyloid aggregation

P30: J. Bágeľová, **D. Fedunová**, Z. Gažová, M. Antalík, Effect of $HClO_4$ on conformational transitions of ferricytochrome c

P31: **Z. Gažová**, A. Bellová , J. Imrich , P. Kristian, Z. Daxnerová, M. Antalík, Anti-amyloidogenic activity of acridines

P32: A. Bellová, **Z. Gažová**, J. Imrich, P. Kristian, Z. Daxnerová, M. Antalík, Acridine derivatives as potent inhibitors of lysozyme aggregation

T1

Effects of lipids on the activity of sarcoplasmic reticulum calcium pump

P. Balgavý[1], J. Karlovská[1], M. Kotalová[1,2], D. Uhríková[1], J. Gallová[1], N. Kučerka[1,3], J. Teixeira[4], T. Murugova[5], A. Kuklin[5]

[1] Department of Physical Chemistry of Drugs, FAF UK, Odbojárov 10, 832 32 Bratislava, Slovakia, e-mail: kfchl@fpharm.uniba.sk

[2] Department of Nuclear Physics and Biophysics, FMFI UK, Mlynská dolina F1, 842 48 Bratislava, Slovakia

[3] Canadian Neutron Beam Centre, National Research Council, Chalk River, Ontario K0J 1P0, Canada

[4] Laboratoire Léon Brillouin (CEA-CNRS), CEA Saclay, 91191 Gif-sur-Yvette, France

[5] Frank Laboratory of Neutron Physics, Joint Institute for Nuclear Research, 141980 Dubna, Russia

P-type ATPases are fundamental in establishing ion gradients by coupling the ATP hydrolysis to ion transport across biological membranes [1, 2]. Of many P-type ATPases known today, Mg^{2+}-dependent Ca^{2+}-ATPase (ATP phosphohydrolase, EC 3.6.1.38, SERCA1) from skeletal muscle sarcoplasmic reticulum (SR) is structurally and functionally the best studied member [3]. SR Ca^{2+}-ATPase is one of the most studied intrinsic membrane proteins because it is a single-chain transmembrane protein [4] with a conveniently measured function that is present in high concentration in the SR membrane. It transports 2 moles Ca^{2+} from the cytoplasm into the reticulum across the SR membrane with concomitant hydrolysis of 1 mol ATP; two or three moles H^{+} are counter-transported. The estimation of crystal structures of the SR Ca^{2+}-ATPase with two bound Ca^{2+} ions in the transmembrane protein region [5] and in the absence of Ca^{2+} ions and in the presence of inhibitor thapsigargin [6] has provided an opportunity to interpret the Ca^{2+}-ATPase conformational changes accompanying the reaction cycle in structural terms [7 - 10]. However, to elucidate fully the structure and function of the Ca^{2+}-ATPase in membrane, and particularly the role of lipid-protein interactions that influence ATP hydrolysis and ion transport, it is necessary to reconstitute it into defined synthetic phospholipids. The most successful approach so far involves the use of various detergents for Ca^{2+}-ATPase solubilization and reconstitution. Using this approach, it has been found that the Ca^{2+}-ATPase activity depends on phase states, hydrocarbon chain lengths, structure and charges of polar head groups of annular lipids surrounding the protein [11 - 15]: a) the activity is practically zero in the solid-like (gel phase) bilayer, high in the fluid (liquid crystalline) bilayer, but the particular value of fluidity in the fluid state has no effect; b) for high activity, a fluid bilayer from lipids with zwitterionic head groups is required - charged lipids support low activities; c) lower activity is observed in lipids under conditions when they form non-bilayer aggregates in isolation; d) the activity in (zwitterionic) diacylphosphatidylcholines is highest in the fluid bilayer of 1,2-dioleoylphosphatidylcholine (DOPC), but lower in fluid bilayers with shorter or longer acyl chains. These results indicate, that the ATPase activity is modulated by a delicate interplay of several physical factors – bilayer hydrophobic thickness, hydrogen bonding potential and hydration, surface charge, dipole potential and curvature frustration of the bilayer seem to be the most important.

We have studied effects of *n*-decane (C10), cholesterol (CHOL) and *N*-dodecyl-*N*,*N*-dimethylamine-*N*-oxide (C12NO) on bilayers of unilamellar vesicles prepared by extrusion from diacylphosphatidylcholines with monounsaturated acyl chains using small-angle neutron scattering (SANS) and turbidimetry [16 - 22]. In the present contribution, we compare bilayer physical parameters obtained from these studies with effects of these bilayer admixtures on the specific Ca^{2+}-ATPase activity of purified protein reconstituted into the same unilamellar vesicles. The effect of CHOL is most probably caused by the bilayer thickening. C12NO inhibits the DOPC-recontituted Ca^{2+}-ATPase activity at concentrations where the DOPC vesicles transform into mixed micelles. At lower C12NO concentrations,

the effect of DOPC bilayer thickness decrease on Ca^{2+}-ATPase activity is compensated by a change in the DOPC conformation in the bilayer polar region observed by ^{31}P-NMR spectroscopy studies of multilamellar vesicles containing C12NO. C10 effect on the bilayer thickness observed by SANS is rather small to affect the Ca^{2+}-ATPase activity. The intrinsic Ca^{2+}-ATPase fluorescence quenching studies using combinations of non-brominated and brominated C10 and DOPC indicate a direct interaction of C10 with protein rather than with annular lipids in the bilayer in DOPC-reconstituted Ca^{2+}-ATPase.

Acknowledgement
This work was supported by the VEGA 1/0295/08 and APVV 51-027404 grants. The SANS experiments were supported by the JINR project 07-4-1031-99/2008 and by the European Commission through the Access Activities of the Integrated Infrastructure Initiative for Neutron Scattering and Muon Spectroscopy (NMI3), supported by the European Commission under the 6th Framework Programme through the Key Action: Strengthening the European Research Area, Research Infrastructures, Contract no: RII3-CT-2003-505925.

References

[1] J. V. Moller, B. Juul, M. le Maire, *Biochim. Biophys. Acta* 1286 (1996) 1-51.
[2] H. J. Apell, *Bioelectrochemistry* 63 (2004) 149-156.
[3] H. J. Apell, *Rev. Physiol Biochem. Pharmacol.* 150 (2003) 1-35.
[4] D. H. MacLennan, C. J. Brandl, B. Korczak, N. M. Green, *Nature* 316 (1985) 696-700.
[5] C. Toyoshima, M. Nakasako, H. Nomura, H. Ogawa, *Nature* 405 (2000) 647-655.
[6] C. Toyoshima, H. Nomura, *Nature* 418 (2002) 605-611.
[7] A. G. Lee, *Biochim. Biophys. Acta* 1565 (2002) 246-266.
[8] A. N. Martonosi, S. Pikula, *Acta Biochim. Pol.* 50 (2003) 337-365.
[9] C. Toyoshima, G. Inesi, *Annu. Rev. Biochem.* 73 (2004) 269-292.
[10] H. S. Young, D. L. Stokes, *J. Membr. Biol.* 198 (2004) 55-63.
[11] A. G. Lee, *Progr. Lipid Res.* 30 (1991) 323-348.
[12] A. G. Lee, *Biochim. Biophys. Acta* 1376 (1998) 381-390.
[13] A. G. Lee, *Biochim. Biophys. Acta* 1565 (2002) 246-266.
[14] A. G. Lee, *Biochim. Biophys. Acta* 1612 (2003) 1-40.
[15] A. G. Lee, *Biochim. Biophys. Acta* 1666 (2004) 62-87.
[16] D. Uhríková, P. Balgavý, N. Kučerka, A. Islamov, V. Gordeliy, A. Kuklin, *Biophys. Chem.* 88 (2000) 165-170.
[17] D. Uhríková, N. Kučerka, A. Islamov, V. Gordeliy, P. Balgavý, *Gen. Physiol. Biophys.* 20 (2001) 183-189.
[18] D. Uhríková, N. Kučerka, A. Islamov, A. Kuklin, V. Gordeliy, P. Balgavý, *Biochim. Biophys. Acta* 1611 (2003) 31-34.
[19] J. Gallová, D. Uhríková, M. Hanulová, J. Teixeira, P. Balgavý, *Colloids Surf. B* 38 (2004) 11-14.
[20] J. Karlovská, D. Uhríková, N. Kučerka, J. Teixeira, F. Devínsky, I. Lacko, P. Balgavý, *Biophys. Chem.* 119 (2006) 69-77.
[21] J. Karlovská, F. Devínsky, P. Balgavý, *Gen. Physiol. Biophys.* 26 (2007) 290-297.
[22] J. Gallová, D. Uhríková, N. Kučerka, J. Teixeira, P. Balgavý, *Biochim. Biophys. Acta* in preparation (2008)

T2

Thermodynamics of protein conformational transitions

M. Antalík

Department of Biophysics, Institute of Experimental Physics, SAS, Watsonova 47 and Department of Biochemistry, Faculty of Science, UPJŠ, Moyzesova 11, Košice, Slovakia, e-mail: antalik@saske.sk

The study of the proteins results to the knowledge that atoms of these structures are sitting in their sites by interactions between neighboring atoms. Proteins present dynamically variable systems allowing their functionality by a number of van der Waals, hydrogen, coulombic and hydrophobic interactions. The intrinsic protein structure is similar to the aperiodic crystal. The important element affecting the global protein structure is solvent which enveloped the molecule. The disturbances in the polypeptide chain as well as in the vicinity can lead to the disruption of the three-dimension structure of the protein. The structural unfolding is associated with small change of the free Gibbs energy. The folding of proteins into the functional structures is spontaneous process which does not require a catalytic assistance principally. Specific interactions between the individual parts of proteins determine cooperativity of the transitions between the functional and unfolding states. The increase of the cooperativity of the unfolding process can be achieved by formation of the supramolecular complexes of proteins. The above mentioned facts will be demonstrate by cytochrome c, one of the most frequently studied proteins in term of the characterization of the thermodynamical principles of protein conformational transitions.

Acknowledgement
This work was supported by Slovak Grant Agency Project No. 2/6167/06.

T3

DNA/RNA aptamers – structure and applications

T. Hianik

Department of Nuclear Physics and Biophysics, FMFI UK, Mlynská dolina F1, 842 48 Bratislva, Slovakia, e-mail: tibor.hianik@fmph.uniba.sk

DNA/RNA aptamers are in vitro synthesized single stranded nucleic acids with high affinity to proteins or to other low and macromolecular compounds, which is comparable with affinity of antibodies. Aptamers are of considerable interest for their potential use in medical diagnostics and therapy. Biosensors based on DNA or RNA aptamers (aptasensors) are of substantial interest as an alternative to the biosensors based on antibodies. Although the first SELEX-related patent was filed in 1989 [1], the potentialities of the aptamer-based biosensors have not been realized in a full scale due to the problems with aptamer stability during immobilization and signal registration. Several problems related to the practical application of aptamers are still under solutions, for example how immobilization of aptamers to the supported films and their microenvironment will affect the aptamer structure and aptamer-ligand interactions. Problems are connected with application of aptamers in complex biological systems, where interferences with other molecules could take place and especially RNA aptamers are unstable due to cleavage by nucleases. So far mostly radio labeled aptamers were used. However, to be widely employed in clinical practice, aptamers must be detected via a nonradioisotope method. Moreover, most reliable and cost effective would be exploitation of the direct physical methods that do not require labeling of aptamers by additional chemical ligands. This highly promising route is currently in considerable focus of many laboratories [2-5]. Novel trends in biophysical research consist in the study of the mechanisms of the ligand-aptamer interactions [6] and of the effect of various conditions on the aptamer structure [7].

This contribution represents introduction into the aptamer structure, properties and their applications in medical diagnostics and therapy.

Acknowledgements
This work was supported by Slovak Grant Agency (Project No. 1/4016/07).

References

[1] C. Tuerk, L. Gold, *Science* 249 (1990) 505-510.
[2] M. Rimmele, *ChemBioChem* 4 (2003) 963- 971
[3] T. Hianik, in: Electrochemical Sensor Analysis, S. Alegret, A. Merkoci, A. (Eds.), Elsevier, Amsterdam, 2007, pp. 801-825.
[4] I. Willner, M. Zayats, *Angew. Chem. Int. Ed.* 46 (2007) 6408-6418.
[5] T. Mairal, V.C. Özap, P.L. Sanchez, M. Mir, I. Katakis, C.K. O Sullivan, *Anal. Bioanal. Chem* 390 (2008) 989-1007.
[6] S. Nagatoishi, Y. Tanaka, K. Tsumoto, *Biochem. Biophys. Res. Commun*. 352 (2007) 812–817.
[7] B.I. Kankia, G. Barany, K. Musier-Forsyth, K. *Nucl. Acids Res.* 33 (2005) 4395-4403.

T4

Possibilities of application of electrochemical techniques in DNA damage studies

M. Fojta

Institute of Biophysics, v.v.i., Academy of Sciences of the Czech Republic, Kralovopolska 135, CZ-612 65 Brno, Czech Republic, e-mail: fojta@ibp.cz

Nucleic acids are electroactive and surface-active substances yielding at mercury, carbon and some other electrodes redox and/or tensammetric signals. Some of these signals exhibit a remarkable sensitivity to alterations in the DNA structure. Electrochemical techniques have proved useful in detecting DNA damage that is usually accompanied with changes in electrochemical activity of particular base residues, changes in the DNA conformation affecting DNA adsorption at the electrode surfaces, and/or may result in appearance of new signals specific for electroactive DNA adducts (reviewed in [1]).

Behavior of double stranded DNA and mercury and some amalgam electrodes is strongly influenced by presence of DNA strand breaks (sb; interruptions of the DNA sugar-phosphate backbone). Upon formation of the sb (due to exposure to DNA damaging agents), a qualitative change in the DNA AC voltammetric response is observed. This principle has been utilized for studies of DNA damage at the electrode surface by *in situ* electrochemically generated reactive species [1]. Analogous technique, in connection with DNA cleavage by DNA repair enzymes, has been applied in detecting damage to DNA bases [2].

The most common electrochemical techniques applied in studies of DNA damage use various types of carbon electrodes and a signal due to electrochemical oxidation of guanine (which is the primary target for a variety of toxic compounds and its modification usually results in a loss of its electrochemical activity [1]). Some approaches employ surface-confined or soluble mediators of electrocatalytic guanine oxidation [3]. In addition to the label-free techniques utilizing intrinsic electrochemical activity of DNA, techniques involving non-covalently bound redox indicators (such as $[Co(bipy)_3]^{2+/3+}$ binding selectively to double-stranded DNA) or covalently bound markers (such as osmium tetroxide complexes, Os,L, selectively modifying single-stranded DNA) have been proposed. Upon extensive DNA damage, its double-helical structure is disrupted, binding of the $[Co(bipy)_3]^{2+/3+}$ indicator is reduced and its signal decreases [4]. Pyrimidine bases in single-stranded regions of damaged (and/or enzymatically post-treated) DNA can be modified by Os,L followed by electrochemical detection of the osmium markers [5].

Acknowledgement
This work was supported by GACR (203/07/1195), GA ASCR (IAA500040701) and MEYS CR (LC06035).

References

[1] M. Fojta, in: E. Palecek, F. Scheller, J. Wang, (Eds.), Electrochemistry of nucleic acids and proteins. Towards electrochemical sensors for genomics and proteomics. Elsevier, Amsterdam, 2005.p. 386-431.
[2] K. Cahova-Kucharikova, M. Fojta, T. Mozga, E. Palecek, *Anal. Chem*. 77 (2005) 2920-2927.
[3] J.F. Rusling, *Biosens. Bioelectron.* 20 (2004) 1022-1028.
[4] J. Labuda, M. Buckova, L. Heilerova, A. Caniova-Ziakova, E. Brandsteterova, J. Mattusch, R. Wennrich, *Sensors* 2 (2002) 1-10.
[5] L. Havran, J. Vacek, K. Cahová, M. Fojta, *Anal. Bioanal. Chem*., in press, DOI 10.1007/s00216-008-1850-1, 2008

O1

Effect of H_2S on intracellular chloride channels

K. Ondriaš, Ľ. Máleková

Institute of Molecular Physiology and Genetics, Centre of Excellence for Cardiovascular Research, SAV, Vlárska 5, 83334 Bratislava, Slovakia, e-mail: karol.ondrias@savba.sk

H_2S is produced endogenously, it is involved in neuromodulation, cell proliferation, apoptosis, regulation of cardiac function and cardioprotection, vasorelaxation, hypertension, and septic, endotoxin and haemorrhagic shocks and inflammation processes [1]. Reduced endogenous H_2S concentration was found in hypertension, coronary heart disease, cataractogenesis, atherosclerosis, choleresis and cirrhosis. Increased endogenous H_2S was associated with inflammation, shock, sepsis, pancreatitis and diabetes. H_2S was reported to either enhance, or to attenuate the relaxant effect of NO in the rat aorta [2]. Molecular mechanisms of the numerous H_2S effects are not fully understood. An activation of K_{ATP} channel, decrease in calcium influx and increase of calcium release by H_2S has been reported [3]. In order to contribute to the understanding of the numerous biological effects of H_2S, we tested whether H_2S can influence intracellular chloride channels.

We characterized the effect of H_2S on single channel properties of the chloride channels derived from the rat heart lysosomal vesicles incorporated into a bilayer lipid membrane. The single chloride channel currents were measured in 250:50 mmol/l KCl *cis*/*trans* solutions. H_2S inhibited the chloride channels by decreasing the channel open probability in a concentration-dependent manner, at the conventration range of 50-100 μmol/l. The inhibitory effect of H_2S was side dependent. We assume that the inhibitory effect of H_2S on chloride channels may be responsible for some of its numerous biological effects.

Acknowledgement
This work was supported by the Slovak Grant Agency VEGA, project No. 2/6012/27.

References

[1] E. Lowicka, J. Beltowski *J. Pharmacol. Reports* 59 (2007) 4-24.
[2] C.Q. Chen, H. Xin, Y.Z. Zhu, *Acta Pharmacol. Sin.* 28 (2007) 1709-1716.
[3] W Zhao, J. Zhang, Y. Lu, R. Wang, *EMBO J* 20 (2001) 6008-6016.

O2

The Effect of Altered Ryanodine Receptor Gating on Generation of Calcium Sparks and Propagation of Calcium Waves in a Cardiac Myocyte Model

I. Valent, I. Zahradník, A. Zahradníková

Institute of Molecular Physiology and Genetics, Slovak Academy of Sciences, Vlárska 5, 833 34, Bratislava, Slovakia, e-mail: alexandra.zahradnikova@savba.sk

Diastolic Ca^{2+} spark frequency, a key regulator of sarcoplasmic reticulum calcium content, is increased in the failing heart as well as in ryanodine receptor (RyR)-mediated stress-induced ventricular arrhythmias (CPVT and ARVD). The increased diastolic calcium release has been implicated as the main causative factor of the increased propensity to arrhythmias in these diseases. Both in heart failure and in CPVT/ARVD, diastolic calcium waves are observed at the cellular level. Several molecular mechanisms leading to calcium wave formation have been implicated in RyR dysregulation; these include changes in the interaction of RyR with FKBP12.6, in intramolecular interactions within RyRs, in the inhibition of the channel by Mg^{2+} ions, or in the RyR activation by luminal Ca^{2+}. We have tested the effects of changes in the thermodynamic and kinetic parameters of RyR gating, as well as the effect of RyR refractoriness in a mathematical model of calcium spark generation.

Release sites composed of clusters of RyR channels with steady-state open probability governed by a calcium-dependent mechanistic gating model were simulated using a stochastic model. A Ca^{2+} spark was activated upon opening of at least one RyR in the cluster. The aEMG model [1], based on intramonomeric allosteric coupling between calcium binding and channel opening, was used for description of RyR gating. The apparent sensitivity of RyRs to cytosolic Ca^{2+} was changed by all regulatory mechanisms in a similar way but with different sensitivity. Diffusion of calcium and its uptake by SERCA were approximated by the fire-diffuse-fire model [2], i.e., it was assumed that release events have constant amplitude u_{max} and constant duration τ_R, and that release events occurring at the same site are separated by at least the refractory time t_{REF} = R τ_R, where R is an integer. Release events could occur only at times M / N τ_R, where M and N are integers.

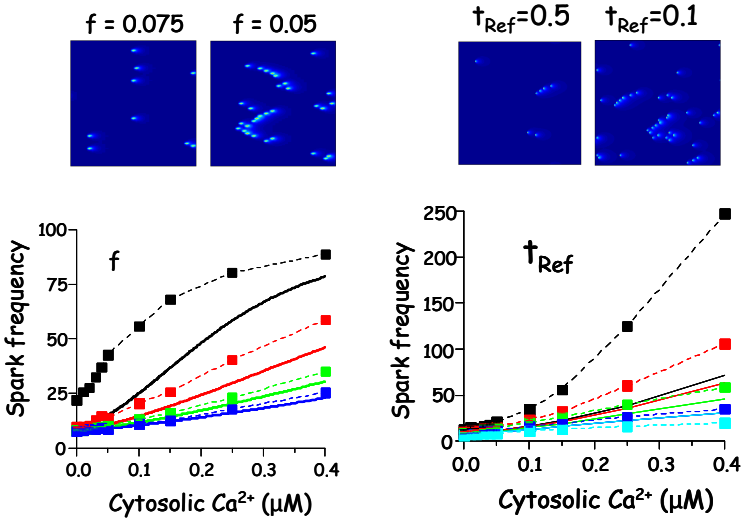

The effect of changes in RyR gating parameters on the calcium dependence of Ca spark frequency. Different colors represent different values of the allosteric coupling factor *f* (left panel) and refractory period t_{Ref} (right panel). Insets show typical simulations for control and modified channels.

The frequency of Ca^{2+} sparks predicted by this model depended steeply on Ca^{2+} con-centration. The calcium dependence of spark frequency was similar to that observed experimentally [3] when the apparent RyR calcium sensitivity was close to physiological (K_{Ca} ~10 μM), and if the remaining RyR gating parameters were unmodified from the original model [1]. Calcium spark frequency was very sensitive to changes in RyR gating parameters because of the

positive feedback of the released Ca^{2+} on the open probability of RyRs in neighboring release sites. Changes in steady-state open probability had the largest impact on spark frequency at diastolic calcium concentrations, while changes in the refractoriness of RyRs had the largest effect at elevated cytosolic calcium concentrations.

In conclusion, we have developed a novel model of calcium spark formation and wave propagation based on RyR gating that can be conveniently used for investigating the mechanisms of altered calcium homeostasis in diseased heart.

Acknowledgement. This work was supported by the EU Contract No. LSHM-CT-2005-018802/CONTICA, and the grants APVV-0139-06 and VEGA 2/0102/08.

References

[1] I. Zahradnik, S. Gyorke, A. Zahradnikova, in *J Gen Physiol.* 126 (2005) 515-527
[2] S. Coombes, R Hinch, Y Timofeeva, in *Prog Biophys Mol Biol.* 85 (2004) 197-216
[3] V. Lukyanenko, S. Gyorke, in *J Physiol.* 521 (1999) 575-585

O3

Effect of luminal Ca^{2+} on the stability of coupled gating between ryanodine receptors from the rat heart

J. Gaburjáková, M. Gaburjáková

Institute of Molecular Physiology and Genetics, Slovak Academy of Sciences, Vlárska 5, 833 34 Bratislava, Slovakia, e-mail: marta.gaburjakova@savba.sk

In cardiac muscle, the intracellular trigger for contraction is a transient rise in intracellular free Ca^{2+} released from the sarcoplasmic reticulum (SR) through ryanodine receptors (RYR2) channels by a process of calcium-induced calcium release (CICR) [1]. The major stimulus for CICR is the entry of a small amount of Ca^{2+} into the cell via a L-type Ca^{2+} channel into the close vicinity of RYR2 channels, resulting in their activation and a massive release of Ca^{2+} from the SR. Local CICR is intrinsically regenerative, and thus a mechanism leading to robust termination of Ca^{2+} release is required to ensure periodic contraction and relaxation of cardiac muscle.

Although identifying such a termination mechanism is an outstanding unsolved problem in the field of cardiac excitation-contraction (E-C) coupling, several termination mechanisms have been suggested and considered [2-4]. One of them is the phenomenon termed “coupled gating” [3]. It is manifested by simultaneous openings and closings of multiple RYR2 channels. Although the physiological importance of coupled gating of RYR2 channels as a termination mechanism is largely open to debate at the present time, it has been considered in a number of E-C coupling models [5,6]. Stern et al. [5] first introduced allosteric interactions between nearest-adjacent RYR2 channels, experimentally manifested by coupled gating, into their model of local control of E-C coupling in order to restore stability to the model. Liang et al. [7] found that the constant coupling between an array of closed RYR channels and an array of open RYR channels would delay the system termination rate; therefore, they proposed a novel working mechanism termed “dynamic inter-RYR coupling,” meaning that allosteric interactions among RYR channels are modulated by the channel functional state. Experimental evidence for destabilization of coupling among open RYR2 channels was already provided by Marx et al. [3]. They noted that most coupled RYR2 channels exhibited a “noisy” open state current level when compared with a baseline. This feature has been more pronounced when the transition from the coupled to fully uncoupled state of individual RYR2 channels was induced. Thus, the extent of noise of the current level likely reflects the strength of coupling in a given functional state.

The aim of our work was to examine in more detail the stability of functional interaction between two RYR2 channels in closed and open states, using the method of reconstitution of an ion channel into a planar lipid membrane. All coupled RYR2 channels exhibited a “noisy” open state current level (Fig. 1a). Mostly, it was manifested by the asymmetric current amplitude peak of open current level (Fig. 1b). In contrast, we did not observe such behaviour for the single RYR2 channel implying that it is solely a result of coupling between RYR2 channels. Thus, the main principle of our analysis was a determination of current amplitude peak asymmetry for a selected current level as a consequence of a transient modification of coupling strength and we introduced a new parameter - the coupling stability.

First, we compared the coupling stability determined for the closed level with that obtained for the open level. Under all tested experimental conditions, closed-closed channel interactions were significantly stronger in comparison with open-open channel interactions. The coupling stability reached almost maximum (>0.99) indicating very strong interaction between channels in the closed state. Indeed, we never saw brief openings from the baseline that would be a manifestation of a tendency for individual channels to escape from the tightly synchronized regime of their functioning.

Second, we quantitatively examined whether luminal Ca^{2+} has the potential to aid the coupled gating of RYR2 channels. We recorded coupled channels at different luminal Ca^{2+} concentrations ranging from 0 mM to 53 mM. Luminal Ca^{2+} significantly influenced the strength of interaction between open RYR2 channels. Remarkable brief closings from the open current level were easily recognized on the raw current traces when luminal Ca^{2+} was either absent or present in concentration of 53 mM. The weaker interaction between open channels was retained during the tested time period (~3 min) and never led to a complete disappearance of the functional communication between channels. From the quantitative point of view, the coupling stability was the highest ~0.95 when luminal Ca^{2+} ranged from 8 mM to 20 mM. At 0 mM and 53 mM luminal Ca^{2+}, the coupling stability was significantly reduced by ~ 0.2. In contrast to the open level, interaction between coupled RYR2 channels in the closed state was not modulated by luminal Ca^{2+} and the coupling stability was almost maximal (~0.99) under all tested conditions.

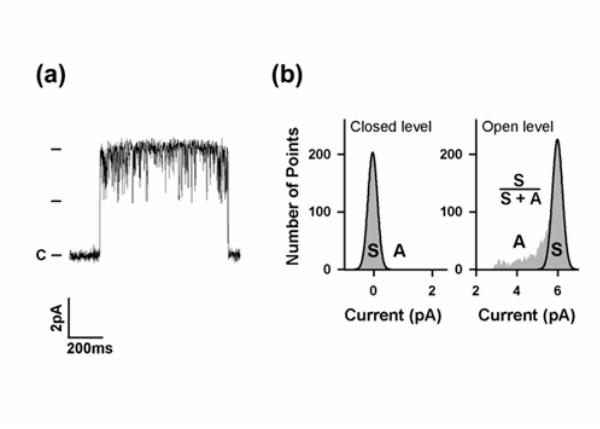

Fig. 1: Analysis of the coupling stability of coupled RYR2 channels. (**a**) Representative current trace of the coupled RYR2 channels with one opening. The channel opening is in the upward direction. Dashes at the left of the tracing indicate closed (C) and open states. (**b**) The current amplitude peaks for the closed and open current levels in generated all-points amplitude histograms were divided into a symmetrical part fitted by Gaussian function (area S) and an asymmetrical part (area A). A new parameter, the coupling stability, was introduced. This parameter is given by S/(S+A), where (S+A) represents the area under the whole current amplitude peak

Our study led to new observations that may have important implications for understanding the principles of the mechanisms triggering the termination of CICR in cardiac muscle. We revealed on single-channel level that the coupling stability of coupled RYR2 channels was significantly reduced when the channels entered the open state. Furthermore, we showed, for the first time, the new role of luminal Ca^{2+} in a recently suggested "dynamic inter-RYR coupling mechanism," a process that could be involved in the acceleration of termination of CICR in cardiac muscle.

Acknowledgement
This work was supported by the Slovak Grant Agency VEGA, project No. 2/6011/26 and by Government of Slovak Republic, project No. SP 51/0280800/0280802 and SP 51/0280900/0280901.

References
[1] A. Fabiato, *J. Gen. Physiol*. 245 (1985) 291-320.
[2] M.D. Stern, *Biophys. J.* 63 (1992) 497-517.
[3] S.O. Marx, J. Gaburjakova, M. Gaburjakova, Ch. Henrikson, K. Ondrias, A.R. Marks, *Circ. Res.* 88 (2001) 1151-1158.
[4] M.D. Stern, H. Cheng, *Cell Calcium* 35 (2004) 591-601.
[5] M.D. Stern, L.S. Song, H. Cheng, J.S. Sham, H.T. Yang, K.D. Boheler, E. Rios, *J. Gen. Physiol.* 113 (1999) 469-489.
[6] R. Hinch, *Biophys. J.* 86 (2004) 1293-1307.
[7] X. Liang, X.-F. Hu, J. Hu, *Biophys. J.* 92 (2007) 1215-1223.

O4

Sensitivity of the cardiac ryanodine receptor to ATP and its impact on kinetics with different luminal Ca^{2+}.

B. Tencerová, J. Gaburjáková, A. Zahradníková, M. Gaburjáková

Institute of Molecular Physiology and Genetics, Slovak Academy of Sciences, Bratislava, Slovakia, e-mail: barbora.tencerova@savba.sk

Introduction

Ryanodine receptor (RyR) is a calcium-activated, calcium-permeable channel of the sarcoplasmic reticulum (SR) that mediates excitation-contraction coupling in cardiac muscle cells. There is growing evidence that Ca^{2+} in the lumen of the SR can be effectively involved in different aspects of RYR channel regulation [1, 2]. To contribute to a deeper understanding of the mechanism by which luminal Ca^{2+} regulates the RyR2 channel it was interesting to investigate its effect on the response of RyR2 channel to different activators. Previously, the effect of luminal Ca^{2+} on RyR activation by cytosolic Ca^{2+} and caffeine has been studied [3]. Luminal Ca^{2+} induced prolongation of both, open and closed dwell times over the whole range of open probability (caffeine) or in the lower range of open probabilities (cytosolic Ca^{2+}). Alteration of gating kinetics provides further evidence of the existence of luminally located Ca^{2+} regulatory sites.

Adenosine triphosphate (ATP) is a well-known activator of the RYR channel with potential physiological importance. ATP binding sites, like those of most RyR ligands, are located on the large cytoplasmic domain.

Aims. In this study, we tested whether luminal Ca^{2+} affects the sensitivity of RyR channels to ATP at diastolic levels of cytosolic Ca^{2+} (~100 nM) and analyzed the gating kinetics of ATP-activated RyR2 channel in the presence of luminal Ca^{2+}.

Methods

RyR2 channels from rat cardiac microsomes were reconstituted into planar lipid membranes. Single-channel currents were recorded at 0 mV potential under voltage-clamp conditions in asymmetric trans/cis environment. The *trans* chamber, corresponding to the SR lumen, was filled with 53 mM Ca^{2+}, mixture of 27.5 mM Ca^{2+} / 27.5 mM Ba^{2+}, 27.5 mM Ca^{2+}, 15 mM Ca^{2+}, mixture of 52 mM Ba^{2+} / 1 mM Ca^{2+} or with 53 mM Ba^{2+} as the charge carrier, and contained additionally 50 mM KCl and 250 mM HEPES (pH = 7.35). Luminal Ba^{2+} mimicked the situation when no Ca^{2+} is present at the luminal face of the channel (53 mM Ba^{2+}), or it was used in a mixture with Ca^{2+} to maintain the concentra-tion gradient for divalent ions. The *cis* chamber, corresponding to the cytosolic side of the channel, contained 0.5 mM $CaCl_2$, 1 mM EGTA (free Ca^{2+} = 90 nM), 125 mM Tris, 50 mM KCl, 250 mM HEPES, pH = 7.35.

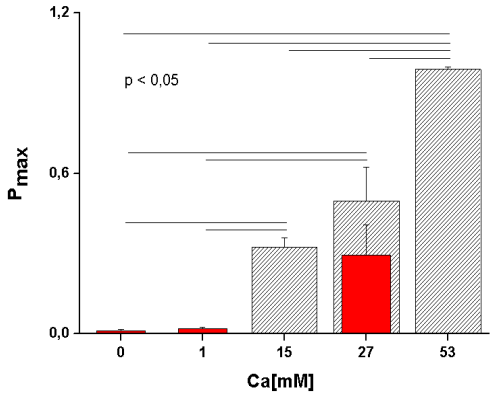

Fig.1. Comparison of the average P_{max} of RyR2 channels in the presence of ATP at 90 nM cytosolic Ca^{2+}, recorded in the presence of 53 mM, 27 mM, 15 mM, 1 mM and 0 mM luminal Ca^{2+}. The graphs show that luminal Ca^{2+} significantly increased the maximal extent of channel activation. Grey and red bars denote conditions, under which ionic current was carried only by Ca^{2+} or by both, Ca^{2+} and Ba^{2+}, respectively.

Results

In the absence of luminal Ca^{2+}, the RyR channels were only marginally activated and displayed short open times. In the presence of luminal Ca^{2+}, ATP induced dose-dependent activation of the channel. The maximum open probability (P_{max}) increased, while the EC_{50} of ATP activation decreased with elevating luminal Ca^{2+} concentration from 1 mM to 53 mM. Both, the increase of P_O and the decrease of EC_{50} showed hyperbolic dependence on luminal Ca^{2+} concentration. In the presence of luminal Ca^{2+}, dwell times were prolonged and frequency of events was increased.

Conclusion

The potency and efficacy of ATP as activator of the cardiac RYR channel at diastolic Ca^{2+} concentrations is dramatically modulated by the luminal Ca^{2+} concentration. Luminal Ca^{2+} positively regulates the responsiveness of the RyR2 channel to ATP and unambiguously accounts for the strong effect of ATP on RyR2 channel gating kinetics.

Acknowledgement This work was supported by the grants APVT-51-031104, VEGA-2/6011/26, EU Contract No. LSHM-CT-2005-018802/CONTICA, and APVV-0139-06.

References

[1] I.Gyorke, S.Gyorke, *Biohys. J.*, 75 (1998) 2801-2810.
[2] L. Xu, G. Meissner, *Biohys. J.*, 75 (1998) 2302-2312
[3] J.Gaburjakova, M.Gaburjakova, *J. Membrane Biol*., 212 (2006) 17-28

O5

New permeation properties of cardiac ryanodine receptor in conflict with single-ion channel model predictions

Z. Tomášková, M. Gaburjáková

Institute of Molecular Physiology and Genetics, Slovak Academy of Sciences, Vlárska 5, 833 34 Bratislava, Slovakia, e-mail: zuzana.vareckova@savba.sk

Ryanodine receptor (RyR) is the major intracellular Ca^{2+} release channel. RyR channels are involved in the process of excitation-contraction coupling in cardiac and skeletal muscles. The crystallographic structure of this channel is currently unavailable. Thus, the mechanism of ion handling, which is tightly connected with architecture of the channel's conductive pore, can be probed only indirectly by examining the permeability properties of the channel. Two distinct mechanisms of ion transport through a conductive pore are known. They differ in the number of ions the conductive pore can contain at a time. An ion channel can be either single-ion or a multi-ion channel.

Two different models describe the possible mechanism of ion permeation through the conductive pore – barrier models and Poisson-Nernst-Planck (PNP) models. The barrier models, based on Eyring rate theory, predict some properties by which single-ion and multi-ion channels could be identified [1]. The first one is the presence of an anomalous mole fraction effect, AMFE. AMFE is measured in a mixture of two ions at one side of the channel. The total ion concentration of the mixture is fixed, but the ratio of the ion concentrations within the mixture is varied. If the conductance of the channel falls below the individual conductances for the two permeant ions present, we talk about AMFE. According to the barrier model, multi-ion channels can exhibit an AMFE, but they are not obliged to do so. The second important property used to identify multi-ion channels is the concentration dependence of the zero-current potential. This property is measured under bi-ionic conditions with only one ion type present at each side of the channel. The zero-current potential is measured when the concentrations of the two ions are raised but the ratio of these concentrations is held constant. The changes of the zero-current potential are predicted specifically for multi-ion channels. Several experiments have been done with a view to determine the mechanism of ion handling in RyR channel [2-3]. The mole-fraction dependence of the conductance was studied by Lindsay et al. [2] in symmetrical mixtures of Na^+-K^+ and Li^+-K^+. No minimum of the conductance was present. Same experiments with one-sided mixtures of divalent ions Mg^{2+}-Ca^{2+} and Ba^{2+}-Ca^{2+} were done by Tinker et al. [3] and gave the same results. No anomaly was present. Tinker et al. used 210 mM concentration of K^+ ions on the other side of the membrane. The concentration of all mixtures studied by Lindsay et al. and Tinker et al. was 210 mM. Tinker et al. measured also the zero-current potential under bi-ionic conditions with K^+ ions on one side of the membrane and Ca^{2+} on the other. The concentration of K^+ was increased from 50 mM to 400 mM. The concentration of Ca^{2+} was matched with K^+ concentration in way that concentration ratio of K^+ to Ca^{2+} was unchanged. The zero-current potential was constant throughout the used concentration range.

The PNP model is based on electrodiffusion. This model is used to fit the experimental data and describes the profile of the electric potential or concentration within the pore. One of the outputs of the PNP model is the number of ions occupying the conductive pore. Recently, a new extended PNP model of RyR channel has been published [4]. The authors simulated various experimental conditions. The model predicted presence of AMFE for mixture of Cs^+ and Na^+ ions and this AMFE was confirmed experimentally. The AMFE is explained differently by the two models. The PNP model does not relate AMFE only to multi-ion channels. But the model of Gillespie et al. [4] calculated the occupancy of a

constrained part of the conductive pore, called selectivity filter. The filter could contain 3 monovalent cations or 2 Ca^{2+} ions. This result directly points to multi-ion character of RyR channel.

Our goal was to re-examine the behaviour of the conductance and of the zero-current potential depending on the mole-fraction of various ion mixtures. We used 8 mM total concentration of divalent mixtures and of combined monovalent-divalent mixtures. The concentration of monovalent mixtures was equal 96 mM. These concentrations approximately correspond to concentrations at which half-maximal Ca^{2+} and Li^{+} current, respectively, occurs. We chose these concentrations because it has been shown that saturation of the pore may mask the presence of AMFE [5]. Further, we have measured the zero-current potential under bi-ionic conditions. Ca^{2+} ions were present on the luminal side of the channel and monovalent cations Li^{+} or Na^{+} were present on the cytosolic side. The concentration of Ca^{2+} ions was in range of 5-53 mM. The concentration ratio of monovalents to Ca^{2+} was set at 1, 5 and 12. In each set of experiments, the chosen concentration ratio was held constant. Microsomes containing RyR channels were isolated from the rat heart. RyR channels were reconstituted into planar lipid membrane and single-channel current was measured. The zero-current potential and the conductance of the channel were determined from the current-voltage relationship obtained under various ionic conditions.

The conductance of RyR channel showed a minimum with varying Cs^{+}/Na^{+} molar fraction at the luminal face of the channel. Under these conditions, the zero-current potential changed monotonically. No extremum of conductance or zero-current potential was observed for other mixtures such as Na^{+}-Li^{+}, Ca^{2+}-Li^{+}, Ca^{2+}-Cs^{+}, Ca^{2+}-Ba^{2+} and Ca^{2+}-Sr^{2+}. The zero-current potential showed significant concentration dependence when Li^{+} or Na^{+} were present at 12-fold concentration of Ca^{2+} concentration at the luminal side of the channel. The concentration dependence of the zero-current potential was less pronounced when the concentration ratio was lowered from 12 to 1.

In the light of the barrier model of ion permeation through channels, the concentration dependence of the zero-current potential is one of the characteristics predicted for multi-ion channels [1]. According to this model, the presence of a minimum of the conductance in mixture of two types of ions is also considered as a feature of multi-ion channels. However, the absence of extremum in either the conductance or the zero-current potential in the other ionic mixtures is not in contradiction with possible multi-ion character of RyR channel. Thus, our results support the hypothesis of the multi-ion nature of the RyR channel conductive pathway, first predicted by Gillespie et al. [4].

Acknowledgement
This work was supported by the Slovak Grant Agency VEGA, project No. 2/6011/26

References

[1] G. Eisenman, R. Horn, *J. Membr. Biol.* 76 (1983) 197-225.
[2] A.R.G. Lindsay, S.D. Manning, A.J. Williams, *J. Physiol.* 439 (1991) 463-480.
[3] A. Tinker, A.J. Williams, *J. Gen. Physiol.* 100 (1992) 479-493.
[4] D. Gillespie, L. Xu, Y. Wang, G. Meissner *J. Phys. Chem. B* 109 (2005) 15598-15610.
[5] D.L. Campbell, R.L. Rasmusson, H.C. Strauss *Biophys. J.* 54 (1988) 945-954.

O6

Volume and compositional fluctuations in phospholipid/sterol vesicles

R. Krivanek , C.G. Jeworrek, L. Okoro, C. Czeslik, R. Winter

Dortmund University of Technology, Department of Chemistry, Physical Chemistry I – Biophysical Chemistry, Otto-Hahn-Straße 6, D-44227 Dortmund, Germany, e-mail: roland.krivanek@tu-dortmund.de

In eukaryotic cells, sterols regulate biological processes and sustain the domain structure of cellular membranes. While cholesterol is the major sterol of vertebrates, ergosterol plays a key role in fungi. Even though phospholipid-sterol interactions are in the focus of interest for decades now, a complete thermodynamic description of these systems is still missing. We have employed a variety of techniques, including ultrasound velocimetry, densimetry, calorimetries (differential scanning and pressure perturbation), and small-angle scattering (both neutron and X-ray) methods, to examine both volume and compositional fluctuations in phospholipid (DPPC)-sterol binary mixtures [1,2].

Fig. 1 shows the temperature dependence of the isothermal compressibility coefficient, β_T^{lipid}, of the lipid mixtures of DPPC and ergosterol (erg). In pure DPPC LUV, β_T^{lipid} has been found to be $3.8 \pm 0.1\times10^{-10}$ Pa^{-1} and $5.8 \pm 0.2\times10^{-10}$ Pa^{-1} in the gel and fluid phase, respectively. These values are ~10 % higher than the corresponding adiabatic compressibility data, β_S^{lipid}. Based on our results we have not found any marked difference in the effect of different sterols (cholesterol and ergosterol) on the various thermodynamic properties studied, namely the partial specific volume, the adiabatic and isothermal compressibility as well as the volume fluctuations. Such behavior is in contrast to the distinct structural and dynamical differences the two sterols exhibit when incorporated into lipid bilayers, where it has been shown that ergosterol orders DPPC chains more effectively than cholesterol [3]. Significant differences in β_T^{lipid} and β_S^{lipid} are seen in the gel and fluid phases of the lipid bilayers, as the solvent and lipid membranes are adiabatically uncoupled in the MHz region by the ultrasound experiment. These differences become dramatic in the gel-fluid transition region, indicating a significant degree of slow relaxational processes in the μs time range in the transition region. Maximum values of the relative volume fluctuations of 15 % are reached for DPPC at the main transition, which are strongly damped upon addition of both sterols. Within the accuracy of the measurements, no significant differences are observed for the two different sterols.

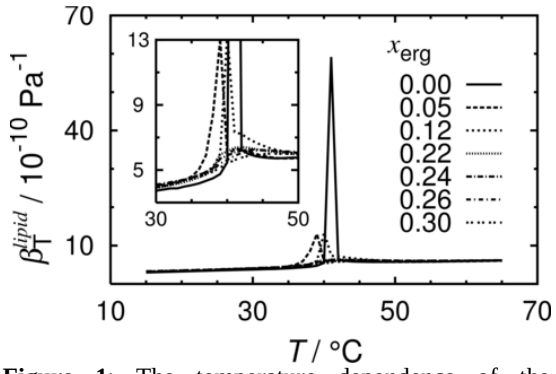

Figure 1: The temperature dependence of the isothermal compressibility coefficient of the lipids, β_T^{lipid}, in DPPC/ergosterol mixtures at different ergosterol molar fractions, x_{erg}.

SANS measurements on DPPC-d_{62}/erg (22 mol% ergosterol, the putative critical concentration) were performed under contrast matching conditions determined from known nuclear scattering lengths and molecular volumes. In Fig. 2, SANS curves measured at various temperatures are shown for sample-to-detector distance of 6 m with λ = 10.62 Å. At temperatures of 26 and 29 °C (see Fig. 2), the DPPC-d_{62}/erg mixture forms coexisting s_o and l_o phases, as can be inferred from the DSC traces. This two-phase region is characterized by a significantly higher SANS intensity as compared to that of the l_d+l_o two-phase region at

36 °C and higher, indicating extended composition fluctuations under these conditions in the lipid membrane of the vesicles. The s_o phase is rich in DPPC-d_{62} and the l_o phase is rich in ergosterol, resulting in a pronounced difference between the scattering length densities of these two phases. Furthermore, a close inspection of the SANS curves measured in the s_o+l_o and the l_d+l_o phase regions reveals that the composition fluctuations of the s_o+l_o membranes are causing the strongest SANS intensity around Q = 0.02 Å^{-1}, corresponding to a length scale of about 300 Å (≈ 2π/Q).

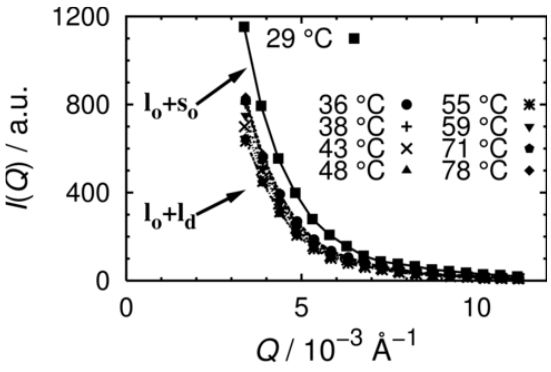

Figure 2: SANS diffraction curves of DPPC-d_{62}/ergosterol MLVs (22 mol% ergosterol) under contrast matched conditions.

As expected, no straight Guinier plots (ln(I(Q)) vs. Q^2) are obtained at all temperatures studied, indicating the absence of well-defined scattering objects of uniform size in the range covered by the SANS experiments. An Ornstein-Zernike analysis of the SANS curves in the critical point region reveals the absence of critical-point-like composition fluctuations with diverging correlation length, ξ, approaching the critical temperature. Furthermore, no large-scale composition fluctuations within the lipid membrane in the l_d+l_o two-phase region were observed. In contrast, significant composition fluctuations within the lipid membrane appear at lower temperatures, where the l_o and s_o phases coexist, on a length scale between 200 and 1800 Å.

Our results indicate that it seems more appropriate to characterize these binary phospholipid-sterol mixtures in the liquid-ordered/liquid-disordered coexistence region in terms of an essentially homogeneous phase of fluctuating nanoscale domains rather than a macroscopically phase-separated two-phase coexistence region as observed for ternary phospholipid-sterol mixtures, such as DPPC/DOPC/cholesterol. Such small domains are expected to have particular properties like an increased line energy, spontaneous curvature and limited lifetimes, which are probably also valid for the small raft-like domains in cellular membranes.

Acknowledgement
Financial support from the Deutsche Forschungsgemeinschaft, the Fonds der Chemischen Industrie, and the country Northrhine Westfalia and the European Union (Europäischer Fonds für regionale Entwicklung) is gratefully acknowledged.

References
[1] R. Krivanek, L. Okoro, and R. Winter, *Biophys. J.* doi:10.1529/biophysj.107.122549 (2008).
[2] R. Krivanek, C.G. Jeworrek, C. Czeslik, and R. Winter, submitted.
[3] C. Bernsdorff, and R. Winter, *J. Phys. Chem. B* 107 (2003) 10658-10664.

O7

Participation of the outermost basic residues in the S4 segments of the $Ca_V3.1$ T-type calcium channel in channel closing.

L. Lacinova[1], M. Pavlovicova[1], M. Kurejova[1], N. Klugbauer[2]

[1] Institute of Molecular Physiology and Genetics, Slovak Academy of Sciences, Vlárska 5, 83334 Bratislava, Slovakia. lubica.lacinova@savba.sk

[2] Institut für Experimentelle und Klinische Pharmakologie und Toxikologie, Albert-Ludwigs-Universität, Freiburg, Germany

Voltage-gated calcium channels (VGCC) play an important role in mediating plasmalemmal calcium ion influx in all electrically excitable cells [1]. The main pore-forming subunit (α_1) of all VGCC consists of four homologous domains (I-IV), each with six transmembrane segments (S1-S6). Segments S4 contain 4-5 basic amino acids and form putative voltage sensor of the channel. It was suggested that the movement of the S4 segment accompanies opening and closing of voltage-gated channels [2]. We examined the significance of the S4 segments of each domain for deactivation of the $Ca_V3.1$ channel. We have neutralised uppermost basic amino acids of the S4 segments from each single domain and in two neighbouring domains by exchanging arginin for cystein (R180C, R834C, R1379C, and R1717C) and compared them to the wild type channel.

All experiments were carried out on HEK 293 cells transiently transfected by wild type or mutant $Ca_V3.1$ channels. The Ca^{2+} current was studied by whole-cell patch-clamp using the HEKA-10 patch clamp amplifier. The extracellular solution contained (in mM): NaCl, 155; $CaCl_2$, 2; $MgCl_2$, 1; CsCl, 5; HEPES, 10; pH 7.4 (NaOH). The intracellular solution contained (in mM): CsCl, 130; EGTA, 10; $MgCl_2$, 5; TEA-Cl, 10; Na-ATP, 5; and HEPES, 10; pH 7.4 (CsOH). Data were recorded with HEKA Pulse 8.5 and analyzed off line using HEKA Pulsefit 8.5 and Origin 7.5 software.

Holding potential (HP) in all experiments was -100 mV. Deactivation was determined by pulse protocol consisting of 10 ms long conditioning pulse to +60 mV followed by 100 ms long repolarisation to membrane potentials varying between –140 mV and 0 mV. Voltage dependencies of deactivation time constants $\tau_{deact}(V)$ were fitted by the equation:

$$\tau_{deact}(V) = 1/(\exp(-(V-V\tau_{deact})/dV) + k_{OI}) \qquad (1)$$

where dV is a slope factor representing voltage sensitivity of each construct, k_{OI} is the rate constant of the transition of each construct from the opne state to the closest inactivated state and $V\tau_{deact}$ is the voltage at which deactivation time constant reaches the value $1/(1 + k_{OI})$ [3].

Removal of a single charged residue in domain II slightly accelerated the kinetics of channel closing while all other single mutations (i.e., in domains III and IV and, to a lesser extent, domain I) slowed down deactivation (Figure 1). Acceleration of channel closing by neutralisation of one basic amino acid in domain II was further enhanced when another basic amino acid in the adjacent domain I or III was neutralised (Figure 1). We can conclude that these mutations destabilised an open channel state. On the other hand, most prominent stabilisation of the open channel state that was reflected in a prolonged time constant of channel closing was caused by neutralisation of the basic amino acid in domain IV. Furthermore, voltage dependencies of deactivation time constants were shifted along the axis x. This effect was quantified by fitting experimental data by the equation (1) (Table 1). Mutations, which increased deactivation time constants, shifted their voltage dependence to more negative potentials (IIIS4, IVS4 and III+IVS4).

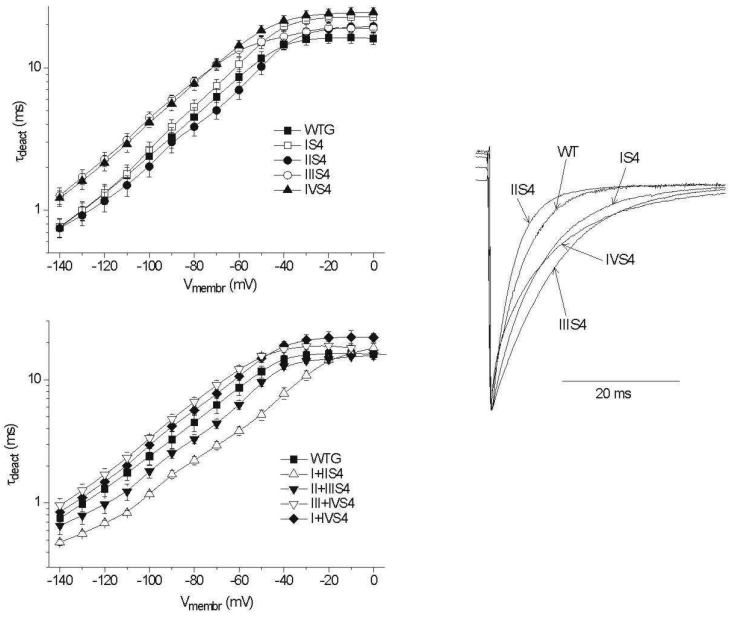

Figure 1. Deactivation time constants for $Ca_V3.1$ constructs calculated according to the equation (1). Examples of current traces recorded during repolarisation to –70 mV are shown on the right.

Decrease of deactivation time constants was accompanied by shift of their voltage dependence in an opposite direction, i.e., towards more depolarised membrane potentials (I+IIS4). Voltage sensitivity of channel deactivation reflected in slope factor of voltage dependence of τ_{deact} was not altered by introduced mutations except for the single mutation in the domain IV.

Table 1.

$V\tau_{deact}$ calculated according to the Equation 1. *, $p<0.05$; **, $p<0.01$.

Construct	WTG	IS4	IIS4	IIIS4	IVS4	I+IIS4	II+IIIS4	III+IVS4	I+IVS4
$V_{\tau deact}$ (mV)	- 110.6±4.6	- 112.5±3.5	- 102.5±4.5	- 134.5±4.4**	- 127.3±2.5**	- 94.5±2.9*	- 105.2±3.1	- 123.6±3.8*	- 116.5±3.3

In conclusion, the kinetics of channel deactivation reflects the stability of the open channel state. Removal of a basic amino acid in domains IV and III and, to a lesser extent, in the domain I stabilised an open channel state while neutralisation of the basic amino acid in domain II destabilised it.

Acknowledgement
This work was supported by the Slovak Grant Agency VEGA, project No. 2/7001.

References

[1] F. Hofmann, L. Lacinova, N. Klugbauer, *Rev. Physiol. Biochem. Pharmacol.* 139 (1999) 33-87.
[2] F. Bezanilla, *Physiol Rev* 80 (2000) 555-592.
[3] K. Talavera, A. Janssens, N. Klugbauer, G. Droogmans, B. Nilius, *J. Gen. Physiol.* 121 (2003) 529-540.

O8

Time resolved luminescence and singlet oxygen formation after illumination of hypericin in complex with low-density lipoproteins

P. Gbúr[1], R. Dedic[2], D. Chorvát jr.[3], J. Hála[2], P. Miškovský [1,3], D. Jancura[1]

[1]Department of Biophysics, P.J.Safarik University, Kosice, Slovakia
[2]Department of Chemical Physics and Optics, Charles University, Praque, Czech Republic
[3]International Laser Center, Bratislava, Slovakia, e-mail: jancura@upjs.sk

Photosensitized generation of singlet oxygen ($^1O_2$) by molecules of a photosensitizer (pts) is a crucial process in photodynamic therapy (PDT). Upon administration into blood stream photosensitizers associate predominantly with serum proteins. Hypericin (Hyp), a natural photosensitizing agent occurring in the plants of the genus *Hypericum*, associates mainly with low density lipoproteins (LDL) and to a lesser extent with human serum albumin.

Time–resolved fluorescence and phosphorescence study of Hyp in complex LDL as well as the evolution of singlet oygen ($^1O_2$) formation and annihilition after illumination of Hyp/LDL complex at room temerature are presented in this work. The observed shortening of the fluorescence lifetime of Hyp at higher Hyp/LDL molar ratios (>25:1) suggests quenching of excited singlet state of monomeric Hyp at these Hyp/LDL concentration ratios. The very short lifetime (~0.5 ns) of Hyp fluorescence at very high Hyp/LDL ratios (>150:1) suggest that at high local Hyp concentration inside lipidic structures fast and ultrafast nonradative decay processes from excited singlet state of Hyp become more important.

The amount of produced $^1O_2$ as well as integral intensity of Hyp phosphorescence after illumination of Hyp/LDL complex show a saturation behavior with respect to the Hyp/LDL ratio. This behavior resembles the dependence of the concentration of molecules of Hyp in monomeric state on this ratio. This fact confirms that only monomeric Hyp is able to produce excited triplet state of Hyp. which consequently, in hypoxic conditions, leads to singlet oxygen production.

The analysis of phosphorescence decay curve of Hyp in the presence of LDL manifests its non-trivial kinetics. We suppose that the primary process of Hyp triplet state depopulation is the energy transfer to ground state of molecular oxygen and formation of singlet oxygen, but the presence of other depopulation processes are not excluded. The value of singlet oxygen lifetime (~8 μs) after its formation from the excited triplet state of Hyp in LDL suggest that molecules of singlet oxygen remain for a certain period of time inside LDL particle and are not immediately released to the aqueous surrounding. Furthermore, it is demonstrated that Hyp exists in the complex with LDL in monodeprotonated state.

Acknowledgements
This work was supported by the Scientific Grant Agency of the Ministry of Education of Slovak Republic under the grant VEGA No. 2278, by the Slovak Research and Development Agency under the contract APVT-20-036104 and by the project MSM0021620835 from the ministry of Education of the Czech Republic.

O9

Sequential spectral unmixing of spectrally-resolved time-correlated single photon counting data

D. Chorvat Jr.[1], A. Mateasik[1], A. Chorvatova[2,3]

[1] International Laser Centre, Bratislava, Slovakia
[2] Research Centre of CHU Sainte-Justine, University of Montreal, Montreal, Canada
[3] Department of Pediatrics, University of Montreal, Montreal, Canada
e-mail: dusan@ilc.sk

Recent advances in time-correlated single photon counting (TCSPC) allowed to experimentally measure sub-nanosecond fluorescence decay kinetics of fluorophores on multiple wavelengths simultaneously [1,2]. In the case of spectrally overlapping emission from several fluorescent species, obtained spectral and temporal decay patterns are often too complex to be analyzed by means of classical multi-exponential analysis, especially in live cell environment. In our contribution we therefore present a newly developed approach, based on sequential spectral unmixing.

The developed method has following steps:

1. Identification of the number of spectral components using area-normalized time-resolved emission spectroscopy (TRANES), or a singular value decomposition
2. Estimation of the spectral profiles of all significant components either by measurement of the pure samples, or by principal component analysis assessing variations in the data following application of specific modulators in the case of cell autofluorescence
3. Sequential spectral unmixing of the recorded multi-wavelength TCSPC datasets according to the database of reference spectra, followed by fluorescence lifetime analysis.

We will discuss both the benefits and the limitations of the developed approach [3] and demonstrate its ability to efficiently separate contributions of individual components from multi-component mixtures of spectrally overlapped fluorophores, such as intrinsic cell autofluorescence and/or fluorescent proteins.

Acknowledgement
This work was supported by the research grant VEGA 2/6158/6 to DC, and by CIHR (MOP 84450) grant to AC.

References

[1] Becker W., *Advanced Time-Correlated Single Photon Counting techniques*, Springer, New York, 2005.
[2] Chorvat D. Jr., Chorvatova A., *Eur Biophys J.* 36 (2006) 73–83
[3] Chorvat D. Jr., Mateasik A., Kirchnerova J., Chorvatova A., *Proc. SPIE* 6771 (2007) 677105 1-12

O10

Interaction of Mn^{2+} ions with DNA studied by microcalorimetry

P. Jasem

Department of Medical Biophysics, LF UPJŠ, Tr. SNP1, 040 66 Košice, Slovakia, e-mail: Pavol.Jasem@upjs.sk

Interest in the study of the thermodynamic properties of DNA metallocomplexes is due to the major role played by metal ions in the functioning of nucleic acids and also by the constantly increasing pollution of the environment by heavy metal salts. For example, they stabilize the structure of nucleic acids, influence the synthesis rate and accuracy of the nucleotide sequence in DNA- and RNA-polymerase systems, take part in the processes of DNA transcription and replication, and cause mutagenesis and carcinogenesis [1]. These effects depend not only on the type of metal, but also on the value of their effective concentration [2]. It is also important to note that the interaction of metal ions with DNA can serve as a simplest model for its binding to more complex ligands, including many drugs, mainly antibiotics, and lends itself to a correct theoretical interpretation [3].

DNA–metal ion interactions and their effects on DNA structure have been investigated using a variety of techniques. From the UV-visible spectroscopy and circular dichroism experiments, it was concluded that the alkaline earths interact primarily with DNA phosphates, stabilizing the double helix through reduced charge repulsion of its complementary strands. For example, they enhance base stacking, probably by reducing electrostatic repulsion along the DNA chain [4].

In this work, we aim to characterize thermodynamic changes that DNA undergoes upon thermal melting in the presence of divalent metal ions. We investigate the effect of manganese ions on the parameters of the helix-coil transition of DNA at low Na^+ concentration. As a target of metal interaction, calf thymus DNA and DNA from chicken erythrocytes in aqueous solution was employed.

Native DNA (Sigma) of molecular mass 1.9×10^7 Dalton, protein content lower than 0.1%, RNA content lower than 0.2%, hypochromic effect of 36% and turbidity (D320 for DNA concentration of 1 mg/ml) lower than 0.025 o.u., was used. The concentration of Na^+, taking into account the counter-ions introduced with DNA, was 4.2×10^{-3} M. The microcalorimetric investigations were made using a DSAM-4 differential scanning calorimeter. The temperature scanning rate was 1°C/ min. This enabled us to observe the complex nature of the process and evaluate the temperature and enthalpy of the transition in a wide range of concentrations of metal ions. As the transition temperature T_m we took the value of the temperature of the maximum of the melting curve, width of the transition interval ΔT was defined as the halfwidth of the peak, the area bounded by the curve of the temperature dependence of the heat capacity $C_p = f(T)$ corresponds to the heat of the observed conversion process ΔH_{cal}. The maximum error of the heat capacity measurements did not exceed 1.5 % in the 0-100 °C.

The helix-coil transition of deoxyribonucleic acid in presence of chloride salt of Mn^{2+} was studied at elevated temperatures in the range from 20 °C. to 100 °C. by microcalorimetry. The Mn^{2+} concentration was varied between 0 and 20 $[Mn^{2+}]/[P]$. The secondary structure of DNA remained in the frame of the B-form family in the whole ion concentration range at room temperature. No significant DNA denaturation was revealed at room temperature even at the highest concentration of metal ions studied. The dependence of the melting temperature of DNA, the width of its melting curve, and the enthalpy of the helix-coil transition on the molar ratio $[Mn^{2+}]/[PO_2^-]$ have been determined. The thermal stability of DNA is affected by the ion concentration and the nature of solvent. It increases at low $[Mn^{2+}]/[PO_2^-]$ ratios and the melting temperature T_m, ΔT increases relative to characteristic for DNA without divalent ions and ΔH_{vH} decrease. This implies than cations stabilize the

DNA structure by reducing the charge repulsion between the phosphate groups. When the concentration Mn^{2+} increases, T_m passes through the maximum and ΔT decreases. It is due to elevating of cooperativity of the helix-coil transition of DNA. With a further increase of the ion concentration T_m, ΔT and ΔH_{cal} changes very slightly, and decreases at high concentrations.

DNA denaturation and a significant decrease of the melting temperature T_m, ΔT and ΔH_{cal} of DNA connected with a decrease of the stability of DNA induced by Mn^{2+} ions occurred and demonstrated sensitivity to DNA condensation and aggregation as well as an ability to distinguish between these two processes [4,5]. No condensation or aggregation of DNA was observed at room temperature at any of the metal ion concentrations studied. DNA condensation was revealed in a very narrow range of experimental conditions at around 2.0 $[Mn^{2+}]/[P]$. DNA aggregation was observed in the presence of Mn^{2+} ions at elevated temperatures during or after denaturation.

References

[1] H. Hays, A.J. Berdis, *Biochemistry* 41 (2002) 4771-4778.
[2] J. Duguid, V.A. Bloomfeld, J. Benevides, G.J. Thomas,,Jr, *Biophys. J.* 69 (1995) 2623-2641.
[3] K. Nazari, N. Gholami, A.A. Moosavi-Movahedi, *Med. Chem. Res*. 16 (2007) 238-257.
[4] A.M. Polyanichko1, V. Andrushchenko, E.V. Chikhirzhina, V.I. Vorob'ev, H. Wieser, *Nucleic Acids Research*, 32 (2004) 989-996.
[5] A. Arslantas, A.K. Devrim, H. Necefoglu, *Int. J. Mol. Sci*. 8 (2007) 1225-1233

O11

Analysis of iron forms in the human spleen

M. Kopáni[1], M. Weis[2], J. Dekan[3], J. Jakubovský[1], M. Miglierini[3]

[1] Comenius University, School of Medicine, Department of Pathology, Sasinkova 4, 811 08 Bratislava, Slovakia
[2]Department of Physics, Slovak University of Technology, Faculty of Electrical Engineering and Information Technology, Ilkovičova 3, 812 19 Bratislava, Slovakia
[3]Department of Nuclear Physics, Slovak University of Technology, Faculty of Electrical Engineering and Information Technology, Ilkovičova 3, 812 19 Bratislava, Slovakia e-mail: martin.kopani@fmed.uniba.sk

Abstract

We examined 3 samples of human spleen tissues with diagnosis of hereditary spherocytosis, hemochromatosis and after splenectomy with no signs of spleen disease. Scanning electron microscopy wit energy – dispersive microanalysis (SEM-EDX), transmission electron microscopy (TEM), Mössbauer spectroscopy (MS), X-ray diffraction (XRD) were used for analysis of iron particles. Mössbauer spectroscopy of studied tissues revealed different phase of iron oxide in the human spleen. On the ground of this consideration we can claim all samples of investigated tissues exhibit presence of two different paramagnetic iron phases, both based on three-valent (Fe^{3+}) atoms. Consequently only 4 different iron-oxides correspond with experimental results. Multielemental composition of iron particles was found by SEM-EDX analysis. We suppose that pH and various chemical elements are significant factors influence biomineralization of iron in the human spleen.

Introduction

Iron can be found in human body mainly in the form of ferritin. This protein creates spherical formation with the size of 12 nm. The core of ferritin is 8 nm big and consists of ferrihydrite - $5Fe_2O_3.9H_2O$ with various amount of phosphorus. Studies performed via nanodiffraction showed that physiological ferritin is from crystalline ferrihydrite and amorphous iron hydroxide [1], pathological ferritin prevailed wüstite (FeO) and magnetite – like structure. In excessive volume of iron in the organism, the iron is stored in cells in the form of hemosiderin [2]. Hemosiderin is considered to be a proteolytic product of ferritin [3]. Besides the differences of diffraction image between the samples of hemosiderin it is found also some differences in their element composition [4,5].

Material and methods

We examined 3 samples of human spleen tissues with diagnosis of hereditary spherocytosis, hemochromatosis and after splenectomy with no signs of spleen disease. Sections were prepared for investigation in light microscopy and stained with Perls' Prussian blue to locate ferric ion (Fe^{3+}) deposits. Tissue probes have been prepared by common methods for SEM-EDX and TEM investigation [6]. For ^{57}Fe Mössbauer spectroscopy 3 powdered samples of spleen tissues were placed in sample holders and measured at room-temperature and liquid nitrogen temperature (LNT). The Mössbauer spectrometry measured in transmission geometry was employed using a ^{57}Co(Rh) source and subsequently evaluation of hyperfine parameters was done by the help of the CONFIT fitting program.

Results

The Mössbauer spectrum typical for paramagnetic particles is observed, consisting of the two paramagnetic doublets (paramagnetic state) with common quadrupole splitting and negligible hyperfine fields. Following data reveal the results from MS of studied tissues.

Table 1 List of possible phases of the iron oxides present in the studied tissues.

Phase of iron oxide	Isomer shift [mm/s]	Quadrupole splitting [mm/s]
Lepidocrocite γ-FeO(OH)	0.37	0.53
Feroxyhyte δ-FeO(OH)	0.36	0.69
Ferrihydrite $5\ Fe_2O_3 \cdot 9\ H_20$	0.35	0.71
$FePO_4$	0.38	0.80

Discussion

The investigation of Perls' Prussian Blue stained slides by light microscope indicates iron depositions in samples with diagnosis of hemochromatosis and hereditary spherocytosis. SEM-EDX microanalysis reveals multielemental composition. Sample of spleen tissue with no signs of spleen disease can contain ferrihydrite (Table 1). Presence of vestigial amounts of some elements significantly influences oxidative-reduction status of iron, its structure, chemical composition and stoichiometry [7,8]. The amount of phosphorus in iron oxides influences iron oxidation [9]. The interaction of iron Fe(II) with ferrihydrite leads to precipitation of goethite, lepidocrocite and magnetite [10]. The magnetite and goethite-like form of hemosiderin that has been observed in some pathological tissues [11] was not detected. The significant source of Fe(II) is the perturbation in erythrophagocytosis, which plays role in several diseases, including hemochromatosis [12]. We suppose that pH and various chemical elements are significant factors influence biomineralization of iron in the human spleen.

Conclusion

Mössbauer spectroscopy of studied tissues revealed different phase of iron oxide in the human spleen. Multielemental composition of iron particles was found by EDX analysis.

References

[1]. J.M. Cowley, D.E. Janney, R.C. Gerkin, P.R. Buseck, *J. Struct. Biol.* 131 (2000) 210-216.
[2]. C. Seldon, M. Owen, J.M. Hopkins, T.J. Peters, *Br. J. Haematol*. 44 (1980) 593-603
[3]. M.P. Weir, J.F. Gibson, T.J. Peters, *Biochem. J*. 223 (1984) 31-38.
[4]. R.J. Ward, R. Legssyer, C. Henry, R.R. Crichton, *J. Inorg. Biochem*. 79 (2000) 311-317.
[5]. C. Quintana, J.M. Cowley, C. Marhic, *J. Struct. Biol.* 147 (2004) 166-178.
[6]. M. Kopani, J. Jakubovsky, S. Polak, *Acta Phys. Slovaca* 51 (2001) 339-345.
[7]. T. Borch, Y. Masue, R.K. Kukkadapu, S. Fendorf, Environ. *Sci. Technol.* 41 (2007) 166-172.
[8]. S.W. Jeen, J.L. Jambor, D.W. Blowes, R.W. Gillham, *Environ. Sci. Technol.* 41 (2007) 989-1994.
[9]. J. Cumplido, V. Barrón, J. Torrent, *Clays Clay Miner.* 48 (2000) 503-510
[10]. C.M. Hansel, S.G. Benner, S. Fendorf, *Environ. Sci. Technol.* 39 (2005) 7147-7153.
[11]. D. Meyrick, J. Webb, C. Cole, *Inorg. Chim. Acta* 339 (2002) 481-487.
[12]. C. Beaumont, F. Canonne-Hergaux, *Transfus. Clin. Biol.* 12 (2005) 123-30.

O12

Detection of dsDNA degradation using impedimetric DNA-based biosensor

J. Labuda, J. Galandová, A. Ferancová

Institute of Analytical Chemistry, Faculty of Chemical and Food Technology, Slovak University of Technology in Bratislava, 812 37 Bratislava, Slovakia, e-mail: jan.labuda@stuba.sk

Simple and disposable DNA-based biosensors with a layer of multiwalled carbon nanotubes (MWNT) and double stranded (ds) calf thymus and herring sperm DNA deposited on the surface of a screen-printed carbon electrode (SPE) have been prepared using both, layer-by-layer and mixed coverages. Electrochemical impedance spectroscopy (EIS) has been utilized as a powerful and effective tool for the investigation of electric features of DNA modified electrodes. The EIS measurements have been performed in 0.1 M phosphate buffer solution pH 7.0 using 1 mM potassium ferricyanide as a redox probe. Cyclic voltammetry (CV) with the redox couple of $[Fe(CN_6)]^{3-}$ / $[Fe(CN_6)]^{4-}$ was used as an independent detection method.

The presence of MWNT at the SPE surface significantly decreases the polarization resistance of the electrode surface due to high MWNT conductivity. On the other hand, the impedance increases at the electrodes modified with the dsDNA layer. To detect the presence of dsDNA on the electrode, the normalized values of the polarization resistance difference, ΔR_p, the anodic to cathodic CV peak potential separation, ΔE_p as well as the cathodic current signal obtained for $[Fe(CN_6)]^{3-}$/$[Fe(CN_6)]^{4-}$ have been evaluated [1]. The application of impedimetric nanostructured DNA-based biosensors to the detection of dsDNA degradation by the reactive oxygen species formed *in situ* and some synthetic compounds are presented.

Acknowledgement: The work was supported by the Application Research Project AV /4/0103/06 and the Grant Agency VEGA (Project No. 1/0852/08) of the Ministry of Education of Slovakia.

References:

[1] G. Ziyatdinova, J. Galandová, J. Labuda, *J. Electrochem. Sci*. 3 (2008) 223-235.

O13

Atomic force microscopy in bio-nanotechnology

F. Kienberger, G. Kada

Agilent Technologies Austria, Aubrunnerweg 11, 4040 Linz, Austria;
e-mail: ferry_kienberger@agilent.com ; gerald_kada@agilent.com

Within the field of scanning probe microscopy, atomic force microscopy (AFM) is extensively used in a wide range of disciplines such as life science, solid-state physics, and materials science. The AFM has evolved into an imaging method that yields structural details of biological samples such as proteins, nucleic acids, membranes, and cells in their native environment [1]. AFM is a unique technique for providing subnanometer resolution at a reasonable signal-to-noise ratio under physiological conditions. As a result of continuous developments in sample preparation, imaging techniques, and instrumentation, AFM is now a companion technique to X-ray crystallography and electron microscopy (EM) for the determination of protein structures, for example. It complements EM by allowing visualization of biological samples in buffers that preserve their native structure over extended time periods. AFM does not rely on symmetry averaging and crystallization, therefore revealing defects and structural anomalies not observable in classical ensemble measurements. Unlike EM, AFM yields three-dimensional maps with an exceptionally good vertical resolution (less than a nanometer) (Figure 1). In addition to high-resolution imaging of proteins, nucleotides, membranes, and living cells, the measurement of mechanical forces at the molecular level provides detailed insights into the function and structure of biomolecular systems [2]. Inter- and intramolecular interactions can be studied directly at the molecular level, as exemplified by the analysis of polysaccharide elasticity, DNA mechanics, the function of molecular motors, and the binding potentials of receptor–ligand pairs involved in cell adhesion. In the latter case, defined forces are exerted on a receptor–ligand complex and the dissociation process is followed over time. With data obtained from force measurements, molecular interactions can be analyzed in terms of kinetic rate constants, structural parameters of binding pockets, molecular dynamics of the recognition process, and the energy landscape of the interaction [3] (Figure 2). Compared with conventional ensemble methods, single-molecule experiments offer several advantages. First, by conducting many sequential measurements, the distribution of molecular properties of inhomogeneous systems can be determined. Second, single-molecule trajectories, since they are direct records of the system’s fluctuations, provide dynamic and statistical information that is often hidden in ensemble-averaged results. Finally, it is possible to monitor rarely populated transients in real time, which are difficult or impossible to capture using conventional methods.

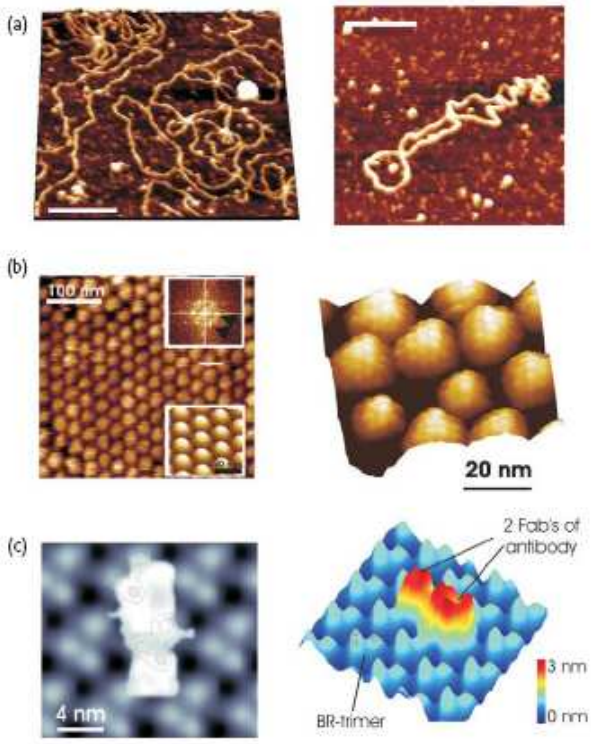

Figure 1. High-resolution topographical imaging of biomolecular assemblies. (a) 3 kbp (base pairs) pDNA on a mica surface imaged in Ni2+ buffer solution. Scale bar 150 nm. (b) Left: crystalline arrangement of human rhinovirus on a lipid bilayer containing receptors. Inset: Fourier spectrum and average lattice. Right: dense packing of virus particles with regular patterns of small protrusions ~0.5 nm high and ~3 nm in diameter corresponding to protein structures protruding from the virus capsid. (c) Topographical image of purple membrane to which a single antibody is bound (left) and a three-dimensional representation (right). The hexagonal arrangement of bacteriorhodopsin trimers and the two Fab fragments of the antibody can be observed with a resolution of roughly 1 nm.

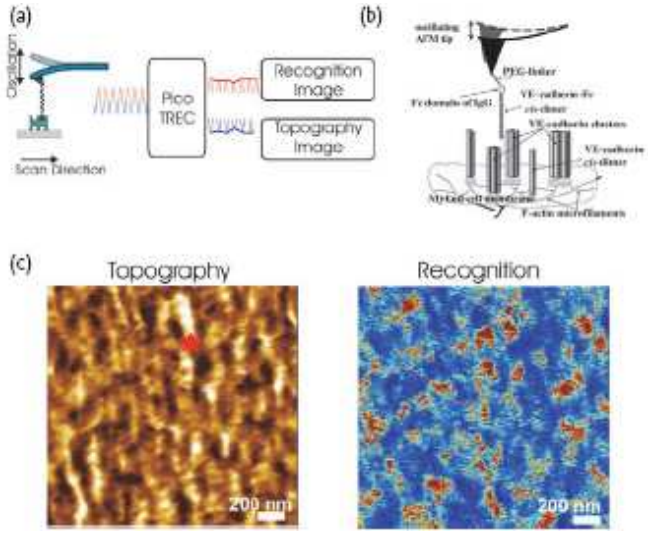

Figure 2. Simultaneous topography and recognition imaging (TREC) of gently fixed cells. (a) Signal processing for simultaneously obtaining topography and recognition images. The cantilever oscillation signal is split via the TREC box into upper (recognition image) and lower (topography image) parts. (b) Schematic of dynamic recognition imaging to visualize VE-cadherin binding sites on a cell surface. (c) Simultaneous topography and recognition images of an endothelial cell surface obtained with VE-cadherin-Fc-functionalized AFM tips.

Acknowledgement
This work was supported by EC grants (Marie Curie RTN-CT-2006-035616; LSHG-CT-2005-512101; BioLightTouch contract No. 028781)

References
[1] G. Kada, F. Kienberger, P. Hinterdorfer. NanoToday 3 (2008) 12-19. Cover story.
[2] F. Kienberger, G. Kada, H. Muller, P. Hinterdorfer. J. Mol. Biol. 347 (2005) 597-606.
[3] F. Kienberger, A. Ebner, H. Gruber, P. Hinterdorfer. Acc. Chem. Res. 39 (2006) 29-36. Cover story.

O14

Modeling DNA chain dimensions in nanochannels

P. Cifra, Z. Benková, T. Bleha

Polymer Institute, Slovak Academy od Sciences, 842 36 Bratislava, Slovakia, e-mail: bleha@savba.sk

Recent developments [1,2] in micro- and nanofluidic devices fabricated by chip lithography provide a new impetus to study the confinement of principal biopolymers such as DNA. Micro- and nanofabrication is a powerful tool to build up channels of precise geometry and of characteristic dimensions on the order of tens or hundreds of nanometres. With the availability of sub-100 nm channels, it has become possible to study with detail the conformation and dynamics of DNA at the length scale of the DNA persistence length. Statistical properties of DNA and other biological polymers confined in the channels deviate from their values in bulk and depend on the strength and geometry of confinement.

We employed Monte Carlo simulations to explore properties of DNA and other semiflexible polymers in confined spaces [3,4]. Simulations were based on the coarse-grained worm-like chain model, where a dsDNA molecule is represented by a string of bead units connected by springs. The relative chain elongation R/L (where L is the contour length) and the persistence length P of DNA were computed as a function of the channel dimension D and chain bending rigidity. In a cylinder and a slit, three regions of DNA elongation were identified and rationalized by the blob and Odijk theories of confined polymers. In a tube an abrupt transition between the blob region (at moderate confinement) and the deflection (Odijk) region (at strong confinement) was found at $R/L \approx 0.8$ and $2D \sim P$. Overall, the simulation results for channel-induced DNA elongation R [3,4] are in harmony with measurements of confined DNA at high salt concentrations [1,2]. The potential occurrence of hairpins was elucidated as a trade-off between confinement and chain stiffness. The persistence length P represents a measure of the bending rigidity of semiflexible chains. Unfortunately, several methods how to determine the value of P are employed in practice. In computations of DNA chains we employed two basic definitions, the projection P_{proj} and the orientational correlation P_{or} functions. For bulk (unconfined) DNA molecules these definitions give practically an identical result $P_3 \approx 50$ nm, representing the intrinsic stiffness of DNA at high salt concentration. However, simulations revealed that the two above functions of P substantially differ in case of DNA in channels. The projection function P_{proj} turns into an apparent quantity at confinement, since, in addition to the intrinsic term P_3, it also involves the external orientational factor from the confining field. Thus, in narrow channels P_{proj} of DNA may reach the values up to about 400 nm. On the other hand, the simple exponential function, suitable for description of orientation correlations in free chains, was found to be applicable in channels only to short distances along the DNA chain contour. As a result, the associated persistence length P_{or} did not include the contribution of confinement and reproduces the intrinsic value of P_3.

Acknowledgement
This work was supported by the VEGA grants 2/6116/26 and 2/6014/26 and in part by the Centre of Excellence COMCHEM.

References

[1] W. W. Reisner, K. J. Morton, R. Riehn, Y. M. Wang, Z. Yu, M. Rosen, J. C. Sturm, S. Y. Chou, E. Frey and R. H. Austin, *Phys. Rev. Lett.* 2005, **94**, 196101.
[2] K. Jo, D. M. Dhingra, T.Odijk, J.de Pablo, M.D. Graham, R. Runnheim, D. Forrest and D.C. Schwarz, *PNAS*, 2007, **104**, 2673
[3] P. Cifra, Z. Benkova and T. Bleha, J. *Phys. Chem. B*, 2007, ***112***, 1367
[4] P. Cifra, Z. Benkova and T. Bleha, *Faraday Discussions* (2008)

O15

What is revealed about the evolution of the genetic code by similarities between tRNA genes?

J. Suchánek

Department of Informatics, University of Trenčín, Študentská 2, 91150 Trenčín, Slovakia,, e-mail: suchanek@tnuni.sk

The genetic code describes translational assignments between codons and amino acids. tRNAs and aminoacyl-tRNA synthetases (aaRSs) are those molecules by means of which these assignments are established. Any aaRS recognizes its tRNAs according to some of their nucleotides called identity elements. Mutation of *major identity elements* leads to the strongest functional effects, while *minor identity elements* have moderate effects and tune specificity. Let S_{IE} be a set of all identity elements of tRNAs, while S_{MMIE} be their most major identity elements so as they are specified in Fig. 2 in our Supplemental Materials (SM) to the chapter 3.1 of the 1st paper at http://web.t-com.sk/hisym. We will often refer to this web page. A pair of codons (N_iN_jG, N_iN_jA) or (N_iN_jC, N_iN_jU) can often be affected by one tRNA thanks to "wobbling" of the 3rd codon base during its interaction with this tRNA (Fig. 1 in SM to 3.3).

We used a program DNAPARS v. 3.67 (http://evolution.genetics.washington.edu/phylip.html) by Felsenstein *et al*., which computes phylogenies finding the minimum number of nucleotide substitutions necessary to obtain extant nucleic acid sequences from their common ancestor. We used it for various groups of related organisms to obtain an ancestor of *tRNA genes separately for each codon*.

Let a similarity between two sequences of *tRNA genes* be the number of sites that have the same nucleotide in the two sequences. Then a *1Mut-similarity* $\overline{\mathrm{Sim}}^{gr}_{1\mathrm{Mut},\,S_i}$ is defined as the average similarity between such *tRNA genes* of a group of related organisms '*gr*' whose codons differ by one point mutation (indicated by '1Mut'). The parameter S_i specifies those sites of *tRNA genes* that are included in computation. When the average similarity $\overline{\mathrm{Sim}}^{gr}_{\mathrm{all},\,S_i}$ is computed between all *tRNA genes*, not only between those whose codons differ by one point mutation, it is called a *plain similarity*.

Saks *et al*. [1] demonstrate by their experiment *in vivo* in *Escherichia coli* that a *tRNA gene* can be recruited from one isoaccepting group to another by a point mutation of its anticodon. They inactivated the original $\mathrm{tRNA}^{\mathrm{Thr}}_{\mathrm{UGU}}$ gene and transformed a $\mathrm{tRNA}^{\mathrm{Arg}}_{\mathrm{UCU}}$ gene by mutating its anticodon UCU to UGU. The recruited tRNA turned out to be fully functional in expression of Thr from a codon ACA, although less efficient.

We developed a genetic algorithm to search a global maximum of 1Mut-similarities $\overline{\mathrm{Sim}}^{species}_{1\mathrm{Mut},\,S_i}$ over a set of $32! \approx 2.63\times10^{35}$ such alternative genetic codes in which assignments of wobbling pairs of codons were preserved or changed simultaneously. This global maximum is reached at the standard code for *tRNA genes* of no *archaeal* or *bacterial* species, but it is done 27 times for 4 sets of identity elements of *eukaryotic* species. However, a global maximum of plain similarities $\overline{\mathrm{Sim}}^{species}_{\mathrm{all},\,S_i}$ is reached at the standard code only 5 times for the *eukaryotic* species (Table 1 in SM to 3.1). We performed analogous experiments with ancestors of *tRNA genes* of these species. A global maximum is reached at the standard code 17 times for $\overline{\mathrm{Sim}}^{species\ ancestors}_{1\mathrm{Mut},\,S_i}$, but only 5 times for $\overline{\mathrm{Sim}}^{species\ ancestors}_{\mathrm{all},\,S_i}$ (Table 1.2). This all approves that point mutations of anticodons were really tested by nature and that

tRNAs were adapting to minimize consequences of such recruitments from one isoaccepting group to another by a point mutation of their anticodon, *which then could not be exceptional events at all*. This confirms the adequacy of our definition of a 1Mut-similarity between *tRNA genes*.

We searched the order of tRNAs in which they were most probably assigned to their codons and amino acids. Because Ala and Val are amino acids with the highest means of their 1Mut-similarities with other amino acids, let us insert eight universal ancestors of *tRNA genes* assigned to eight present codons of Ala and Val into our chronology (1) as the set our algorithm starts from. Ala and Val also belong among the first four amino acids in a chronology of Trifonov [2] searching a consensus between 40 most important hypotheses about the evolution of the code. Then we obtain a chronology:

AVPIKRWMDCSTFHGXYLEQZN (1)

The beginning Ala, (Val), Pro, Ile, Lys, Arg, Trp, Met, Asp, Cys, (Ser) of this chronology lies under a plateau on a graph of $\overline{\mathrm{Sim}}^{univ.\,ancestors}_{1\mathrm{Mut},\,S_{\mathrm{IE}}}$ plotted over (1) for S_{IE} of *tRNA genes* (Fig. 4[b] in SM to 3.3). This plateau could not appear by chance because it has remained preserved along the whole line of evolution of the code. The plateau occurs in universal ancestors only for S_{IE}, while it occurs for both S_{MMIE} and S_{IE} in their domain ancestors (Fig. 5) and only for S_{MMIE} in their kingdom ancestors (Fig. 6). In this way, these plateaux have shifted from S_{IE} to S_{MMIE} during evolution. Therefore, they must represent some very profound and principal feature of organization of the code.

Our cascades of plateaux correlate with observations of Ribas de Pouplana and Schimmel [3]. There are two classes of aaRSs that have nothing in common except biochemistry of the reactions they catalyze. They bind opposite sides of a tRNA acceptor stem. The authors noticed that active-site domains of specific pairs of synthetases – one from each class – can be docked simultaneously onto the acceptor stem. Most striking is the way that PheRS and TyrRS are mutually accommodating. If their conclusions were correct, then aaRSs would be incorporated in the early reduced code approximately by octets of codons in each step of its transformation from a possible earlier form to a new organization utilizing tRNAs or their precursors. For example, this would mean that all codons coding Ile and Thr today should be simultaneously assigned to one of these two amino acids initially and a half of them would be reassigned to the other amino acid only additionally. The plateau over the beginning of (1) well correlates with the pairs of mutually accommodating aaRSs indicated by the authors.

All our computations were performed with our application tRNALab running under Windows, whose installation file is available at the same web pages as SM. What we wrote personally in it is about 54,000 lines of the code in our files *.cpp and *.h. It provides a rich interface (57 windows) with many intermediate results with commentaries as well as many additional functions. We are going to explain its main features at the lecture.

Acknowledgement
This study was supported by the Slovak Grant Agency VEGA 1/0253/03 and APVT-51-013802.

References

[1] M. E. Saks, J. R. Sampson, J. Abelson, *Science* 279 (1998) 1665-1670.
[2] E. N. Trifonov, *Gene* 261 (2000) 139-151.
[3] L. R. Ribas de Pouplana, P. Schimmel, *Trends Biochem. Sci.* 26 (2001) 591-598.

O16

Phylogenetic analysis of influenza A virus neuraminidase

I. Kinclová, G. Ruttkay-Nedecký, I.K. Haverlík

Department of Nuclear Physics and Biophysics, FMFI UK, Mlynská dolina F1, 842 48 Bratislava, Slovakia, e-mail: kinclova@fmph.uniba.sk

Influenza viruses evolve by means of two different mechanisms, which are gene reassortment (in the case of influenza A viruses it causes genetic shift) and genetic drift (gradual changes in antigenic places caused by mutations) [1].

Virulence of influenza A type is controlled by multiple genes, the most important is RNA segment 4 which codes for hemagglutinin (HA) and segment 6 coding for neuraminidase (NA), both being integral membrane proteins radiating outward from the lipid envelope of influenza virus. At present, sixteen subtypes of influenza A virus hemagglutinin are known which are denoted H1-H16 and nine subtypes of influenza A virus neuraminidase, N1-N9 [2].

The aim of this work was to find the percentage divergences between neuraminidases within individual neuraminidase subtypes.

Material and methods

The total number of 611 complete amino acid sequences of influenza A virus neuraminidase were compared, the sequences were obtained from the GenBank database [3]. For a particular virus subtype (various combinations of HA and NA subtypes, e.g. H1N1, H2N1, etc.), one neuraminidase isolate was always chosen for a particular year.

Clustal [4] was used to align the sequences, with gap opening 10.00, gap extension 0.20. Percentage divergence between two isolates was calculated on the basis of alignment.

Results and discussion

Table 1 shows the number of isolates belonging to specific subtypes that were compared to each other. It brings information about the chain lengths, and percentage divergences among the compared sequences belonging to specific subtypes. Average percentage divergences between isolates belonging to specific subtypes were at least 4.3% (N9 subtype) and maximum 11.5% (N1 subtype), which shows a high degree of homology among isolates belonging to a specific neuraminidase subtype.

Table 1. Comparison of percentage divergences between isolates within different neuraminidase subtypes, based on amino acid sequence comparison.

Subtype	Number of isolates used	Chain length (Number of amino acid residues)		Percentage divergences between isolates (%)	
		Min.	Max.	Max.	Average
N1	128	445	470	23.7	11.5
N2	171	440	469	19.4	10.5
N3	67	441	469	23.2	7.5
N4	17	469	470	35.3	7.2
N5	31	464	473	14.2	6.5
N6	52	446	471	13.0	7.3
N7	27	469	471	21.1	11.1
N8	67	454	470	21.3	9.1
N9	51	469	470	10.9	4.3

The present study showed that neuraminidase sequences are well conserved. Maximum values of percentage divergence between isolates within individual subtypes were between 10.9 to 35.3%.

Sequence analysis of neuraminidase showed that also the amino acid residues in the enzyme active site are well conserved, as published elsewhere [5].

Acknowledgement
This work was partially supported by the Slovak Grant Agency VEGA, project No. 1/3037/06.

References

[1] N.J. Cox, N.J., and K. Subbarao, *Annu. Rev. Med* 51 (2000) 407-421.
[2] R.A.M. Fouchier, V. Munster, A. Wallensten, T. M. Bestebroer, S. Herfst, D. Smith, G. F. Rimmelzwaan, B. Olsen, and A. D. M. E. Osterhaus, *J. Virol.* 79 (2005) 2814-2822.
[3] D.A. Benson, I. Karsch-Mizrachi, D.J. Lipman, J. Ostell, B. A. Rapp, and D. L. Wheeler, *Nucl. Acids Res.* 28 (2000) 15-18.
[4] J. D. Thompson, D. G. Higgins, and T. J. Gibson, *Nuc.l Acids Res.* 22 (1994) 4673-4680.
[5] I.K. Haverlik, G. Ruttkay-Nedecky, I. Kinclova, Phylogenetic analysis of influenza A virus – neuraminidase active site. *In this proceedings.*

O17

What is known (and what is not) about neuronal mechanisms controlling the cough reflex

I. Poliaček, J. Jakuš

Institute of Medical Biophysics, JLF UK, Malá Hora 4, 037 54 Martin, Slovakia,
e-mail: poliacek@jfmed.uniba.sk

Cough is the most important defensive reflex of the airways. It participates on a proper function of the respiratory system by an active removing of irritants and foreign particles from the airways [1]. Cough reflex is a complex and complicated behavior that interacts with the respiratory, cardiovascular, and other functions of organisms.

At the level of pre-motoneurons the motor pattern of cough is completely developed [2]. However, the role of medullary mechanisms in modification of this pattern is not fully understood. It was confirmed that the medullary respiratory neurons substantially participate on the production of the cough motor pattern [3,4]. E.g. expiratory neurons with incrementing firing pattern (E-aug) or expiratory units with decrementing firing (E-dec) are involved in production of cough expulsions [4-6]. It seems that rhythmic and temporal characteristics of the cough are produced by common respiratory / cough central pattern generator (CPG) [4,5]. This CPG is located in a rostral extension of the ventral respiratory group (VRG) within the medulla oblongata. Nevertheless, pathways transmitting the neuronal signal of the cough pattern from the CPG to the inspiratory and expiratory pre-motor outputs are unknown. E.g. direct connections of rostral VRG expiratory neurons (mostly E-aug units) that fire in correlated manner with abdominal expiratory muscles during cough [6] to the expiratory pre-motoneuronal area in caudal VRG (other population of E-aug neurons with axonal output toward the expiratory motoneurons in the spinal cord) are mostly inhibitory [7].

To date very little is known about additional spontaneously active and recruited neurons being involved in a process of coughing [4]. Particularly, their role and connectivity are still uncovered. We exposed some new areas beside the main medullary respiratory groups that are involved in production and modulation [8-11] of the cough. These areas include e.g. structures of the midbrain where cough-related activated neurones were found [11] in addition to a former view, that midbrain does not contain neuronal structures being necessary for reflex coughing [12].

The attenuation of the cough by e.g. central antitussives is realized almost exclusively by a reduction in cough number and expiratory amplitudes of the coughs. Temporal characteristics of the cough pattern are not significantly modified [13]. The mechanisms of action of central antitussives, the receptors involved in this processes [14], neuronal populations affected by these drugs, and regions where are antitussive sensitive neurons located retain obscure.

An interaction of several reflex and / or spontaneous behaviors including defensive airway reflexes is arranged in order to establish an optimal function of the organism [1,15]. Such functioning can be disrupted e.g. under pathological condition leading to unproper reflex functions (gastroesophageal reflux) [16]. On the other hand, some another reflexes as there are aspiration reflex and cough might provide stabilizing function for respiratory (at a hypoxic apnea), cardiac (rhythmicity), and other systems [17]. Also the function, cooperation, and hierarchy of central structures under the condition of multiple behaviors (e.g. simultaneous stimulations) such there is the cough – aspiration reflex co-interaction are still dimmed and mostly unknown.

In spite of a significant improvement of our knowledge about the generation and control of the cough and other reflex behaviors we are still far away from the proper

understanding of mollecular, cellular, and neuronal network properties guiding these behaviors.

Acknowledgement
This work was supported by Grant APVV No. 20-047705 „Cardio-pulmonary-cerebral resuscitation and autoresuscitation by gasps and coughing“ to professors Z. Tomori (Košice) and J. Jakuš (Martin)

References

[1] J. Korpáš, Z. Tomori, *Cough and other respiratory reflexes,* Karger S., Basel, 1979.
[2] R. Shannon, D.C. Bolser, B.G. Lindsey, *Neural control of coughing and sneezing*, in *Neural control of the respiratory muscles*, A.D. Miller, A.L. Bianchi, B.P. Bishop (Eds.), CRC press, Boca Raton, New York, London, Tokyo, 1996.
[3] J. Jakus, Z. Tomori, A. Stransky, *Physiol. Bohemoslov.* 34 (1985) 127-136.
[4] R. Shannon, D.M. Baekey, K.F. Morris, S.C. Nuding, L.S. Segers, B.G. Lindsey, *Pulm. Pharm. Ther.* 17 (2004) 369-376.
[5] R. Shannon, D.M. Baekey, K.F. Morris, Z. Li, B.G. Lindsey, *J. Physiol.* 525 (2000) 207-224.
[6] F. Bongianni. D. Mutolo, G.A. Fontana, T. Pantaleo. *Am. J. Physiol.* 274 (*Regulatory Integrative Comp. Physiol.* 43) (1998) R1015-R1024.
[7] C. Jiang, J. Lipski, *Exp. Brain Res.* 81 (1990) 639-648.
[8] J. Jakuš, A. Stránsky, I. Poliaček, H. Baráni, Ľ. Bošeľová, *Physiol. Res.* 47 (1998) 203-213.
[9] J. Jakuš, A. Stránsky, I. Poliaček, H. Baráni, Ľ. Bošeľová, *Physiol. Res.* 49 (2000) 387-398.
[10] I. Poliaček, J. Jakuš, A. Stránsky, H. Baráni, E. Halašová, Z. Tomori, *Physiol. Res.* 53 (2004) 155-163.
[11] J. Jakuš, I. Poliaček, E. Halašová, P. Muríň, J. Knociková, Z. Tomori, D.C. Bolser, *Respir. Physiol. Neurobiol.* 160 (2008) 289-300.
[12] D.C. Bolser, *J. Appl. Physiol.* 71 (1991) 2325-2331.
[13] D.C. Bolser, J.A. Hey, R.W. Chapman. *J. Appl. Physiol.* 86 (1999) 1017–1024.
[14] I. Poliaček, L.W. Corrie, C. Wang, M.J. Rose, D.C. Bolser, *J. Appl. Physioll* 102 (2007) 1014-1021.
[15] D.C. Bolser, I. Poliacek, J. Jakus, D.D. Fuller, P.W. Davenport, *Respir. Physiol. Neurobiol.* 152 (2006) 255-265.
[16] A.J. Ing, *Pulm. Pharmacol. Ther.* 17 (2004) 403–413.
[17] Z. Tomori, R. Beňačka, V. Donič, J. Jakuš, *Monaldi Arch. Chest. Dis.* 55 (2000) 398-403.

O18

Review of medical imaging methods

P. Jasem[1], P. Jasem,Jr.[2] Ľ. Horovčák[1]

[1] Department of Medical Biophysics, LF UPJŠ, Tr. SNP1, 040 66 Košice, Slovakia, e-mail: Pavol.Jasem@upjs.sk

[2] Department of Cybernetics and Artificial Intelligence, TU, Němcovej 3, 042 00 Košice, Slovakia

There are some basic methods of imaging the body, using x rays, gamma rays, sound waves, or electromagnetic waves. Each method has its own place; the techniques are complementary, not mutually exclusive. The history of medical imaging methods and its use in medicine, started around 1900 concentrate on using x rays, ionising radiation.

What is ionising radiation? Ionising radiation is part of the electromagnetic spectrum and is used in imaging techniques in the form of either x rays—for conventional radiography, angiography, mammography, fluoroscopy and computed tomography - CT or gamma rays for imaging in nuclear medicine, PET- and SPECT- methods.

Whereas imaging with ionising radiation uses x-rays or gamma rays, non-ionising radiation uses either sound waves, in the case of ultrasound, magnetisation of protons in magnetic resonance imaging (MRI), or near-infrared light in optical tomography.

Apart from the standard two dimensional ultrasound, other forms of ultrasound exist, such as classical- mode, Doppler, colour Doppler and three- or four- dimensional ultrasound.

MRI uses a strong magnetic field to align all the hydrogen protons in the tissue. The alignment is then disrupted by a specific radio frequency energy called the Larmor frequency as the protons recover their alignment, they emit radio signals and these can be measured and converted by a computer using Fourier transforms to produce an image. Each tissue produces different radio signals which the computer recognises and thus the image is made up of shades of grey or colour.

P1

Influence of sterols on the egg yolk phosphatidylcholine bilayer: a small-angle synchrotron X-ray diffraction study.

J. Gallová[1], M. Svorková[1], D. Uhríková[1], S.S. Funari[2], P. Balgavý[1]

[1] Comenius University in Bratislava, Faculty of Pharmacy, 832 32 Bratislava, Slovakia, e-mail: gallova@fpharm.uniba.sk

[2] HASYLAB at DESY, Notkestrasse 85, Hamburg, Germany

Sterols are ubiquitous components of biological membranes. Mammalian cells contain one major sterol – cholesterol. It is known that cholesterol ensures proper fluidity, passive permeability and mechanical strength of membrane, it plays an important role as a signalling molecule and as a modulator of lateral organization of membrane. In higher plants, sterols are present as complex mixtures. β-sitosterol is one of the predominat plant sterols. It differs stucturally from cholesterol by the presence of an additional ethyl group at C-24 in the side chain. β-sitosterol, together with other plant sterols, effectively reduces the absorption of dietary cholesterol and thus protects from cardiovascular diseases. Furthermore, β-sitosterol was shown to have anti-carcinogenic, anti-inflammatory, anti-microbial, anti-bacterial and anti-fungal effects [1].

The aim of this work is to compare the effect of cholesterol and β-sitosterol on the structural properties of model membranes. Multilamellar liposomes of egg yolk phosphatidylcholine (EYPC) were chosen as an appropriate model of lipid part of biological membranes. Effect of increasing concentration of both sterols up to molar ratio sterol:EYPC=1 on the repeat period was studied using small-angle synchrotron X-ray diffraction.

Weighted amounts of EYPC, cholesterol and β-sitosterol were dissolved in chloroform. An appropriate volume of EYPC solution was mixed with the sterol solution and the solvent was evaporated to dryness. After adding water, the dispersions were homogenized by hand shaking, brief sonication and vortexing.

Small- (SAXD) and wide-angle (WAXD) synchrotron radiation diffraction experiments were performed at the soft-condensed matter beam line A2 at HASYLAB at the Deutsches Elektronen Synchrotron (DESY) in Hamburg (Germany), using a monochromatic radiation of wavelength λ=0.15 nm. The evacuated double-focusing camera was equipped with two linear delay line readout detectors. The SAXD detector was calibrated using rattail tendon and the WAXD detector by tripalmitin. Difractograms were measured at 25°C.

From the SAX region, the positions of the first- and second-order reflections were directly determined by fitting the peaks by Lorentzian function above a linear background. The positions of the first- and second-order reflections are typical for lamellar structure where lipid bilayers with the thickness d_l are separated by water layers with the thickness d_W. The repeat period $d=d_l+d_W$ was determined as a reciprocal value of the position of the first-order reflection. The dependence of the repeat period d on the molar ratio sterol:EYPC is shown on the Fig. 1. It is evident that the repeat period of EYPC in the presence of sterol was higher than in pure EYPC in the whole concentration range. For molar ratio sterol:EYPC>0.1, β-sitosterol was more effective in increasing d than cholesterol. Repeat period d increases approximately linearly up to molar ratio 0.4 with higher slope for β-sitosterol compared to cholesterol. A plateau was observed at SIT:EYPC=0.4-0.9 molar ratio. At the same range, a small decrease of repeat period is seen in the presence of cholesterol.

WAXD patterns exhibited one wide diffuse scattering peak characteristic of liquid-like carbon chains of phospholipid in the whole studied concentration range of cholesterol +EYPC and of β-sitosterol+EYPC up to molar ratios 0-0.5.

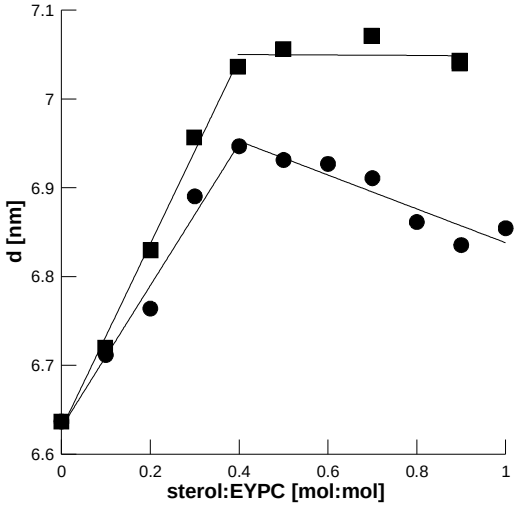

Fig. 1: Dependence of the repeat period on the molar ratio sterol:EYPC.
Circles – cholesterol, squares - β-sitosterol.

Difractograms showed anomalous behavior in the presence of β-sitosterol at molar ratio higher than 0.5. In SAX region, a new peak appeared in the vicinity of the second-order lamellar phase peak. Changes are evident also in the WAX region where a reflection spacing at about 0.59 nm was observed.

The increase of repeat period of EYPC in the presence of cholesterol is probably connected with the increase of the bilayer thichness. It is caused by decreased number of *gauche* conformers in acyl chains of EYPC and the increase of ordering [2]. The increased thickness of lipid bilayer in the presence cholesterol was observed using diacyl monounsaturated phosphatidylcholines [3]. But the abrupt change in the repeat period at molar ratio sterol:EYPC=0.4 is not explained and needs further study.

In conclusion, the effect of cholesterol and β-sitosterol on the structure of EYPC bilayer is qualitatively similar but marked quantitative differences were observed that might be physiologically relevant.

Acknowledgement
This study was supported by VEGA 1/0295/08, APVV 51-013802, JINR 07-4-1031-99/2008 and European Community – Research Infrastructure Action under the FP6 "Structuring the European Research Area" Programme Contract RII3-CT-2004-506008 (HASYLAB projects II-20052037 EC and II-20052018 EC)

References
[1] Z. Ovesná, A. Vachálková, K. Horváthová, *Neoplasma* 51 (2004) 407-414.
[2] M. Svorková, A. Annus, J. Gallová, *Acta Facult. Pharm. Univ. Comeniane* 53 (2006) 238-244.
[3] N. Kučerka, J. Pencer, Nieh M.P., Katsaras J., *Eur. Phys J. E* 23 (2007) 247-254

P2

SANS study on extruded unilamellar DOPC+DOPS liposomes containing long-chain aliphatic 1-alcohols

M. Kotalová[1,2], D. Uhríková[2], J. Teixeira[3], P. Balgavý[2]

[1] Department of Nuclear Physics and Biophysics, FMFI UK, Mlynská dolina F1, 842 48 Bratislava, Slovakia, e-mail: kotalova@fmph.uniba.sk

[2] Department of Physical Chemistry of Drugs, FaF UK, Odbojárov 10, 832 32 Bratislava, Slovakia

[3] Laboratoire Léon Brillouin, CEA-Saclay, 911 91 Gif sur Yvette Cedex, France

According to Meyer-Overton rule [1,2], the anesthetic (or another biological) potency should increase with the partition coefficient between lipoidal medium and water. The breakdown of this rule was first observed for aliphatic 1-alcohols [3]. The general anesthetic potency of 1-alcohols (CnOH, n is the number of carbons in alkyl chain) increases up to C11OH and than decreases, compounds with n > 13 are non-anesthetic. This cut-off effect is not caused by anomalies in the partition equilibria – the molar partition coefficent increases exponentially in whole region. Similar cut-off type dependences have been observed also in other CnOH biological effects. Within the context of lipid mediated mechanism of general anethesia, the solubilization of an anesthetic molecule in the membrane bilayer influences such property of the bilayer that alters protein conformational equilibria, and this depends on the identity of the solute. However, which property of the membrane bilayer is altered upon incorporation of anesthetic 1-alkanols is still not known. Cantor [4] has suggested that anesthetic molecules cause a redistribution of lateral pressures in the membrane bilayer, which in turn shifts the conformational equilibria of membrane proteins such as ligand-gated ion channels, which are associated with anesthesia. Using ^{2}H-NMR spectroscopy, it was found that C8OH orders the acyl chains of dimyristoylphosphatidylcholine (DMPC), unlike C12OH and C14OH, which have little effects [5]. Vibrating tube densitometric study has demonstrated that the volume change of transferring of CnOH from its pure state into the DMPC bilayers was positive for small (C4OH - C6OH) 1-alkanols while it was negative for larger (C7OH - C12OH) 1-alkanols [6]. All these results suggest that the packing of CnOH and lipid molecules in bilayers depends on the CnOH alkyl length and bilayer depth.

In the present communication, we report our preliminary results of SANS study of the effect of CnOHs on fluid lipid bilayers in unilamellar vesicles, prepared by extrusion through 50 nm pores in carbohydrate filters from mixtures of CnOH, dioleoylphosphatidylcholine (DOPC) and dioleoylphosphatidylserine (DOPS), dispersed in heavy water. The small amount (4%) of DOPS present in bilayers charged the bilayer surface negatively and thus prevented oligolamellar vesicle formation during extrusion and vesicle aggregation after extrusion. The SANS measurements were performed at the small-angle neutron scattering diffractometer PAXE at the extremity of the guide G5 (cold source) at LLB Saclay. The diffractometer was equipped with the xy position sensitive detector.

The experimental data were evaluated using the small-angle form of the Kratky–Porod approximation based on homogenous neutron scattering density distribution in the bilayer. From the SANS spectra in the Guinier region ($0.001\text{Å}^{-2} \le Q^2 \le 0.006\text{Å}^{-2}$), the bilayer gyration radius R_g was obtained by fitting the SANS intensity using function $I(Q) \sim I(0)\exp(-Q^2R_g^2)Q^{-2}$, where Q is the scattering vector value, and the thickness parameter $d_g = 12^{0.5}R_g$ which is the scattering length density weighted bilayer thickness. The bilayer thickness d_g was studied as a function of temperature in the 25 - 55ºC region. From these data, the coefficient of thermal expansibility $\beta = \partial \ln d_g(T)/\partial T$ was obtained.

Bilayer thickness parameter as a function of alcohol alkyl chain length, at 0.4 :1 alcohol : lipid molar ratio, at different temperatures is shown in Fig.1 (left panel). For each temperature a linear increase of bilayer thickness with increasing alcohol chain length was observed. The average increase presented ~ 1.5Å. With increasing alcohol : lipid molar ratio

further increase of bilayer thickness parameter was observed, with a maximum of ~ 41.9Å for C16OH at 1 : 1 molar ratio. At the same time, for a given 1-alcohol, we observed a temperature induced decrease of bilayer thickness, with a minimum of ~ 40.7Å for C8OH at 51°C. The decrease was more significant for longer of studied 1-alcohols. This decrease may be due to the increased *trans*-gauche isomerization and lateral bilayer expansion in the fluid phase. The coefficient of thermal expansibility as a function of alcohol alkyl chain length is shown in Fig.1 (right panel). With increasing alcohol chain length a linear increase of coefficient β was observed. This observation is in contrast with theoretical assumption, according to which longer 1-alcohols induce higher phospholipid chain packing and thus stabilize the bilayer.

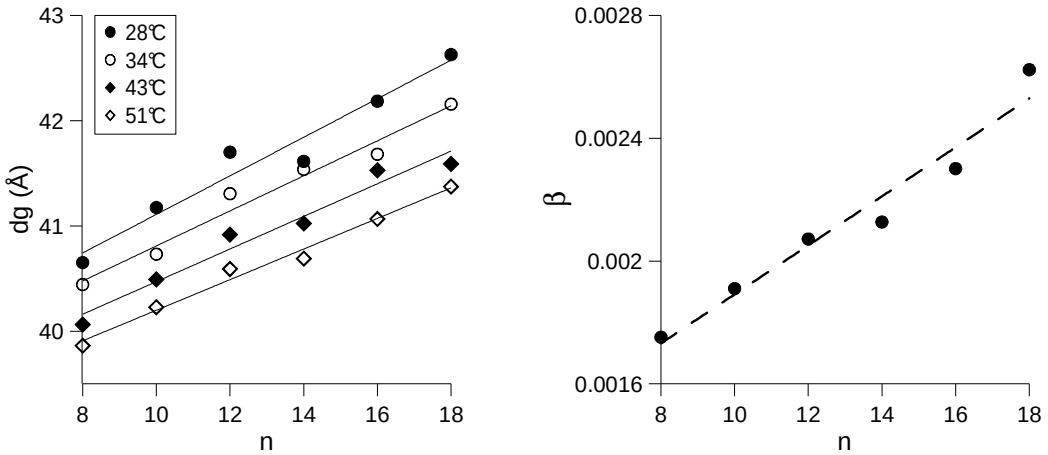

Fig.1 Bilayer thickness parameter (left panel) and coefficient of thermal expansibility (right panel) as a function of alcohol alkyl chain length at 0.4 : 1 alcohol : lipid molar ratio

Acknowledgement
This work was supported by the VEGA 1/0295/08 and APVV 51-027404 grants and by the JINR project 07-4-1031-99/2008. The SANS experiments were supported by the European Commission through the Access Activities of the Integrated Infrastructure Initiative for Neutron Scattering and Muon Spectroscopy (NMI3), supported by the European Commission under the 6th Framework Programme through the Key Action: Strengthening the European Research Area, Research Infrastructures, Contract no: RII3-CT-2003-505925.

References
[1] H.H. Meyer, *Arch. Exp. Pathol. Pharmakol.*, 42 (1899) 109-118.
[2] C.E. Overton, *Studien über die Narkose zugleich ein Beitrag zur allgemeinen Pharmakologie.* Verlag von Gustav Fischer, Jena, 1901.
[3] K.H. Meyer, H. Hemmi, *Biochem. Z*, 277 (1935) 39-72.
[4] R.S. Cantor, *Biophys. J.*, 80 (2001) 2284-2297.
[5] P.W. Westerman, J.M. Pope, N. Phonphok, J.W. Doane, D.W. Dubro, *Biochim. Biophys. Acta*, 939 (1988) 64-78.
[6] T.H. Aagaard, M.N. Kristensen, P. Westh, *Biophys. Chem.*, 119 (2006) 61-68.

P3

Voltage-dependent channels in native and NGF-differentiated rat PC12 cells

A. Caro, M. Zana, Ľ. Lacinová

Institute of Molecular Physiology and Genetics, Slovak Academy of Sciences, 5, Vlarska St., 833 34 Bratislava, Slovakia, e-mail: anton.caro@hotmail.com

The aim of the current study was to characterize the voltage dependent channels expressed in native and differentiated (treated with neuronal growth factor) cells. PC12 cell line was derived from a pheochromocytoma of the rat adrenal medulla. PC12 cells stop dividing and undergo terminal differentiation when treated with nerve growth factor, making the line a useful model system for neuronal differentiation [1].

In the following experiment the cells were divided into two groups depending on their condition – Group A comprised of non-treated PC12 cells and Group B comprised of cells treated with neuronal growth factor (NGF). NGF was identified for its trophic role for different populations of neurons in the peripherial nervous system. [2]

Both groups were cultured in (DMEM 500 ml, 20% Foetal Bovine Serum, 1% Penicillin Streptomycin, 1% L-Glutamine) with 200 ng/ml NGF added for group B. The whole cell patch clamp technique was used. Two types of solutions were used; one favoring measurement of voltage dependent K^+ and Na^+ channels (I) and one favoring measurement of voltage dependent Ca^{2+} channels (II). The composition of both solutions was as follows (mM): Pipette solution I - KCl 130, EGTA 10, Mg-ATP 3, Na_2-ATP 0.4, HEPES 10, pH 7.2 (KOH). Pipette solution II (mM) – CsCl 130, Na_2-ATP 5, TEA-Cl 10, HEPES 10, EGTA 10, $MgCl_2$ 5, pH 7.4 (CsOH). The external (bath) solution I contained (mM): NaCl 110, KCl 3, HEPES 10, CaCl2 10, $MgCl_2$ 1, Glucose 5, pH 7.4 (NaOH). The solution II contained (mM): NMDG 115, CsCl 5, $MgCl_2$ 1, HEPES 10, $BaCl_2$ 20, Glucose 5 (10), pH 7.3 (CsOH).

Whole cell currents were measured using EPC 10 patch clamp amplifier (HEKA Electronic). A standard patch clamp set-up was used. Experiment was controlled by HEKA™ PatchMaster software. The patch pipettes were pulled from borosilicate glass. Cell capacitance varied between 6 and 16 pF in non differentiated and from 20 to 60 pF in differentiated PC 12 cells. The results were analyzed with FitMaster and Origin 8.5.

Current-voltage (IV) relation for potassium current was measured by a series of 500 ms long depolarizing pulses from a holding potential (HP) of –60 mV to voltages between –20 mV and +80 mV. IV relation for sodium current was measured by a series of 5 ms long depolarizing pulses from a HP of –100 mV to membrane voltages between –90 mV and +60 mV. IV relation for calcium current was measured by a series of 50 ms long pulses applied from a HP of –80 mV to voltages between –70 mV and +70 mV.

In non-differentiated cells two types of outward potassium current were detected – delayed rectifier (I_{KD}) and transient outward current (I_{KA}) (Fig. 1). In minor part of the cells barium-carried current through the calcium channels was observed (Fig.1 and Table 1). Na^+ current was not detected neither in Group A, nor in Group B.

After differentiation the absolute values of the registered ionic currents increased, but as the cells increased also in size, this lead to decrease in current density. Furthermore, proportion of cells expressing I_{KA} slightly increased and proportion of the cells expressing functional calcium channels more than doubled.

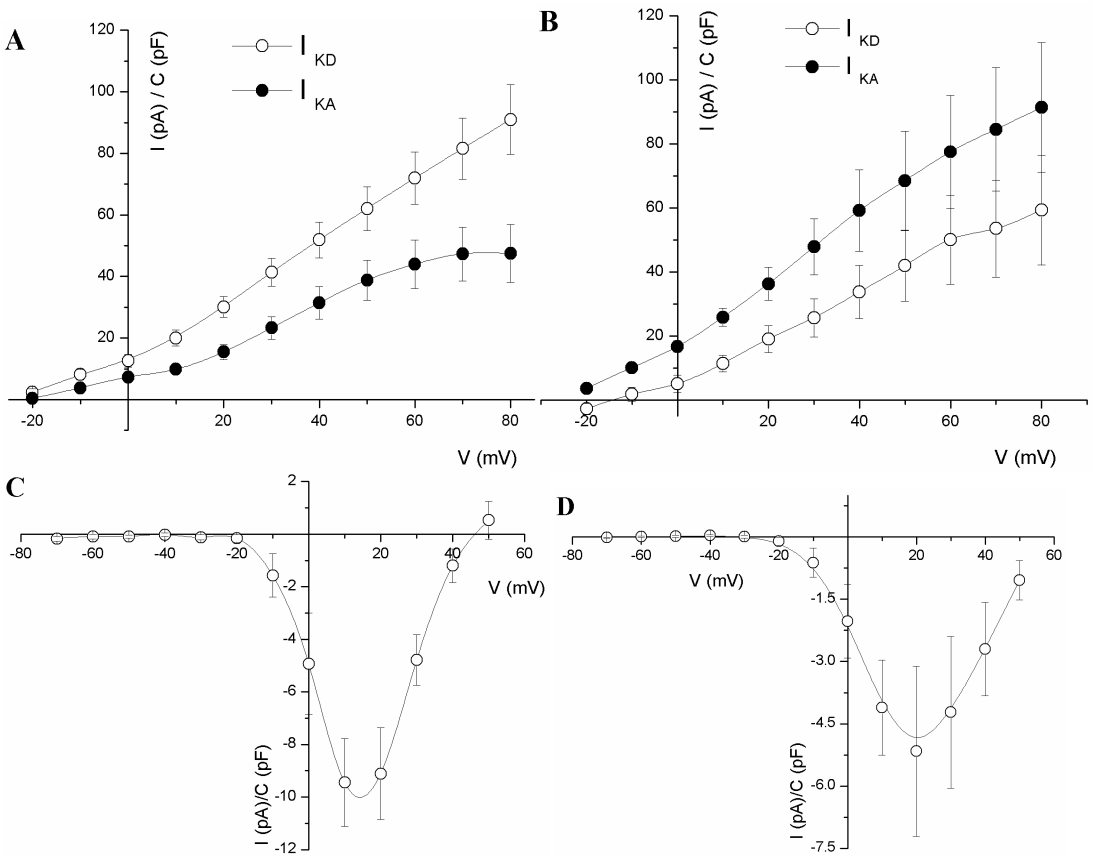

Figure 1. A – averaged I_{KA} and I_{KD} IV relation measured from non-differentiated cells; B – averaged I_{KA} and I_{KD} IV relation measured from differentiated cells; C – averaged I_{Ba} IV relation measured from non-differentiated cells ; D – averaged I_{Ba} IV relation measured from differentiated cells.

Table 1. Average current density amplitude measured at the peak of the IV-relation (I_{Ba}) or at membrane depolarization to +70 mV (I_{KD}, I_{KA}). n – number of tested cells; m – number of cells with detected current.

Group	I_{KD} (m/n)	I_{KA} (m/n)	I_{Ba} (m/n)	I_{Na} (m/n)
A	90±12 (24/24)	47±9 (9/24)	-5±2 (6/26)	(0/24)
B	84±19 (7/7)	42±11 (3/7)	-9±2 (8/15)	(0/7)

The results obtained with native and NGF-treated cells confirm that our PC 12 cells function in the same way as it has been described by others. It was demonstrated that NFG treatment did not result in increase in the expression of Na^+ channels, but favored the expression of Ca^{2+} channels and K^+ outward channels.

PC12 line is a useful neurobiological model system for neurobiological and neurochemical studies and will be used for analysis of effects of silencing genes for calcium channels on cell physiology.

Acknowledgement
This work was supported by the Marie Curie Research Training Network Ca_vNet MRTN-CT-2006-035367.

References
[1] K. Fujita, P. Lazarovici, G. Guroff, *Environ Health Perspect*, 80 (1989) 127-142.
[2] R. Goetz, *J. Neural Transm. Suppl*. 60 (2000 247-259.

P4

Monitoring possibilities of the mitochondrial membrane potential by a thiadicarbocyanine tribromide fluorescent probe

M.Zvarík, L. Šikurová

Department of Nuclear Physics and Biophysics, FMFI UK, Mlynská dolina F1, 842 48 Bratislava, Slovakia, e-mail: zvarikmilan@gmail.com

Introduction

Membrane potential is one of the most substantial physiological parameters of living cells and their organelles. Mitochondrial membrane potential arising from ionic gradients plays the major role in cell bioenergetics. It is appropriate to exploit fluorescent probes for measurements of the membrane potential in organelles, such as mitochondria, and in the cells that are too small for microelectrodes. Carbocyanine dyes belong to the first and widely used potentiometric fluorescent probes [1]. Thiadicarbocyanine tribromide (TCBr) is a fluorescent probe from the group of carbocyanines, which was used only a short time ago [2, 3], and even without an appropriate explanation of its spectral changes. That is why we will examine, in the submitted work, the changes of the fluorescent characteristics of TCBr at its supposed interaction with mitochondria and we compare them with the ions triggered changes.

Materials and methods

Mitochondria were isolated from hearts of adult male Wistar rats by differential centrifugation (Hettich Zentrifugen Universal 320 R) while the inner membrane was functionally fully preserved [4]. The isolation procedure was performed at 4 ºC and the isolated mitochondria were diluted to the final concentration of 1.25 mg/ml in a buffer solution. The mitochondria were stained with a fluorescent probe N,N'-di(3trimethylammoniumpropyl) thiadicarbocyanine tribromide (TCBr), purchased from Molecular Probes and used at the final concentration of $5x10^{-6}$ mol/l. The fluorescence spectra were obtained using a LS45 (PerkinElmer) luminescence spectrometer. All the sample preparations and measurements were carried out at 22±2ºC and protected from light.

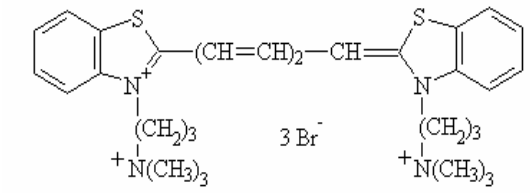

Thiadicarbocyanine tribromide (TCBr)

Results and discussion

The fluorescence emission spectrum of water solution at excitation of 520 nm provides two fluorescent maxima at 570 nm and at 667 nm (Fig 1a). By addition of KCl into the water solution of TCBr, decrease of fluorescence intensity at 667 nm will occur without any significant change of fluorescence intensity at 570 nm. Dependence of fluorescence intensity at 667 nm on KCl concentration indicates a non-linear decrease of the intensity with increase of KCl concentration (Fig. 2). The decrease is probably caused by creation of non-fluorescent species, maybe aggregates [5].

Presence of mitochondria in water solution induces only decrease of the fluorescence intensity at 667 nm, while position of the peaks is simultaneously preserved (Fig 1c).

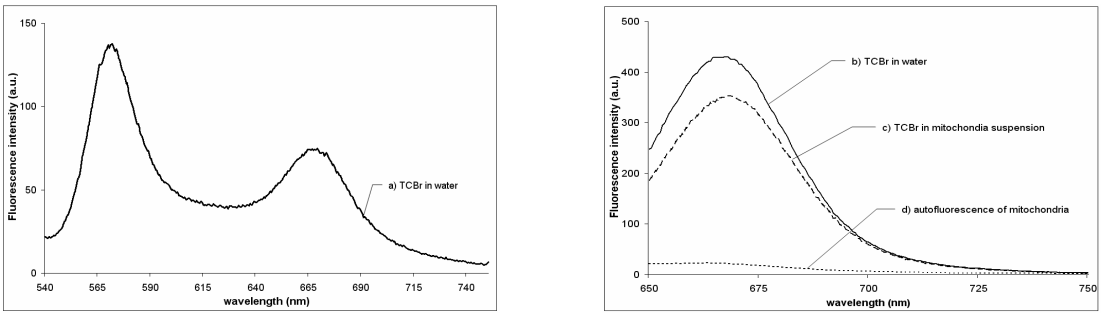

Fig. 1 Fluorescence spectrum of: a) TCBr in water (excitation 520 nm), b) TCBr in water (excitation 630nm) c) TCBr in mitochondria suspension, d) mitochondria.

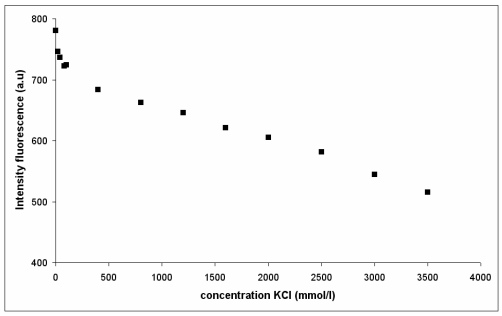

Fig. 2 Relationship between 667 nm-fluorescence intensity of TCBr (5 µmol/l) and concentration of KCl.

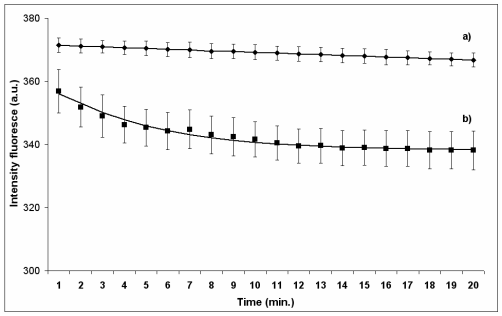

Fig. 3 Time dependence of 667 nm-fluorescence intensity of TCBr a) without presence of mitochondria, b) in presence of mitochondria. The data are expressed as the means ±SD of 6 independent experiments.

Interaction of the TCBr probe with mitochondria was recorded during the period of 20 minutes. Fluorescence intensity decreases with time and it reaches the plateau after 12 minutes (Fig. 3b). Fluorescence of TCBr water solution does not change within the measurement error during the time of 20 min (Fig. 3a).

The presented results could be interpreted as accumulation of the cationic carbocyanine dye TCBr in intact mitochondria with preserved membrane potential [5].

Acknowledgement

This work was supported by the Slovak Grant Agency VEGA, project No. 1/3037/06.

References

[1] P.J. Sims, A.S. Waggoner, C.H.Wang, J.F. Hoffman. *Biochemistry 13* (1974) 3315-3330

[2] Ch. Zhao, T. Nguzen, L. Ming Boo, T. Hong, C. Espiritu, D. Orlov, W. Wang, A. Waring, I.R. Lehrer, *Antimicrob. Agents Chemother* 45 (2001) 2695-2702

[3] M. Ferko, D. Habodászová, I. Waczulíková, J. Mujkošová, J. Kucharská, L. Šikurová, A. Ziegelhöffer, in *Potential Therapeutic Targets in Cardiovascular and Other Diseases*, N. Tribulová. Ľ. Okruhlicová.. (Eds.) Bratislava: Veda, 2006.

[4] A.L. Lehninge, E. Carafoli, C.S. Rossi, *Adv. Enzymol. Relat. Areas Mol. Biol.* 29 (1967) 259-320

[5] J. Plasek, A. Vojtıskova, J. Houstek, *J Photochem Photobiol – Biol* 78 (2005) 99=108

P5

Effects of changes of ryanodine receptor gating on the susceptibility to arrhythmias in heart myocytes: a modeling study

E. Cocherová, J. Parulek, A. Zahradníková

Institute of Molecular Physiology and Genetics, Slovak Academy of Sciences, Vlárska 5, 833 34, Bratislava, Slovakia, e-mail: elena.cocherova@savba.sk

Changes in ryanodine receptor (RyR) gating were suggested to be responsible for several types of arrhythmias. It has been suggested that increased RyR calcium sensitivity and/or enhanced RyR activity at diastolic calcium levels leads to an increase in cytosolic calcium at the diastole and to activation of the sodium/calcium exchanger, thus initiating cell depolarization and generation of delayed afterdepolarizations and/or spontaneous action potentials [1]. These events occur only upon adrenergic stimulation.

Here we have investigated the effect of changed basal activity and changed luminal regulation of the ryanodine receptor (RyR) on the propensity of the cardiac myocyte to arrhythmias. A model of rabbit ventricular myocyte action potential (AP), based on the Shannon-Bers AP model [2,3], was developed and the influence of changed RyR channel properties on initiation of heart arrhythmias was investigated.

The simulation was run for 300 s at a predefined stimulation frequency to obtain steady-state values of variables characterizing ion currents, membrane potential, and calcium concentration in individual cell compartments. External stimulation was then excluded and spontaneous behavior of the cell was observed. Under physiological conditions of a healthy cell, no delayed afterdepolarizations leading to triggered action potentials were observed.

Upon adrenergic stimulation, the sensitivity of RyR to calcium increases. At the same time, calcium concentration in the lumen of the sarcoplasmic reticulum is elevated, thus leading to increased activation of RyRs. Under these conditions we were able to observe triggered APs for certain values of RyR gating parameters. At a stimulation frequency of 2 Hz, triggered APs appeared in a certain interval of the K_{oCa} parameter, which controls the regulation of the cytosolic calcium sensitivity of the RyR by luminal calcium (see Fig. 1). Increasing the basal activity of the RyR by changing the parameter K_{leak} led to an increase in the frequency of spontaneous APs (see Fig. 2). Decreasing the stimulation frequency led to a strong decrease of the frequency of the spontaneous APs at all RyR gating parameter values; the spontaneous APs had also a much lower tendency to persist after stopping the stimulation. Specifically, increase of the basal RyR activity without concomitant changes of RyR calcium sensitivity was not sufficient to

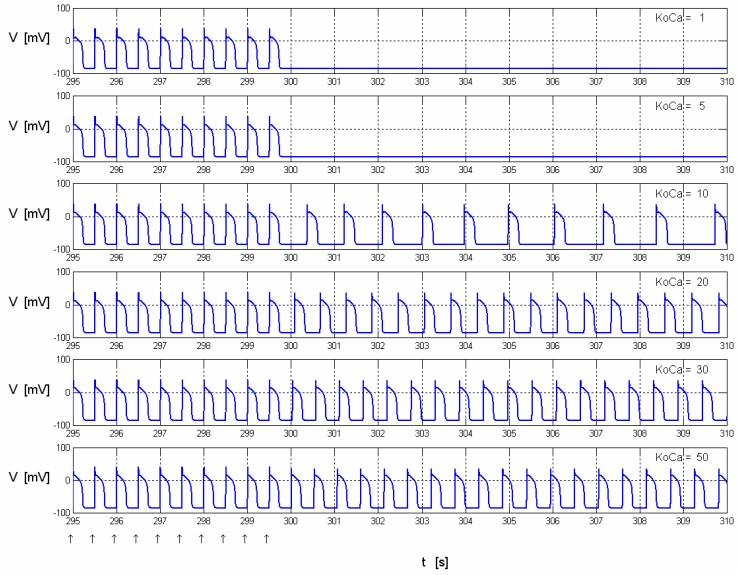

Fig. 1 The effect of varying the K_{oCa} parameter on the generation of spontaneous APs (times of stimulation assigned by arrows).

generate spontaneous APs.

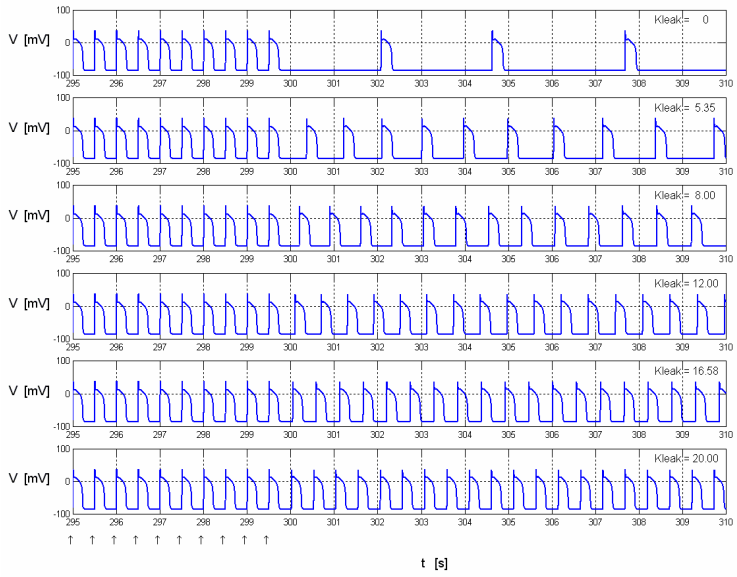

Fig. 2 The effect of varying the K_{leak} parameter on the generation of spontaneous APs (times of stimulation assigned by arrows).

In conclusion, we have demonstrated that changes in RyR gating (without changes in other properties of the myocyte) may lead to generation of spontaneous action potentials. The model predicts that decreasing the frequency of APs (i.e., lowering the heart rate) may be a useful strategy to prevent RyR-generated arrhythmias.

Acknowledgement
This work was supported by the EU Contract No. LSHM-CT-2005-018802/CONTICA

References
[1] L. A. Venetucci, et al, *Ann. N. Y. Acad. Sci.* 1099 (2007) 315-325.
[2] T. R. Shannon, et al, *Biophys. J.* 87 (2004) 3351-3371.
[3] T. R. Shannon, F. Wang, D. M. Bers, *Biophys. J.* 89 (2005) 4096-4110.

P6

Calcium channels and calcium signaling in cardiac excitation-contraction coupling

I. Zahradník, A. Zahradníková, jr., Z. Kubalová, E. Poláková, J. Pavelková, A. Zahradníková

Institute of Molecular Physiology and Genetics SAS, Vlárska 5, 833 34 Bratislava, Slovakia.
e-mail: ivan.zahradnik@savba.sk

The principal role of calcium channels and calcium ions in triggering calcium release and contraction of cardiac myocytes is well recognized. However, the mechanism by which calcium signaling controls the intensity of calcium release is not well understood due to stochastic nature of ion channel gating. This involves voltage-dependent activation of dihydropyridine receptor (DHPR) calcium channels, calcium-dependent activation of ryanodine receptor (RyR) calcium channels and calcium-dependent inactivation of DHPR calcium channels. To disclose relations among these processes, calcium release activation by I_{Ca} was investigated at the level of local release sites units (dyads) in rat ventricular myocytes using patch-clamp, confocal microscopy and mathematical modeling. Calcium spikes, the fluorescent signals proportional to intensity of local calcium release, were activated by temporally synchronized calcium current triggers. Synchronization of calcium current triggers was achieved by generating instantaneous "tail" I_{Ca}, switched on by stepping the membrane potential from the calcium reversal potential (V_{Ca}) to negative potential. The synchronized trigger was modulated by duration of the prepulse to V_{Ca} that modulated the number of recruited DHPRs, and by the tail potential that modulated single DHPR channel current amplitude and deactivation kinetics, and by the DHPR agonist BayK8644 that prolongs the mean DHPR channel open time. Effects of synchronized triggers on calcium release were measured using the calcium dependent inactivation of calcium current and the calcium spikes as local sensors of calcium release. Experimental records were approximated by mathematical models of calcium current kinetics and of calcium spike kinetics that allowed to estimated parameters related to calcium signaling within dyads, the tubulo-reticular junctions. The coupling fidelity between DHPR and RyR channels mediated by Ca^{2+} ions was determined using the temporal distribution of calcium spike latencies and a model based on exponential distribution of DHPR channel open times. The analysis provided the first *in situ* estimate of DHPR mean open time of ~0.5 ms and estimate of about 8 active DHPR channels per dyad. The DHPR-RyR coupling fidelity was found low in agreement with prevalence of very short DHPR openings, inherent to stochastic gating, that did not provide enough calcium to activate RyR channels. However, despite low DHPR-RyR coupling fidelity, the probability of calcium release activation was high, due to activation of many DHPRs at individual release sites. Moreover, the difference between efficiency of the first and subsequent DHPR openings, and between parallel and sequential DHPR openings, was revealed and characterized.

It can be concluded that metabolic control of DHPR calcium channels is tuned to control the calcium release intensity by physiological stimuli that control function of DHPR channels. These include modulation of single DHPR channels, like number and duration of their openings, and transfer the stochastic molecular behavior to reliable cardiac function by avoiding the danger of inadvertent triggering of calcium release.

Acknowledgement
This work was supported by the Slovak Grant Agency VEGA, project No. 2/0102/08 and by Agency for Promotion Research and Development under the contract No. LPP-0099-06.

P7

Inhibition of the $Ca_v3.1$ T-type calcium channel by silver ions

Zs. Kohuš[1], Ľ. Lacinová[2]

1 Comenius University in Bratislava, Faculty of Natural Sciences, Department of Animal Physiology and Ethology, e-mail: zsolt.kohus@gmail.com
2 Institute of Molecular Physiology and Genetics, Slovak Academy of Science, Vlárska 5, 833 34 Bratislava, Slovakia

T-type or low-voltage activated calcium channels are characterized by a low voltage treshold of activation, small unitary conductance and fast inactivation [1]. T-type channels are blocked by multiple classes of drugs, including antiepileptics, antihypertensives, and anestethics [2]. They have high affinity to divalent [3] and trivalent [4] cations.

Interaction of monovalent silver ions ($Ag^{+)}$ with $Ca_v3.1$ calcium channel has been described by Gromová and coautors [5], who tested two different silver salts: AgCl and $AgNO_3$. Both forms of Ag^+ blocked the $Ca_v3.1$ calcium channel. These experiments were made using bath solution with nominal concentration of Cl^- ions 171 mmol/l. High chloride concentration may facilitate precipitation of Ag^+ ions. The aim of our study was to investigate the effect of Ag^+ on $Ca_v3.1$ in bath solution with low concentration of Cl^- ions.

Experiments were carried out on HEK 293 cells stably expressing the $Ca_v3.1$ subunit of T-type Ca^{2+} channel. The cells were grown in minimal essential medium (MEM) with Earle's salts, containing 10% fetal calf serum (v/v), 100 U/ml penicillin-streptomycin, and 0.04 % (w/v) G418 at 37°C in a humidified atmosphere of air/CO_2 95:5. The cells were harvested from their culture flasks by trypsinization and plated out 24-48 h before use in electrophysiological experiments.

Ion currents were recorded in whole cell configuration of the patch-clamp method using the EPC-10 patch clamp amplifier. All experiments were carried out at room temperature in a bath solution containig (mmol/l): CH_3SO_3Na 135, HEPES 10, $CaCl_2$ 2, $MgCl_2$ and CsCl 5; pH 7.4 (NaOH). The pipette solution contained (mmol/l): CsCl 130, NaATP 5, TEA-Cl 10, HEPES 10, EGTA 10 and $MgCl_2$ 5; pH 7.4 (CsOH). Osmolarity of the pipette solution was approximately 300 mOsm and osmolarity of the bath solution was approximately 2-3 mOsm lower. 10 μmol/l Agcl, 1 μmol/l AgCl and 10 μmol/l $AgNO_3$ solutions were prepared freshly before each experiment (Fig. 1).

Patch-clamp pipettes were manufactured from borosilicate glass with input resistance ranging between 1.6 and 2.5 MΩ. The capacitance of individual cells ranged between 8 and 32 pF. The holding potential (HP) in all experiments was -100 mV. The effect of the salts was investigated using series of 50 ms long depolarizing pulses applied from the HP to -30 mV with frequency 0.2 Hz. Current-voltage relations were measured by a series of 40 ms long depolarizing pulses applied from HP to membrane potentials between -90 and + 70 mV. Data were recorded using HEKA Pulse 8.5 and analyzed with HEKA Pulsefit 8.5 and Origin 7.5 software.

$AgNO_3$ in concentrations 10 μmol/l inhibited the calcium current through the expressed $Ca_v3.1$ channels in a concentration-dependent manner. The block was irreversible.

Higher concentration (100 μmol/l) of $AgNO_3$ were not fully soluble in our solution and therefore were not tested.

AgCl dissolves relatively poorly in water, with maximum soluble concentration 15 μmol/l. Maximal concentration used in our experiment was 10 μmol/l. This concentration blocked about 10% of the calcium current amplitude, but 1 μmol/l AgCl had no significant effect on the calcium current.

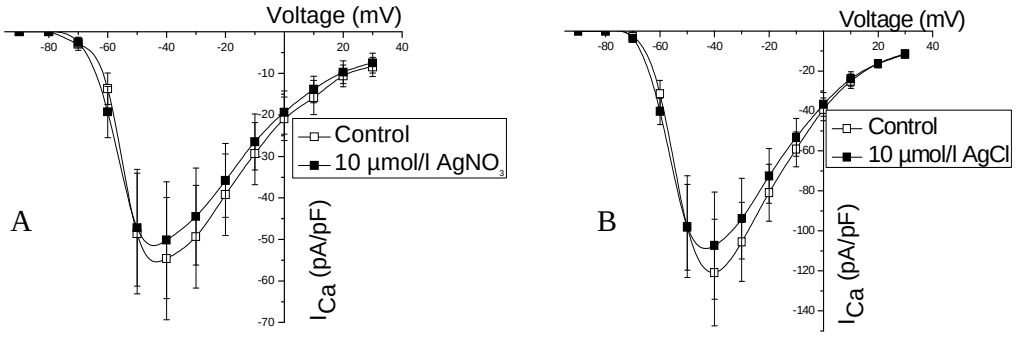

Figure 1 A: Voltage dependence of current densities (IV) measured under the control condition and in the presence of 10 µmol/l $AgNO_3$. B: Voltage dependence of current densities (IV) measured under the control condition and in the presence of 10 µmol/l AgCl.

The comparison of results of Gromová et al. with our our results is in the Table 1.

Table 1

	Gromová et al. (2003)	**This work**
Concentration	Amplitude inhibition (%)	Amplitude inhibition (%)
1 µmol/l AgCl	16.2	No effect
10 µmol/l AgCl	24.3	12.1
10 µmol/l $AgNO_3$	20.3	5.5

Silver ions moderately inhibited the current through the expressed $Ca_v3.1$ calcium channels. This inhibition was irreversible suggesting trapping Ag^+ ion in a channel pore. Blocking efficiency depend on composition of bath solution being more effective in the presence of high concentration of Cl^- ions.

References

[1] B. S. Freeye, M. M. McNulty, D. A. Hanck, *Mol. Pharmacol.* 70 (2006) 718-726
[2] E. Perez-Reyes, *Physiol. Rev.* 83 (2003) 117-161
[3] J. H. Lee, J. C. Gomora, L. L. Cribbs, E. Perez-Reyes, *Biophys. J.* 77 (1999) 3034-3042
[4] A. M. Beedle, J. Hamid, G. W. Zamponi, *J. Membr. Biol.* 187 (2002) 225-238
[5] P. Gromorová, M. Kurejová, Ľ. Lacinová, *Gen. Physiol. Biophys.* 22 (2003) 515-523

P8

SAX diffraction study of DNA-phospholipid-gemini surfactants aggregates

P. Pullmannová[1], D. Uhríková[1], S. S. Funari[2], I. Lacko[3], F. Devínsky[3], P. Balgavý[1]

[1] Department of Physical Chemistry of Drugs, [3]Department of Chemical Theory of Drugs, Faculty of Pharmacy, Comenius University, Odbojárov 10, 832 32 Bratislava, Slovakia, e-mail: pullmannova@fpharm.uniba.sk

[2] Hasylab at DESY, Notkestr. 63, D-22603 Hamburg, Germany.

The microstructure of aggregates formed by interaction of DNA with neutral phospholipids either dioleylphosphatidylethanolamine (DOPE) or dioleylphosphatidyl-choline (DOPC), and alkane-α,ω-diyl-bis(dodecyldimethylammonium bromide) (CnGS, spacer n = 2, 4, 6, 8, 10, 12) was studied using small angle X-ray diffraction. The gemini surfactants contain two alkyl chains and two quaternary ammonium groups connected by a polymethylene chain (spacer). They are attracting growing interest due to ability to form aggregates with DNA [1,2]. They are perspective gene delivery vectors showing very good transfection activity *in vitro* [3] and *in vivo* [4].

Three types of condensed organized cationic surfactant-lipid-DNA microstructures were identified: i) spaghetti-like structures in which DNA is covered by a cylindrical lipid bilayer [5], ii) condensed columnar inverted hexagonal phase (H_{II}^c) with linear DNA molecules surrounded by lipid monolayers forming inverted cylindrical micelles arranged on a hexagonal lattice [6], iii) condensed lamellar phase (L^c) with ordered DNA monolayers intercalated between lipid bilayers [7] (so called sandwich structure). Recent data indicate that lamellar complexes (L^c) have transfection efficiencies as high as those formed by hexagonal phase (H_{II}^c) [8].

Small-angle (SAXD) synchrotron radiation diffraction experiments were performed at the soft condensed matter beamline A2 at HASYLAB at the Deutsches Elektronen Synchrotron (DESY) in Hamburg (Germany). The aggregates were prepared at isoelectric point, CnGS:DNA = 0.5:1 mol/base in 0.1 M NaCl, and the molar ratio CnGS:phospholipid = 0.15 mol/mol.

The fully hydrated DOPC forms a lamellar phase with the repeat distance $d = 6.24 \pm 0.01$ nm and the fully hydrated DOPE forms a hexagonal phase with the lattice parameter $a = 7.67 \pm 0.01$ nm at 20°C. The repeat distance d was determined according to equation $d = 1/s_1$, and for hexagonal phase, the lattice parameter a is given by $a = 2/\sqrt{3}s_1$, where s_1 is the position of the first order diffraction peak's maximum. In presence of CnGS and DNA, the aggregates have shown temperature dependent structural diversity, as documents the Fig.1.

At 20 °C, the DNA–C4GS–DOPC aggregate forms the lamellar phase with $d = 7.24 \pm 0.01$ nm, and also the DNA–C4GS–DOPE forms the lamellar phase ($d = 6.89 \pm 0.01$ nm). While the DNA–C4GS–DOPC aggregates have kept their lamellar phase with increasing temperature (not shown), in the DNA–C4GS–DOPE we have observed $L_\alpha^c \rightarrow H_{II}^c$ phase transition. At 60° C, the coexistence of the lamellar phase ($d = 6.29 \pm 0.01$ nm) and the hexagonal phase ($a = 7.05 \pm 0.02$ nm) is observed in DNA–C4GS–DOPE aggregates (Fig. 1). After heating the aggregate up to 80 °C, the hexagonal phase becomes dominant. We have not observed any peak related to the DNA organization between lipid bilayers what indicates irregular packing of DNA strands in the sandwich structure aggregates. Structural parameters of the aggregates DNA-CnGS-phospholipid were evaluated as a function of the length of the spacer.

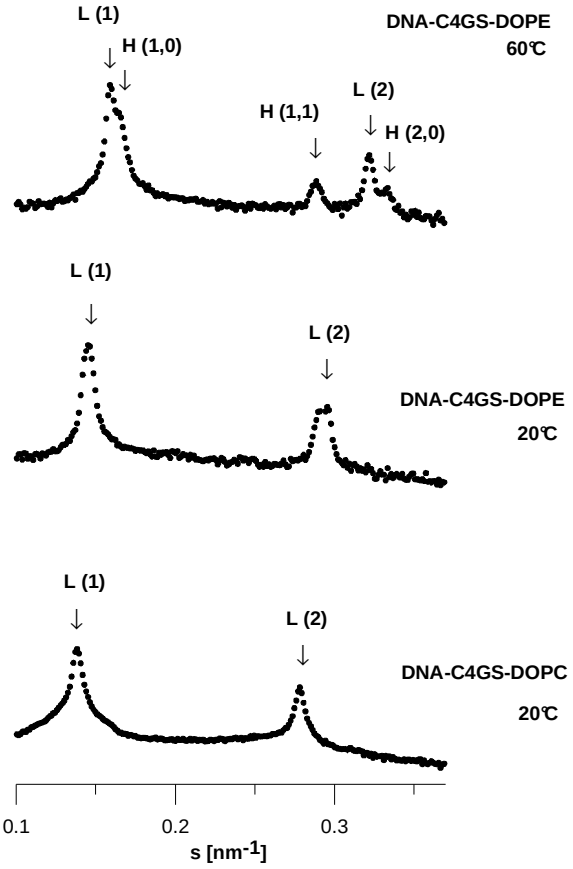

Fig. 1: SAXD patterns of DNA-C4GS-DOPC and DNA-C4GS-DOPE aggregates.

Acknowledgement
This work was supported by the European Community - Research Infrastructure Action under the FP6 "Structuring the European Research Area" Programme Contract RII3-CT-2004-506008 (HASYLAB project II-20052037 EC), by the JINR project 07-4-1031-99/2008 and by the VEGA grant 1/3029/06 to DU.

References

[1] A. J. Kirby, P. Camilleri, J. B. F. N. Engberts, M. C. Feiters, R. J. M. Nolte, O. Soderman, M. Bergsma, P. C, Bell, M. L. Fielden, C. L. G. Rodriguez, P. Guedat, A. Kremer, C. McGregor, C. Perrin, G. Ronsin, M. C. P. van Eijk, *Angew. Chem. Int. Ed.* 42 (2003) 1448 – 1457.
[2] D. Uhríková, G. Rapp, P. Balgavý, *Bioelectrochemistry* 58 (2002) 87 – 95.
[3] P. Camilleri, A. Kremer, A.J. Edwards, K.H. Jennings, O. Jenkins, L. Marshall, C. McGregor, W. Neville, S.Q. Rice, R.J. Smith, M.J. Wilkinson, A.J. Kirby, *Chem. Commun.* (2000) 1253.
[4] I. Badea, P. Verral, M. Baca-Estrada, S. Tikoo, A. Rosenberg, P. Kumar, M. Foldvari, *J. Gene Med.* 7 (2005) 1200 – 1214.
[5] B. Sternberg, F. L. Sorgi, L. Huang, *FEBS Lett.* 356 (1994) 361- 366.
[6] I. Koltover, T. Salditt, J. O. Radler, C. R. Safinya, *Science* 281 (1998) 78 – 81.
[7] T. Salditt, I. Koltover, J. O. Radler, C. R. Safinya, *Phys. Rev. Lett.* 79 (1997) 2582 – 2585.
[8] A. J. Lin, N. L. Slack, A. Ahmad, C. X. George, Ch. E. Samuel, C. R. Safinya, *Biophys. J.* 84 (2003) 3307 – 3316.

P9

The use of trivalent cations for a measurement of gating current from the $Ca_v3.1$ channel.

M. Drígeľová, M. Pavlovičová, Ľ. Lacinová

Institute of Molecular Physiology and Genetics, Slovak Academy of Science, Vlárska 5, 833 34 Bratislava, Slovakia, e-mail: maria.drigelova@savba.sk

Voltage-operated calcium channels consist of four homological domains each containing six transmembrane segments S1-S6 [1]. The S4 segments contain five to six basic amino acids forming putative voltage sensors. Voltage-dependent openings and closings of these ion channels are accompanied by movements of the S4 segments, which could be detected as so-called gating current. Gating current is observable when inward ion current is fully blocked. The aim of our study was to evaluate suitability of trivalent cations – gadolinium (Gd^{3+}), yttrium (Y^{3+}) and erbium (Er^{3+}) as possible blockers of the $Ca_v3.1$ calcium channel enabling measurement of gating current.

$Ca_v3.1$ calcium channel was permanently transfected into HEK 293 cells. Cells were grown in EMEM (Eagle's modified essential medium), containing 10% foetal calf serum, 100 U/ml penicillin and streptomycin and 0.04% G 418. Cells were harvested from culture flasks by trypsinization and plated out 24-48 h before use in electrophysiological experiments. Inward and gating currents were measured by whole cell patch-clamp method.

10 mM stock solution of $ErCl_3$, $GdCl_3$, YCl_3 were prepared daily in deionized water and diluted into experimental concentration prior to the experiment.

The bath solution contained (in mM): HEPES 10, $CaCl_2$ 2, $MgCl_2$, NMDG 140; pH 7.4 with HCl. The pipette solution contained: (in mM): CsCl 130, Mg-ATP 5, EGTA 10, HEPES 10; pH 7.4 with CsOH. Osmolarity of pipette solutions was measured (typical value approximately 300 mOsm) and osmolarity of bath solution was adjusted by adding glucose so that the final value was by 2-3 mOsm lower, than osmolarity of bath solution.

Whole cell currents were measured using EPC 10 patch clamp amplifier (HEKA Electronic). Patch pipettes were pulled from borosilicate glass. Typical cell size was between 16 and 45 pF. Access resistance was typically between 3.0 and 5.0 MΩ.

Data were recorded with HEKA Pulse 8.5 software and analyzed with HEKA Pulsefit 8.5 and Origin 7.5 software.

Holding potential was -100 mV in all experiments. Gating currents were measured by 50 ms long depolarizing pulses to membrane potentials between -90 mV and +70 mV. Symmetrical capacity transients and linear leak current were subtracted by P/-8 procedure. Three identical pulses were averaged for each trace. Charge movement was consistently observed in cells with amplitude of inward current 1 nA or bigger. Asymmetrical charge movement was evaluated by integrating the area below charge transient observed at the beginning (Q_{on}) and after the end of each depolarizing pulse (Q_{off}).

Three criteria were used to evaluate suitability of each cation:

1. efficiency of the inward current inhibition
2. kinetics of current block development
3. cation must not influence charge movement itself.

First, we tested the concentration dependence of the inward current block. Experimental data were fitted by Hill equation. Fitting procedure resulted in IC_{50} and Hill coefficient values 3.1±0.7 nM and 0.87±0.12 for Er^{3+}, 37±3 nM and 0.76±0.05 for Gd^{3+} and 35±7 nM and 0.55±0.50 for Y^{3+}. Er^{3+} blocked the $Ca_v3.1$ channel ten times more effectively than Gd^{3+} and Y^{3+}. All three tested cations inhibited inward calcium current with comparable kinetics.

Finally, we evaluated the effect of concentration of trivalent cations necessary for complete block of current on gating current. Both Gd^{3+} and Y^{3+} in concentration necessary for complete current block inhibited also the gating current. Er^{3+} in concentration of 30 µM was

able to inhibit fully calcium inward current without interfering with the gating current.

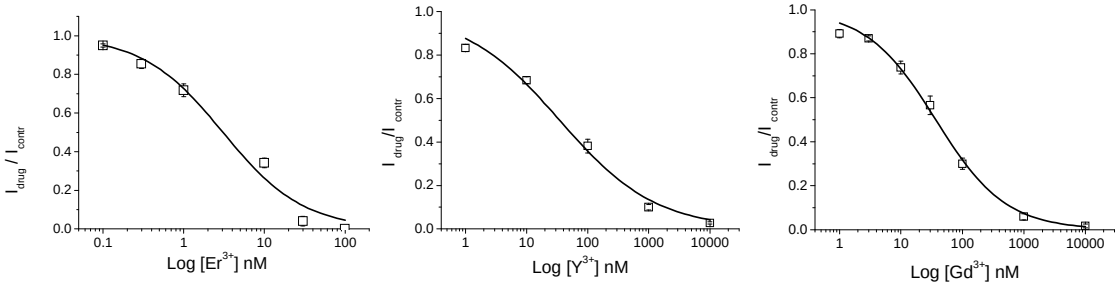

Figure 1. Dose-response curves of the inhibition of inward calcium current through $Ca_v3.1$ channel by trivalent cations.

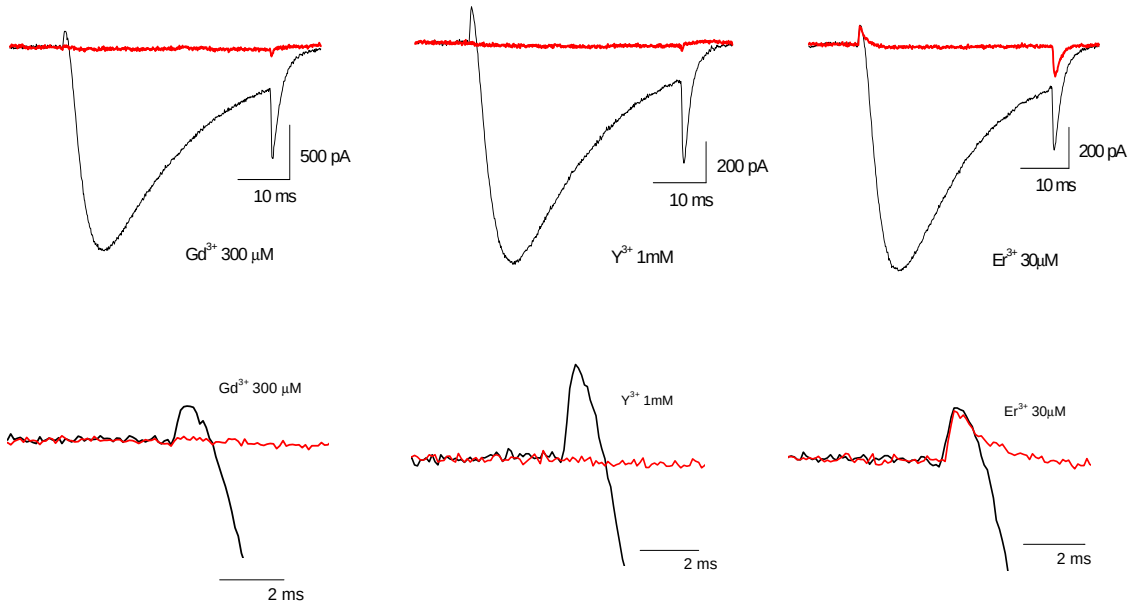

Figure 2. Block of inward calcium current through $Ca_v3.1$ channel by trivalent cations. Beginnings of each current record are enlarged in the botton panel.

In conclusion, most suitable calcium current blocker for the analysis of gating currents originating from the $Ca_v3.1$ channels was Er^{3+}.

Acknowledgement
This work was supported by the Slovak Grant Agency VEGA, project No. 2/7001.

References
[1] F. Hofmann, Ľ. Lacinová, N. Klugbauer, Rev. Physiol. Biochem. Pharmacol. 139 (1999) 33-87.

P10

Interdisciplinary proof of lead in placenta – contribution for diagnostic practice

M. Šimera[1,2], V. Foltin[2,3], M. Morvová[4], E. Neu[5], J. Foltinová[1]

[1] Institute of Histology and Embryology, Faculty of Medicine, Comenius University, Sasinkova 4, 81108 Bratislava, Slovakia, e-mail: msimera@gmail.com
[2] Department of Experimental Physics – Plasma Physics Division, Faculty of Mathematics, Physics and Informatics, Comenius University, Mlynská dolina 84248 Bratislava, Slovakia,
[3] Institute of Natural Sciences, Humanities and Social Sciences – Division of Physics, Faculty of Mechanical Engineering, Slovak Technical University Bratislava, Námestie slobody 17, 812 31 Bratislava, Slovakia
[4] Department of Astronomy, Physics of the Earth and Meteorology – Enviromental Physics Division, Faculty of Mathematics, Physics and Informatics, Comenius University, Mlynská dolina 84248 Bratislava, Slovakia
[5]Umweltmedizin Institut, Feucht bei Nürnberg, Germany

Introduction

Environment plays important role in the rise of diseases not only in case of the respiratory system [1, 5] but also in case of other systems of human organism [2, 3, 6, 12, 13]. Lead is toxic for hemopoetic, nervous and excretory system of developing fetus. Normal placental levels of lead were found to be 0,29 ± 0,9 μg/g, whereas lead in placentas from stillborns was 0,45 ± 0,32 μg/g [8]. The mechanism for the transport of lead to the placenta is not well defined [7, 10]. The microscopic studies and immunohistochemical analyses have demonstrated that the syncytiotrophoblast is the site of metalothionein synthesis, a protein that binds cadmium, lead and may also enhance transport of the essential trace metals zinc and copper [9, 10]. The primary mechanism for transplacental lead transport is probably simple diffusion and is probably related to fetal blood flow rate. It is suggested, however that fetal tissue levels may be influenced by calcium transport and intracellular calcium metabolism. However, although maternal and umbilical cord blood Pb levels were low, maternal blood Pb concentration was significantly linked to a decrease in Ca^{2+} uptake by syncytiotrophoblast. This suggests that exposure to even very low levels of Pb significantly modifies Ca^{2+} transfer in syncytiotrophoblasts [4, 6, 8]. In this interdisciplinary study we have paid attention to placenta, which represents important organ in the life of developing fetus.

Material and methods

In this work we prepared and evaluated sections from excisions of placentas of 104 healthy patients. Excisions from placenta were fixed in AFO – alcohol:formol: acid in the ratio 12:6:1 for light microscopy and in 3 % glutaraldehyd for SEM. On the 7 μm thick paraffin sections we carried out the following histological staining methods:

1. New methodical approach after Foltinová et al. [6], which is combination of Mallory and Parker method for proof of lead. Documentation was done by light microscope Nikon Labophot 2, (Japonsko, Tokyo) at magnifications 100 – 400x and by Olympus Camedia C707. Positivity in lead is manifested by turquise green colour.
2. Concerrently we have studied identical samples from placenta by means of SEM using X–ray microanalysis. We used SEM JEOL JXA 840 A electron probe microanalyzer.
3. Concerrently we have studied identical samples from placenta by means of infrared spectrometry using Kbr pellet making technique. We used infrared spectrometer SPECORD M80, Carl Zeiss, Jena (Germany).

Results and discussion

In the microscopic structure of placenta lead shows positivity and character of

phagocytosis in the same places of the surface part of syncytiotrophoblast that is neighbouring to the flowing mother's blood (Figure 1, 2).

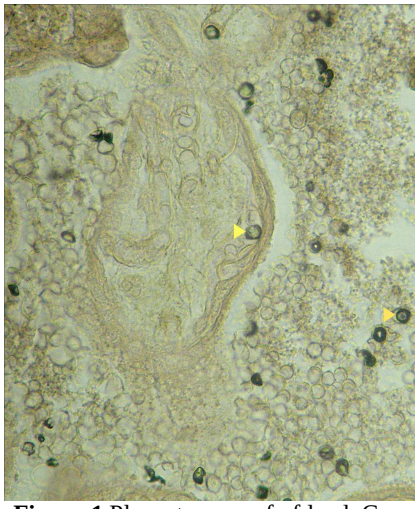

Figure 1 Placenta – proof of lead. Cumulation of lead deposit in erythrocyte (►). Proved by new methodical approach after Foltinová et al. Magnified 400 x.

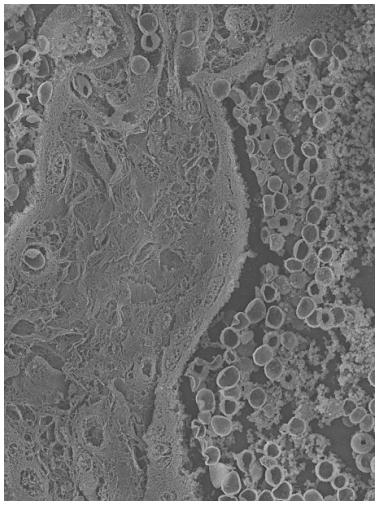

Figure 2 Placenta – the same sample 1 μm bellow, in SEM. Magnified 400 x.

On the IR spectrum of placenta (Figure 3) a decay of protoporfin (denoted as 4) into bilirubin (3) can be seen. From metals presence of lead in water soluble $Pb(NO_3)_2$ was recorded (denoted as 6). This compound is soluble in blood too. If we assume that lead comes from exhaust gases or as a residuum deposited in fruits of trees located near highways, we may conclude that interaction of the metal with NO_x often occurs giving

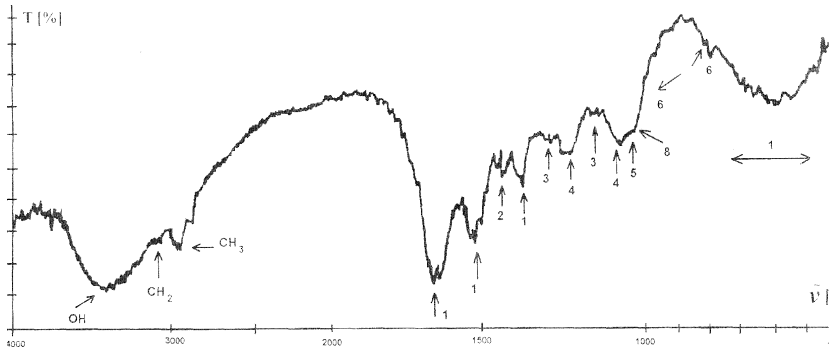

Figure 3 IR spectrum of placenta.

$Pb(NO_3)_2$ as a result. This compound frequently occurs in smokers. $(PO_4)^{3-}$ residues have their origin in reactions and processes occuring on the level of RNA, DNA, ADP, and ATP. Because of large amount of moisture in the original excisions and impossibility to dry them at high temperature there remained 10-30 % of moisture in them. As a result – OH band at 3600 cm^{-1} appeared in the spectrum.

Conclusion

Lead accumulated in placenta and found by a reliable and quick method, as we have done and presented, may help in prevention of the hyperkinetic syndrome of children immediately after the childbirth in the hospital, because the presence of lead in the body is one of the reasons of this syndrome. Validity of this method has the same degree of importance as the method for

proof of IgE for revealing allergic terrain in a newly born child. These results emphasize importance of physicists for the work in a medical research team.

References

[1] J. Foltinová, Histológia pre poslucháčov biomedicínskej fyziky. Vysokoškolská učebnica. Univerzita Komenského Bratislava, 2003, 242p.
[2] J. Foltinová, M. Morvová, V. Foltin, E. Neu, M. Šimera, I. Lettrichová, Programme and Abstract Book of the 41st International Congress of Slovak Anatomical Society. Bratislava. 2007.
[3] J. Foltinová, M. Morvová, V. Foltin, E. Neu, In: Proceedings of International Congress on Enviromental Health. Hanover. Germany. Fraunhofer. ITA. 2000. p.80.
[4] J. Foltinová, V. Foltin, E. Neu, *Neuroendocrinology Letters* 28 (2007) 335 – 340.
[5] J. Foltinova, A. Schrott–Fisher, V. Žilinek, V. Foltin, W. Freysinger, In. Laryngoscope Lippincott Williams & Wilkins Inc. Philadelphia 112 (2002) 713–719.
[6] J. Foltinová, V. Foltin, M. Šimera, M. Morvová, E. Neu, *Int. J Prenatal and Perinatal Psychology and Medicine* 18 (2006) 19-26.
[7] J.G. Pounds, G.J. Long, J.F. Rosen, *Enviromental Health Perspective* 91 (1991) 17-32.
[8] J. Lafond, A. Hamel, L. Takser, C. Vaillancourt, D. Mergler, *J. Toxicol. Environm. Health. Part A*, 67 (2004) 1069-1079.
[9] R.A. Goyer, *Enviromental Health Perspectives* 89 (1990) 101-105.
[10] E. Reichrtová, P. Doročiak, L. Palkovičová, *Hum. Exp. Toxical*. (1998) 176-181.
[11] M.H. Ross, W. Pawlina, Histology a text and atlas with correlated cell molecular biology. Baltimore. Lippincott Williams & Wilkins, 2006, pp. 906.
[12] TJ.B. Simons, J. Physiol. 387 (1986) 267-286.
[13] V. Vráblová, M. Šimera, W. Seidenbusch, Interdisciplinary approach to study of placenta. Morfológia v Súčasnosti, Zborník. Univerzita Komenského v Bratislave Lekárska Fakulta. (2006) 90-94.

P11

Influence of storage of insulated erythrocytes membranes on membrane fluidity

P. Slezák, L. Šikurová

Department of Nuclear Physics and Biophysics, FMFI UK, Mlynská dolina F1, 842 48 Bratislava, Slovakia, e-mail: peter.slezak5@gmail.com

Introduction

Several studies were elaborated, which examined the influence of storage on the whole blood or erythrocytes, eventually. They monitored the influence on electric properties of membrane [1], biophysical, morphological and rheological changes [2 - 4] and also influence of storage on other kinds of biological membranes, for example plasmatic membranes of sperms, was studied [5]. However, we did not succeed till now in finding an article in literature, which is devoted to storage of insulated erythrocyte membranes. That is why the aim of this work, with reference to other measurements, was to find out the influence of storing of insulated erythrocyte membranes on the values of fluorescence anisotropy, as well as to investigate the possibility of objective comparison with the results of measurements, which are performed on samples of membranes of human erythrocytes prepared on the day of blood taking and also on the stored samples.

Material and methods

Biological material – human blood – came from seven voluntary normal (healthy) adult donors of both genders aged from 20 to 25 years. All the donors agreed with utilisation of the blood and they were informed about its use. The blood was taken in cooperation with the Neurologické oddelenie Fakultnej nemocnice (Neurology Department of Faculty Hospital) in Bratislava. A blood sample was processed within 12 hours after the taking, while it was stored in coldness at the temperature of 4°C all the time. Preparation of erythrocyte membranes – ghosts – was carried out by a standard method according to Hanahan and Ekholm [6] with petty adjustments. The samples were stored at -30°C to -40°C in darkness for the period of 2 days. Membrane fluidity was evaluated with the degree of fluorescence anisotropy. Measurements of the fluorescence stationary anisotropy in erythrocytes membranes were performed at spectrofluorimeter Perkin-Elmer LS 45. During the measurements, fluorescent probe DPH (1.6 – diphenyl - 1,3,5 – hexatriene) was used. The resulting DPH concentration in the sample was $1.5 \cdot 10^{-7}$ mol/l, the final concentration of the insulated membranes was 0.5 %. The measurements were carried out at the room temperature (22±2°C) and at the temperature of a human body (37±2°C). The Student pairing t-test was used for the differences within the same group, caused by the influence of the storage. As the criterion of the statistical significance, the value $\alpha = 0.95$ was chosen for the level of statistical significance.

Results and discussion

We found out that after the storage of the samples (freezing and defrosting) integrity of the membranes retained, which is testified by the measured values of the fluorescence anisotropy in the range 0.194 – 0.229 measured at 37±2°C, and range 0.236 – 0.260 measured at 22±2°C. If corruption of the membranes integrity occurred, the values of the fluorescence anisotropy would have the span about 0.1. The measurements were carried out on the samples also after approximately 10 months, however, values about 0.12 were measured, which provides the testimony on corruption of membranes intactness.

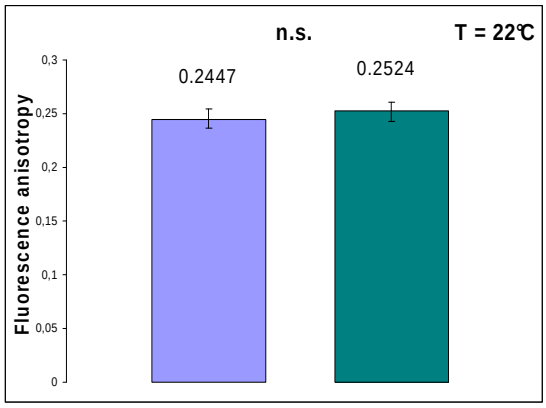

Fig. 1 Storage effect of insulated membranes of erythrocytes on the value of fluorescence anisotropy of probe DPH (blue – check, green – stored sample), the measurement was carried out at 22±2°C. The values are introduced as the mean ± S.D. from 7 independent experiments

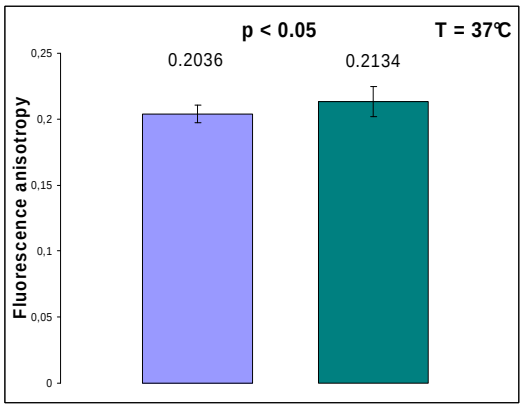

Fig. 2 Storage effect of insulated membranes of erythrocytes on the value of fluorescence anisotropy of probe DPH (blue – check, green – stored sample), the measurement was carried out at 37±2°C. The values are introduced as the mean ± S.D. from 7 independent experiments. Significantly different with $p < 0.05$

When measuring the anisotropy at room temperature 22±2°C, no significant change for stored erythrocytes membranes was observed in comparison with the fresh prepared samples (Fig. 1). When measuring the fluorescence anisotropy at temperature 37±2°C, a significant increase of stationary fluorescence anisotropy by 4.54 % occurred for the stored samples, in comparison with the fresh prepared samples (Fig. 2). The effect is probably caused by increased peroxidation of lipids at a higher temperature, which will not manifest itself at temperature 22±2°C yet.

Acknowledgement
This work was supported by the Slovak Grant Agency VEGA, project No. 1/3037/06.

References:

[1] A.G. Kriebaedis, *J. Cell. Mol. Med.* 11 (2007) 148–155
[2] F. Leterierre, J. Saint–Blancard, J.F. Stoltz, Biophysical, Morphological and Rheological Modifications of the Erythrocyte During Storage, Clinical Hemorheology, Vol. 3, Pergamon Press, 1983, pp. 53–95
[3] Y. Űlgen, M. Sezdi, Physiological Quality Assessment of Stored Whole Blood by Means of Electrical Measurements, International Federation for Medical and Biological Engineering, 2007
[4] W.F. Wolkers, L.M. Crowe, N.M. Tsvetkova, F. Tablin, J.H. Crowe, *Mol. Membr. Biol*. 19 (2002) 59-65
[5] X.F. Wang, G.H. Zheng, S.J. Yang, X.M. Jing, *Chinese Sci. Bull.* 44 (1999) 1008–1014
[6] D.J. Hanahan, J.E. Ekholm, in: Methods in Enzymology V. 31, Acad. Press, New York, 1974, 168-177

P12

NAD(P)H/flavin autofluorescence imaging of INS-1E insulinoma cell metabolism

J. Kirchnerová[1], P. Topor[1], M. Uherek[1], V. Štrbák[2], D. Chorvát jr.[3]

[1] Department of Nuclear Physics and Biophysics, FMFI UK, Mlynská dolina F1, 842 48 Bratislava, Slovakia, e-mail: kirchnerova@fmph.uniba.sk
[2] Institute of Experimental Endocrinology, Slovak Academy of Sciences, Bratislava, Slovakia
[3] International Laser Centre, Bratislava, Slovakia.

Introduction

Insulin secretion is coupled to cytoplasmic and mitochondrial metabolism of pancreatic β cells, techniques assessing live cell redox state are therefore of interest. NAD(P)H/Flavin redox fluorimetry is based on modulation of the intrinsic cell fluorescence by change in the cell redox state; NAD(P)H exhibiting increase of fluorescence in reduced and flavins exhibiting increase of fluorescence in oxidized state. Due to their spatial overlap and overlap in their fluorescence excitation and emission spectra, microscopy using multiple excitation wavelengths is necessary for understanding the complex autofluorescence signal. To apply multiple excitation fluorescence microscopy approach to monitor cellular autofluorescence changes, to decipher NAD(P)H and flavoprotein autofluorescence changes and relate them to actual mitochondrial and cytoplasmic redox state in living cells.

Materials and methods

Rat insulin-secreting INS-1E cells [1] were cultured as described previously [2]. Before the experiments, cells were washed and equilibrated in basal solution and placed in POC-mini (Zeiss) open chamber equipped with 35±2 °C perfusion at 0.5ml/min. Fluorescence imaging was done using Axiovert 200 (Zeiss) microscope equipped with mercury lamp Fluo Arc HBO 100 (Zeiss) (25% output power) illumination with a Plan-Neofluar 20x/0.5 NA. Nondescanned autofluorescence was collected through combined standard Filter Set 40 (Zeiss) (BP 360/51,485/17,560/18 / TFT 440+450+570 / TBP 460+520+600) using CCD camera PentaMAX (Princeton Instruments) controlled by WinSpec/32 (Princeton Instruments) and in-house developed software MTB Experiment. Regions of interest (≈100 pixel ≈40μm^2) of intracellular areas in background corrected images were outlined and fluorescence intensity extracted using in-house developed SPE Counter.

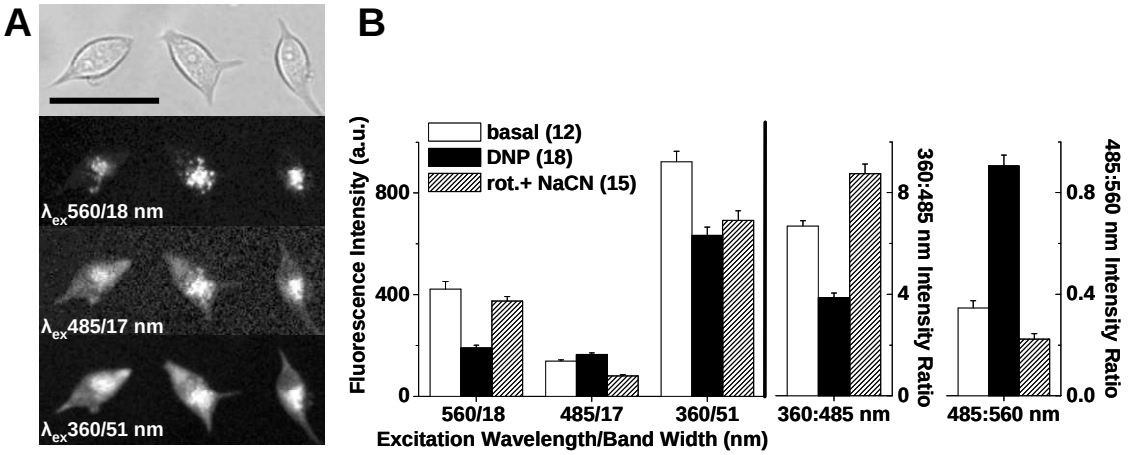

Fig. 1 Triple channel excited INS-1E cell autofluorescence. **(A)** Wide field (top) and fluorescence microscopy images of cellular autofluorescence in response to band pass excitation light. Cells are equilibrated in basal solution containing 50 μM 2,4-DNP, bar corresponds to 50 μm. **(B)** *Left* Mean±SEM (number of cells) fluorescence intensity of cells equilibrated in basal (2.5 mM glucose) solution (basal) and basal solution containing 50 μM 2,4-DNP (DNP) or 10μM rotenone and 4mM NaCN (rot.+NaCN). *Right* 360:485 nm intensity ratio and 485:560 nm intensity ratio changes.

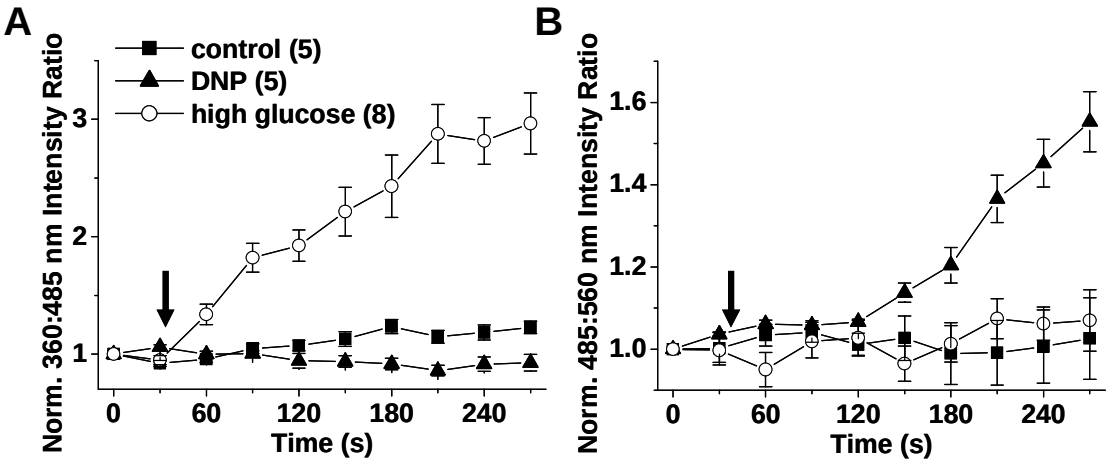

Fig. 2 Autofluorescence imaging of cellular metabolism. Time-course of normalized **(A)** 360:485 nm intensity ratio and **(B)** 485:560 nm intensity ratio responses to basal (2.5 mM glucose) perfusion solution change (denoted by arrow) to basal solution containing 50 μM 2,4-DNP (DNP) or 15 mM glucose (high glucose). (Number of cells, mean±SEM)

Results and discussion

To achieve simultaneous monitoring of multiple channel excited autofluorescence, using combined filter set and in-house developed software MTB Experiment we minimized the total fluorescence acquisition time to 30s. The 560/18 nm excited INS-1E autofluorescence is localized to bright spots. The source of this redox non-responsive signal could be lipofuscin deposits and lysozomes [3]. The source of 485/17 nm excited redox responsive autofluorescence are flavins and flavoproteins localized in mitochondria, however in addition there were also high intensity fluorescence spots overlapping with 560/18 nm excited autofluorescence. We therefore introduced the 485:560 nm intensity ratio that reflects flavin autofluorescence changes at 360/51 nm excitation, the fluorescence of both flavins and NAD(P)H is responsible for the cellular autofluorescence signal. We therefore introduced the 360:485 nm intensity ratio that reflects the NAD(P)H changes. Observed changes of both ratios correspond to increased oxidation of coenzymes induced by uncoupler 2,4-Dinitrophenol or increased pool of reduced coenzymes after inhibition of respiration by rotenone and sodium cyanide. To apply this approach on imaging of INS-1E cell metabolism, we recorded autofluorescence changes of cells exposed to continuous perfusion. Cellular response to application of 2,4-DNP was delayed by about 120 s and observable in both intensity ratios, suggesting that mitochondrial oxidation caused the of autofluorescence changes. On the other hand, 15mM glucose stimulation resulted in immediate autofluorescence response, however, increase in 360:485 nm intensity ratio was not accompanied by simultaneous 485:560 nm intensity ratio change, suggesting that predominantly cytoplasmic NADPH reduction is responsible for the 360:485 nm intensity ratio increase.

Conclusions. We have successfully applied multiple excitation fluorescence microscopy to record INS-1E cell intrinsic fluorescence, introduced approach to decipher NAD(P)H and flavin autofluorescence changes and demonstrated its possible use for detection of cellular metabolic stimuli responsiveness.

Acknowledgement

This work was supported by the Slovak Grant Agency VEGA, project No. 2/6158/27 and by Grant UK/387/2007. JK is supported by ESF JPD BA 3 2004/4-053.

References

[1] A. Merglen, S. Theander et al., *Endocrinology* 145 (2004) 667-78
[2] Z. Bačová, J. Benický et al., *Cell. Physiol. Biochem* 16 (2005) 59-68
[3] J.V. Rocheleau, W.S. Head et al., *J Biol. Chem.* 279 (2004) 31780-7

P13

Study of the interaction of hypericin with phospholipids and low-density lipoproteins by a surface-enhanced Raman and fluorescence spectroscopy

G. Lajoš[1], S. Sánchez-Cortés[2], G. Fabriciová[1], P. Miškovský[1,3], J. V. García-Ramos[2], D. Jancura[1]

[1]Department of Biophysics, PF UPJŠ, Jesenná 5, 040 01 Košice, Slovakia

[2]Instituto de Estructura de la Materia, CSIC, Serrano 121, 28006 Madrid, Spain

[3]ILC, Ilkovičova 3, 812 19 Bratislava, Slovakia, e-mail: gabriela.fabriciova@upjs.sk

Surface-enhanced Raman and fluorescence spectroscopy (SERS and SEFS) were applied in the study of the interactions of photodynamically active compound hypericin (Hyp) with low density lipoproteins (LDL) and phosphatidylcholine (PCH). The SERS and SEFS spectra of Hyp in the presence of LDL and PCH were recorded using excitation line 514 nm in the interval 200-8000 cm^{-1}, which enabled us to obtain simultaneously information about vibrational and fluorescence properties of Hyp from the same spectrum. The fluorescence part of the spectra informs about the state of aggregation of Hyp molecules, which is an essential information from the point of view of the biological activity of Hyp. The Raman part of the spectra provides information about vibrational properties of Hyp due to significant enhancement of the Raman bands of the molecules of Hyp, which are in the vicinity of the surface of the Ag colloid particles used in our study as the substrate for the surface-enhanced spectroscopy.

At constant concentration of Hyp, the intensity of SERS spectra of Hyp increases with the increasing of Hyp/LDL ratio. With respect to the theory of the enhancement of intensity of Raman signal in SERS it was suggested, that at low Hyp/ LDl ratios (Hyp/LDL< 30:1) the molecules of Hyp are localized in the inner part of LDL particles, which prohibits the direct contact of Hyp with the metal surface. When the number of Hyp molecules per one LDL particle is high (>100 :1), certain amount of them is localized in the phospholipid outer shell of LDL and in this situation these molecules are near the surface of colloid particles, which consequently lead to the enhancement of Raman signal of Hyp. Fluorescence part of the spectra shows a new band in the red region of the spectra (~750 nm) at high Hyp/LDL ratios (>100:1). This band is attributed to the formation of excimers of Hyp. The increasing of PCH concentration leads to the higher intensity of both fluorescence and Raman spectra of Hyp. This is due to higher solubility of Hyp in the presence of high concentration of PCH. Small, but detectable changes in the positions and relativve intensities of Raman bands of Hyp were registered upon interaction of Hyp with LDL and/or PCH in comparison with the SERS spectrum of Hyp alone.

Acknowledgement

This work was supported by the Scientific Grant Agency of the Ministry of Education of Slovak Republic under the grants VEGA No. 2278 and 1/4449/07 , by the Slovak Research and Development Agency under the contract APVT-20-036104, by SPP Foundation (G. L.) and the NATO project ref. CBP.EAP.CLG 981432.

P14

Determination of binding constants and kinetics of hypericin incorporation into serum albumins

E. Jacobsen[1], J. Staničová[1], P. Gbur[2], P. Miškovský[2,3], D. Jancura[2]

[1] Institute of Biophysics and Biomathematics, UVM, Komenského 73, 041 81 Košice, Slovakia, e-mail: stanicova@uvm.sk
[2] Department of Biophysics, PF UPJS, Jesenná 5, 041 81 Košice, Slovakia
[3]ILC, Ilkovičova 3, 812 19 Bratislava, Slovakia

Serum albumins are the most abundant plasma proteins and contribute significantly to many transport and regulatory processes. These proteins bind a wide variety of substrates such as metals, amino acids, fatty acids, hormones and an impressive spectrum of therapeutic drugs [1]. The effectivity of drug transport in biological organism depends also on the binding ability and kinetics of interaction of transported drugs with plasma proteins including serum albumins.

Hypericin (Hyp) is a natural photosensitizing pigment occurring in plants of the genus *Hypericum.* Hyp under light illumination displays antiproliferative and cytotoxic effects on many tumor cell lines [2, 3]. These properties together with minimal dark toxicity, tumor selectivity and high clearance from the host body make Hyp a very promising agent in photodynamic therapy of cancer.

Because of the perspective of pharmaceutical utilization of Hyp, its interaction with albumins (human serum albumin (HSA) and bovine serum albumin (BSA)) has been widely studied [4, 5]. The binding constant and binding site for the interaction of Hyp with HSA have been determined [4, 5]. On the other hand, the binding constant of the interaction of Hyp with BSA has not been determined yet, however, Raman spectroscopy studied revealed different mode of Hyp interaction with BSA in comparison with HSA [5].

The increase of the Hyp fluorescence with the increasing of albumins (BSA and HSA) concentrations in aqueous solution was used for the determination of the binding constants for the interaction of Hyp with both HSA and BSA. Our experiments show that the affinity of Hyp for binding to HSA is higher in comparison with binding to BSA.

Fluorescence spectroscopy was also used for the study of the kinetics of the incorporation of Hyp into BSA, and HSA. It has been shown that Hyp is incorporated into both albumins with characteristic lifetime about tens of minutes. We can conclude that binding of Hyp into serum albumins is relatively slow process and this fact should be considered when Hyp is administered into a biological organism.

Acknowledgement
This work was supported by the Slovak Grant Agency KEGA, project No. 3/5115/07, by Agency for Promotion Research and Development under the contract No. APVT-20-036104, and UVM fund for providing of E.J. diploma thesis.

References

[1] T. Peters, *Adv. Protein Chem.* 37 (1985) 161-245.
[2] I. Lopez-Bazzocchi, J.B. Hudson, G.H.N. Towers, *Photochem. Photobiol.* 54 (1991) 95-98.
[3] A. Andreoni, A. Colasanti, P. Colasanti, M. Mastrocinque, P. Riccio, G. Roberti, *Photochem. Photobiol.* 59 (1994) 529-533.
[4] V. Senthil, J.W. Longworth, C.A. Ghiron, L.I. Grossweiner, *Biochim. Biophys. Acta* 115 (1992) 192-200.
[5] P. Miškovský, J. Hritz, S. Sanchez-Cortés, G. Fabriciová, J. Uličný, L. Chinsky, *Photochem. Photobiol.* 74 (2001) 172-183.

P15

Investigation of Hypericin fluorescence in isolated mitochondria and U-87MG cells

L. Bryndzova[1], M. Andrasova[1], V. Huntosova[1], Z. Nadova[1], P. Miskovsky[1,2]

[1] Department of Biophysics, UPJS, Jesenna 5, 040 01 Kosice, Slovakia, e-mail: lenka.bryndzova@yahoo.com,
[2] International Laser Center, Ilkovicova 3, 812 19 Bratislava, Slovakia

Hypericin (7,14- dione- 1,3,4,6,8,13- hexahydroxy 10,11- dimethyl- phenanthrol [1,10,9,8- o*pqra*] perylene) (Fig. 1) is a naturally occurring anthraquinone synthesized by plants of the genus *Hypericum* and is for its photosensitive properties very interested for photodynamic therapy (PDT) of cancers [1]. Photoactivated hypericin shows antiproliferative and cytotoxic effects towards various cancerous cell-lines [2]. After its light activation generate the reactive oxygen species as singlet oxygen, superoxide anion, hydrogen peroxide and as well as activates cell death signaling pathways [1]. Hypericin can be localized in different cells organelles (mitochondria, endoplasmatic reticulum, Golgi complex) [3, 4, 5].

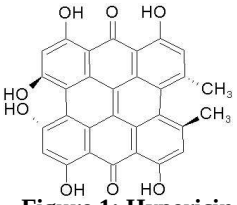

Figure 1: Hypericin

Concentration and localization of photosensitizers (including Hypericin) in cells significantly affect the efficiency of PDT. By using fluorescence spectroscopy we investigated behavior of hypericin in isolated mitochondria and human glioma cells U-87 MG, respectively. The measurements were performed on fluorescence spectroscope Shimadzu RF-5301 PC by excitation wavelength 488 nm and emission between 500-700 nm.

It was demonstrated that the intensity of hypericin fluorescence depends on its concentration and incubation time in both model systems. An initial increase of hypericin fluorescence due to its dissolving in lipid environment of mitochondria was followed by gradual decrease of fluorescence in all studied concentrations (Fig. 2A). On the other hand, we also demonstrated that after extraction of intra-mitochondrial content of hypericin in 100% DMSO the fluorescence intensity increases linearly (Fig. 2B). This implies that there is an aggregation effect at higher hypericin concentrations in isolated mitochondria. Similar results were obtained in U-87 MG cells. High concentration of hypericin in culture medium, which didn't affect the cell survival, was used for uptake time course study. Measurement of intracellular hypericin fluorescence levels showed an initial increase following by a slight decrease with incubation time.

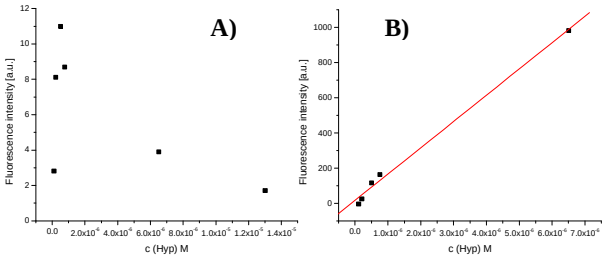

Figure 2: Saturation of isolated mitochondria with hypericin. A) Saturation of mitochondria with hypericin in PBS B) Mitochondria loaded with hypericin in DMSO.

Our results indicate that concentration of biological active monomeric form of hypericin could be significantly lower in comparison with overall amount of hypericin incorporated in mitochondria or cells.

Acknowledgement
This work was supported by the Agency for Promotion Research and Development under contract LPP-0337-06 and by Faculty of Science UPJS project No. VVGS-7/2008/F.

References
[1] T. A. Theodossiou, A. Noronha-Dutra, J.S. Horthersall, *The International Journal of Biochemistry& Cell*

Biology, 38 (2006) 1946-1956.
[2] P. Miskovsky, *Current Drug Targets*, 3 (2002), 55-84.
[3] A.B. Uzdensky, L.W. Ma, V. Iani, G.O. Hjortland, H.B. Steen, J. Moan, *Laser Med. Sci*., 16 (2001), 276-283.
[4] G. Siboni, H. Weitman, D. Freeman, Y. Mazur, Z. Malik, B. Ehrenberg, *Photochem. Photobiol. Sci.*, 1 (2002), 483-491.
[5] T. A. Theodossiou, M.D. Spiro, J. Jacobson, J.S. Hothersall, A.J. Mac Robert, *Photochem. Photobiol. Sci*., 80 (2004), 438-443.

B,

P16

Iterative deconvolution algorithms in confocal data reconstruction

Topor P.[1], Šrámek M.[2], Mateašík A.[3]

[1] Department of Nuclear Physics and Biophysics, FMFI UK, Mlynská dolina F1, 842 48 Bratislava, Slovakia, e-mail: peter.topor@fmph.uniba.sk
[2] Department of Applied Informatics, FMFI UK, Mlynská dolina, 842 48, Bratislava, Slovakia
[3] International Laser Center, Ilkovičova 3, 812 19 Bratislava, Slovakia

Introduction. Fluorescence confocal microscopy is a powerful technique for observing intracellular structural and metabolic details. Unfortunately, microscopy data is distorted by several types of signal degradation and noise sources. Deconvolution can be used to overcome or minimize most of these drawbacks [1]. Many known deconvolution algorithms are sensitive to proper PSF estimation and parameters specification.

Aim. To investigate influence of parameters of selected deconvolution algorithms on their behavior, to optimize their performace by means of measuring the image quality by wide-spread assessment criteria and to apply these tuned algorithms to fluorescence microscopy data.

Materials and Methods. The tested algorithms were: the Richardson-Lucy (R-L) algorithm for Poisson noise distribution (RLP), the R-L algorithm with Tikhonov-Miller regularization (RLPTM), the R-L algorithm with total variation regularization (RLPTV) and the R-L algorithm based edge preserving algorithm with 4 different regularization functions (RLEDGE1-4) [2]. Data format and used algorithms were based on an open-source project f3d [3].

In testing, artificial computer generated set was used , consisting of several voxelized three dimensional geometrical objects with controlled noise level and degraded by confocal microscope's PSF estimated using ImageJ (NIH) plugin (http://bigwww.epfl.ch/demo/deconvolution3D/). Real confocal data was scanned using the LSM 510 Meta (Zeiss) microscope with Plan Apochromat 100x/1,4 objective, Hoechst stained and excited with 405 nm UV laser. Data was provided by Dr. Farkaš (UEE SAV, Bratislava).

Performance of selected algorithms with different values of a regularization parameter λ (weighting factor) was evaluated using established image quality measures – the MSE (Mean Squared Error) and SSIM (Structural Similarity index). These measures were implemented according to [4].

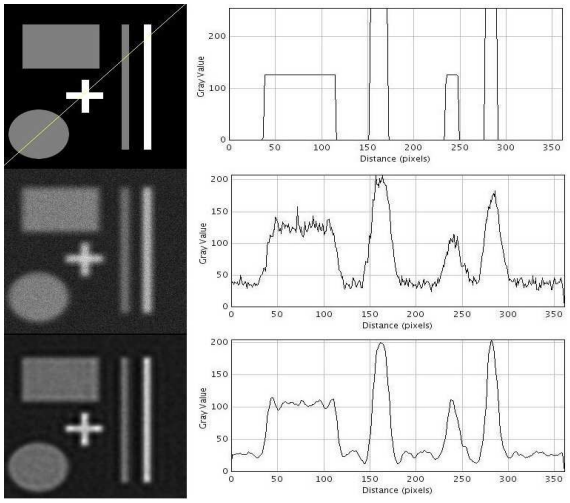

Fig. 1: Generated test data, z-axis central slice (top-left), cross section intensity lapse on line outlined (top-right). Blurred original data (middle-left) and its intensity cross section (middle-right). Deconvolved test data using RLP algorithm – 18 iterations (bottom row).

Results and Discussion. Deconvolved data showed reduced noise level for every algorithm. Distorted light intensities were assigned to their origin spots due to deconvolution more than in original data. Best deconvolution results for both measures were achieved using the RLEDGE3 algorithm. MSE was minimal for regularization parameter λ = 0,001, but SSIM was optimal for λ = 0,1. This difference showed a need for another – cross section intensities comparison, where the RLEDGE3 algorithm caused degradation of homogenous

intensity areas and its results were outperformed by the RLP algorithm. Our results indicate, that the MSE and SSIM measures alone are not robust enough for specification of optimal deconvolution parameters and optimal number of iterations. Further investigation in this area - such as proposal of different quality measurement criteria, is needed.

Confocal chromosomal data was deconvolved using the parameter optimized RLEDGE3 algorithm and the RLP algorithm. RLEDGE3 algorithm reassigned fluorescence to narrower bands with higher intensity values when compared to RLP. Results of both algorithms showed reduced noise level and significantly improved z-axis resolution - thus allowing us to distinguish fluorescent chromosomal structure bands, which were otherwise blurred by neighboring layers and noise. Such processed images are eligible for precise DNA cytometry, segmentation algorithms and further 3D cell model processing.

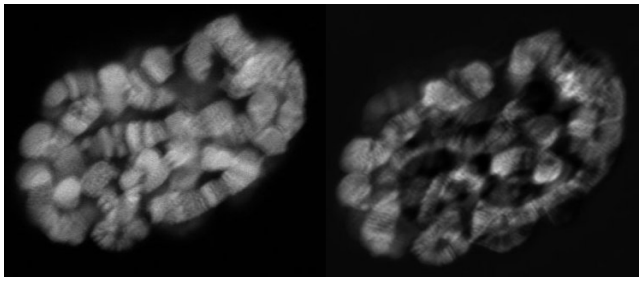

Fig. 2: Central slice of Drosophila melanogaster chromosomes, original data (left), deconvolved using RLP 18 iterations (right), Hoechst, LSM 510 Meta (Zeiss) 100x/1,4, 405 nm excitation. Dr. Farkaš (UEE SAV, Bratislava).

Conclusions. Deconvolution algorithms are important in fluorescence microscopy when dealing with noise and blurred data. Regularization parameters are noise- and specimen dependent and should be carefully investigated for each specific application.

Acknowledgement
This work was supported by the Agency for Promotion Research and Development under the contract No. APVV-20-056105 and by the Comenius University under the contract No. UK/374/2007.

References

[1] Pawley B.(ed.) (2006), Handbook of biological confocal microscopy, 3rd edition, Springer.
[2] Zimányi M. (2006), Model based reconstruction for volume visualization, *PhD thesis*, Comenius University, Bratislava.
[3] Šrámek M., Dimitrov L.I., Straka M., Červeňanský M. (2004), The f3d tools for processing and visualization of volumetric data, *Journal of Medical Informatics and Technologies.*
[4] Begin I., Ferrie F.P. (2006), Comparison of Super-Resolution Algorithms Using Image Quality Measures, *Proceedings of the 3rd Canadian Conference on Computer and Robot Vision.*

P17

A CD spectroscopy study of the formation of guanine quadruplexes by DNA aptamers that selectively bind thrombin at different exosites.

S. Poniková[1], M. Antalík[2,3], T. Hianik[1]

[1] Department of Nuclear Physics and Biophysics, FMFI UK, Mlynská dolina F1, 842 48 Bratislava, Slovakia, e-mail: slavomira.ponikova@gmail.com

[2] Department of Biophysics, Institute of Experimental Physics, SAS, Watsonova 47, Kosice, 040 01, Slovakia

[3] Department of Biochemistry, Faculty of Science, P.J. Safarik University, Moyzesova 11, Košice, 041 54, Slovakia

Thrombin is a multifunctional serine protease with procoagulant and anticoagulant functions. Because of its pivotal role in both thrombosis and hemostasis, thrombin is a major target for anticoagulant and cardiovascular diseases therapy. A novel approach in thrombin activity regulation is based on its interaction with DNA aptamers. The first aptamer developed for thrombin was reported in paper by Bock et al. [1]. This aptamer is composed of 15 nucleotides of the sequence 5'-GGT TGG TGT GGT TGG-3' (FIBRI) and specifically binds thrombin at its fibrinogen binding site [2]. Later, Tasset et al. [3] developed longer DNA aptamer against heparin binding site of the thrombin of following basic sequence: 5'-A GTC CGT GGT AGG GCA GGT TGG GGT GAC T-3'. The underlined part (HEPA) corresponds to the binding motif of this aptamer that is also composed of 15 nucleotides. A unique peculiarity of these aptamers is formation of specific binding motif composed of guanine quadruplex. This is shown on figure below where the structures of FIBRI and HEPA are presented. It is seen that quadruplex consists of two guanine quarters that are stabilized by cyclic hydrogen bonds and connected by specific loops. In the case of FIBRI there are two TT loops and one TGT loop, while for HEPA T_4 is substituted by A_4 and GCA replaces TGT loop. It has been suggested, that substitutions of nucleotides in the loops of HEPA should have unfavorable structural consequences on quadruplex formation and additional stabilizing factors of flanked sequences of spacers and duplex in 29-mer are necessary in order to provide stability of quadruplex core [3, 4]. However, this assumption has not been confirmed so far experimentally.

In this work we performed comparative analysis of the properties of G-quadruplex in FIBRI and HEPA by means of CD spectroscopy at presence of potassium and sodium ions. In the first series of experiments we measured the CD spectra of the two aptamers at presence of various concentrations of potassium ions. In absence of potassium, CD spectra showed low band amplitudes, indicating small content of guanine quadruplexes. With increasing K^+ concentration the amplitude of positive and negative bands increased. The sharp maximum at 292 nm and deep minimum around 267 nm indicates formation of antiparallel guanine quadruplex [5]. Presence of sodium ions in a concentration of 140 mM has unfavorable effect on binding of potassium for HEPA, whereas FIBRI-K^+ complex were only slightly affected. In spite of hindered interaction of aptamer with potassium at presence of sodium ions, HEPA aptamers form stable guanine quadruplexes at higher potassium concentrations. We have shown that the substitution of certain nucleotides in HEPA by purines and absence of flanked

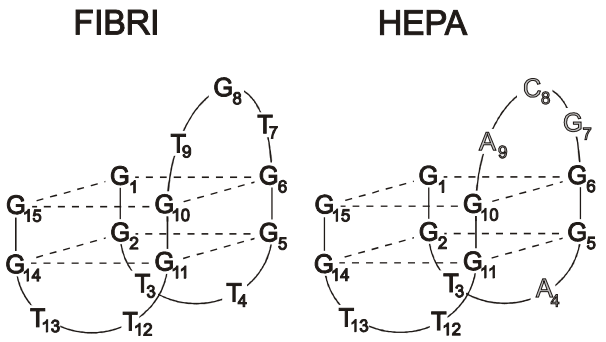

Figure 1: Structures of FIBRI and HEPA aptamer binding motifs

sequences did not disrupt formation of high ordered guanine quadruplexes at presence of potassium ions. From quantitative analysis of aptamers folding we estimated dissociation constants and determined changes in Gibbs energy. These values showed slightly lower stability of HEPA-K^+ complexes in comparison with those for FIBRI.

For further comparative analysis of the stability of both aptamers we investigated their thermal stability from CD melting profiles at presence of either sodium or potassium or both cations. The plot of the amplitude of ellipticity at 292 nm as a function of temperature for both aptamers has sigmoidal shape and with increasing of the temperature the CD magnitudes decreased. At 50 mM KCl, the results of thermal melting analysis indicate slightly higher thermal stability of FIBRI-K^+ in comparison with HEPA-K^+ complex. Presence of sodium ions caused decrease of melting temperature and changes in van't Hoff entalpy of both aptamer – potassium complexes. However, larger unfavorable influence of Na^+ on the stability of HEPA-K^+ complex was observed. Decrease in thermal stability at presence K^+ and Na^+ ions is probably caused by competition between these two cations.

Different thermodynamic properties of both aptamers follow also from analysis of their transition temperatures as a function of aptamer concentrations. We observed increase of T_m with increasing HEPA concentration, but for FIBRI the T_m value did not depend on aptamer concentration. This phenomenon for FIBRI was reported earlier and suggests that this aptamer is in monomer form at wide concentration range [6, 7]. This suggests different behavior of both aptamers in solution. While FIBRI is in monomeric form at rather wide concentration range, the HEPA forms aggregates at higher concentrations that could stabilize quadruplex structure.

Acknowledgement
This work was supported by European Commission 6 FP program STREP DVT-IMP (Contract No. FP6-2005-034256), by the Slovak Grant Agency (Projects No. 2/6167/06 and 1/4016/07) and by Comenius University (Project No. UK /368/2007).

References

[1] L.C. Bock, L.C. Griffin, J. A. Latham, E. H. Vermaas, J. J. Toole, *Nature* 355 (1992) 546-566.
[2] Q. Wu, M. Tsiang, J.E. Sadler, *J. Biol. Chem.* 34 (1992) 24408-24412.
[3] D.M. Tasset, M.F. Kubik, W. Steiner, *J. Mol. Biol.* 272 (1997) 688-698.
[4] M. Tsiang, C.S. Gibbs, L.C. Griffin, K.E. Dunn, L.K. Leung, *J. Biol. Chem.* 270 (1995) 19370-19376.
[5] M. Lu, Q. Guo, N.R. Kallenbach, *Biochemistry* 32 (1993) 598-601.
[6] B.I. Kankia, L.A. Marky, *J. Am. Chem. Soc.*123 (2001) 10799-10804.
[7] Ch-F. Tang, R.H. Shafer, *J. Am. Chem. Soc.* 128 (2006) 5966-5973.

P18

Magnetic beads-based electrochemical nucleic acids and protein sensing strategies

M. Fojta[1], L. Havran[1], P. Horáková[1,2], H. Pivoňková[1], S. Hasoň[1], P. Kostečka[1], J. Vacek[1], K. Němcová[1], E. Paleček[1]

[1] Institute of Biophysics, v.v.i., Academy of Sciences of the Czech Republic, Kralovopolska 135, CZ-612 65 Brno, Czech Republic, e-mail: fojta@ibp.cz
[2] Department of Analytical Chemistry, Faculty of Chemical Technology, University of Pardubice, nam. Cs. legii 565, CZ-532 10 Pardubice, Czech Republic

Magnetic particles coated with various biorecognition elements (such as antibodies, oligonucleotides, streptavidin, etc.) have proved to be powerful tools for specific capture and separation of biomolecules [1]. In connection with electrochemical detection, the magnetic beads have successfully been applied in analysis of nucleotide sequences, antibody-antigen, aptamer-ligand or DNA-protein interactions, chemical modification of DNA, monitoring of DNA *in vitro* synthesis etc. Contrary to electrochemical biosensors comprising an electrode modified with the biorecognition layer, in the magnetic beads-based (double-surface, DS) techniques the interaction and detection steps are performed on different surfaces. One interacting partner (e.g., capture DNA probe or antibody) is anchored to the magnetic beads. The beads possess large surface and offer efficient accumulation and separation of the target molecules. Then, optimum detection electrodes and electrochemical methods can be chosen only with respect to properties of the target molecule. A variety of DS techniques have been proposed to detect DNA hybridization and/or mutations in nucleotide sequences. These approaches include label-free determination of purine bases at mercury, amalgam or carbon electrodes, DNA labeling with electrochemically active osmium complexes, enzymes, nanoparticles or carbon nanotubes [1]. A novel DNA labeling strategy has recently been proposed, based on synthesis of deoxynucleoside triphosphate conjugates with various electroactive moieties (such as ferrocene [2], amino or nitro phenyl groups [3]) and incorporation of the modified nucleotides into DNA by DNA polymerases. Similar DS techniques have been employed in ultrasensitive electrochemical immunoassays as well as in monitoring DNA-protein interactions [4].

Acknowledgement
This work was supported by GACR (203/07/1195), GA ASCR (IAA500040701) and MEYS CR (LC06035).

References

[1] E. Palecek, and M. Fojta, *Talanta* 74 (2007) 276-290.
[2] P. Brazdilova, M. Vrabel, R. Pohl, H. Pivonkova, L. Havran, M. Hocek, and M. Fojta, *Chem-Eur. J.* 13 (2007) 9527-9533.
[3] H. Cahova, L. Havran, P. Brazdilova, H. Pivonkova, R. Pohl, M. Fojta, and M. Hocek, *Angew. Chem. Int. Ed.* in press (2008).
[4] M. Masarik, K. Cahova, R. Kizek, E. Palecek, and M. Fojta, *Anal. Bioanal. Chem.* 388 (2007) 259-270.

P19

Formation of thin lipid films on glassy carbon, gold and Si/SiO_2 wafers by the method of electrostriction

M. Karabaliev

Department of Physics and Biophysics, Faculty of Medicine, Trakia University, 11 Armeiska, Stara Zagora 6000, Bulgaria, e-mail: mi_karabaliev@abv.bg

Solid-supported lipid films have proved very useful both as biomembrane mimetic analogs and as a basis for electrode modifications in the construction of sensor devices [1]. The films are prepared in quite different manner, including liposome spreading, self-assembly, Langmuir-Blodgett (LB), transfer of lipid monolayers from air/water interface to a hanging mercury drop electrode surface or cast film technique [2 and refs. therein].

Alternative methods of formation are achieved through successive thinning of layers of lipid material deposited directly onto the solid substrate [1, 3]. The films in this work are prepared from forming solution containing natural lecithin dissolved in n-hexane - with concentration 10 mg/ml. This film-forming solution is placed above an electrolyte solution (0,1M KCl). With an electrode immersed into the film-forming solution of lipids two interfaces are formed: 1) lipid solution/electrode interface; and 2) electrolyte/lipid solution interface. Due to the amphiphylic nature of the lipid molecules a spontaneous lipid adsorption begins and generation of ordered molecular structures in the form of self-assembled monolayers on the two phase boundaries takes place. Thereafter, the development of a thin wetting film is achieved gradually approaching the above-mentioned interfaces one to another. The process of film thinning starts with their contact. The thicknesses of these self-thinned films in most cases are of the order of 100-200 Å when glassy carbon or gold are used as solid supports. Films formed on the SiO_2 surface of a Si/SiO_2 wafer are usually 500-1000 Å thick.

Additional thinning of these wetting films and preparation of monolayer or bilayer lipid films is achieved by the method of electrostriction. An external electrical voltage U is applied to the self-thinned lipid films. The electrostriction generates additional external pressure P that leads to the thinning of the film. This forced process of thinning stops at a new equilibrium film thickness when equilibration of the film disjoining pressure $\Pi(h)$ with the pressure P caused by electrostriction is achieved, i.e [4]:

$$\Pi = P = \frac{\varepsilon_0 \varepsilon_l U_{LF}^{\ 2}}{2h^2} \qquad (1)$$

Here U_{LF} is the external potential on both sides of the lipid film; h is the film thickness obtained from the film capacitance value; ε_l is the dielectric constant of the film; ε_0 (8.8542×10^{-12} F/m) is the permittivity of free space.

Depending on the type of the solid support different characteristics of the external potential are necessary for obtaining stable mono- or bilayer films.

Representative results for glassy carbon (GC) are shown in Fig. 1. As seen from the figure the process of thinning undergoes three different stages: 1) a stage where the changes in the thickness of a "thick" film are reversibly dependent on the applied potential, 2) a stage where the film spontaneously undergoes an irreversible transition to a new stable state and 3) a stage where the applied potential practically does not change the thickness. Thus using electrostriction caused by DC-potential with voltage in the range above +0,7 V vs. Ag/AgCl a stable thin lipid film is obtained. According to the estimated thickness and bearing in mind the hydrophobicity of GC the type of these films could be considered as monolayer.

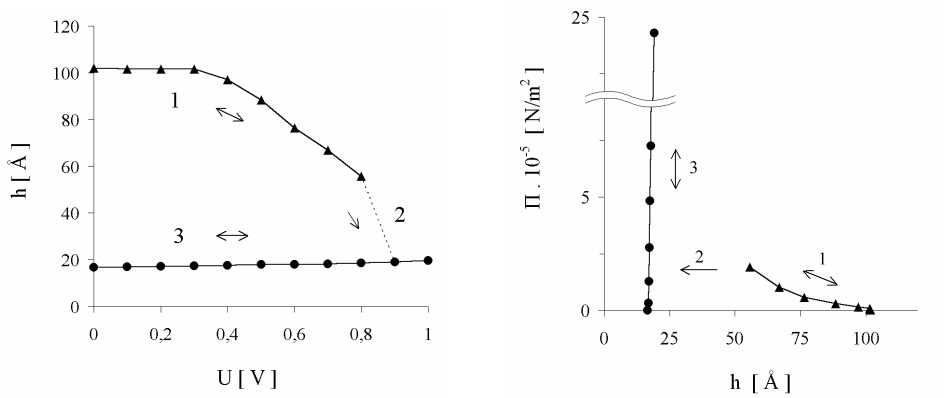

Fig.1. a) Dependence of the apt film thickness *h* on the applied DC-potential (vs. Ag/AgCl) for film on glassy carbon; b) isotherm of the disjoining pressure Π(*h*), obtained from the results in fig.1a and from eq.1.

In the case of gold electrode the picture is qualitatively the same. However much smaller value of the DC-potential of the order of +0,2 to +0,3 V vs. Ag/AgCl is sufficient to obtain films with apparent thickness of 20 to 30 Å.

Completely different is the case of films on Si/SiO_2 wafers, subjected to electrostriction. The use of DC-potentials of up to +2V does not allow the thinning of the films and they remain with thickness of the order of 500-1000 Å. However if the films on Si/SiO_2 are subjected to electrostriction with AC-voltage, they undergo the transition to stable films with thickness of 30-40 Å. The amplitude of the AC-voltage that is sufficient for this transition is 0,4V peak-to peak, at frequency 1200 Hz. All this could be explained taking into account the impedance of the SiO_2 dielectric layer. In the case of conducting supports, such as the GC and the gold, the impedance of the electrode/lipid film interface is smaller than the film impedance and could be neglected. With Si/SiO_2 the potential U_{EXT} applied between the Si/SiO_2 and the reference Ag/AgCl electrode is distributed between the lipid film and the SiO_2 dielectric layer, so that $U_{EXT}=U_{LF}+U_{SiO2}$. The ratio of the voltage drops U_{LF} and U_{SiO2} depends on the ratio of the impedances, $U_{LF}/U_{SiO2}=Z_{LF}/Z_{SiO2}$. At zero frequency or DC potential the current is passing through the resistive parts of the impedances, so $U_{LF}/U_{SiO2}=R_{LF}/R_{SiO2}$. Because $R_{LF}<<R_{SiO2}$, it follows that $U_{LF}<<U_{SiO2}$, and respectively $U_{LF}<<U_{EXT}$. Thus the applied DC-voltage is mainly located on the SiO_2 dielectric layer and the electrostriction on the lipid layer is not sufficient enough. At high frequencies of the applied voltage the current is passing mainly through the capacitive parts of the impedances, so that $U_{LF}/U_{SiO2} \approx C_{SiO2}/C_{LF}$. Since $C_{SiO2} \approx 2$ μF/cm^2 *and* C_{LF}=0,01 to 1 μF/cm^2 it follows that for the whole range of film thicknesses and especially for the thicker films the applied voltage is located on the lipid film.

Conclusions. By the aid of electrostriction substantial thinning of the films could be achieved. Depending on the type of the support different frequencies and amplitudes of the applied potentials could be used in order to prepare lipid films of mono- or bilayer type.

References

[1] T. Hianik, *Rev. Mol. Biotech*. 74 (2000) 189-205.
[2] S. Heyse, T. Stora, E. Schmid, J.H. Lakey, H. Vogel, *Biochim. Biophys. Acta* 1376 (1998) 319.
[3] V. Kochev, M. Karabaliev, *Adv. Coll. Interface Sci*. 107 (2004) 9
[4] P.M. Krugliakov, Y.G. Rovin, *Physical chemistry of black hydrocarbon films. Bimolecular lipid membranes*, Nauka, Moscow, 1978.

P20
Development of biosensor with aptamer as bio-recognition element for QCM detection of IgE

M. Šnejdárková[1], L. Bábelová[1], V. Polohová[1], T. Hianik[2]

[1] Institute of Animal Biochemistry and Genetics SAS, 900 28 Ivanka pri Dunaji, Slovakia ,
[2] Department of Nuclear Physics and Biophysics, FMFI UK, Mlynská dolina F1, 842 48 Bratislava, Slovakia
e-mail: Maja.Snejdarkova@savba.sk

Allergic diseases concern approximately 30% of population and thus become a serious clinical as well as social problem. Ishizaka et al. [1] discovered the presence of immunoglobulin E (IgE) in human serum. Concentration of IgE in a blood of healthy adults is between 240-290 $ng.ml^{-1}$, whereas a substantial increase of IgE concentration is observed in allergen sensitive patient. IgE plays a central role not only in the mechanisms of the allergic diseases but also in mammalian defense system against parasites [2]. Therefore for the purpose of medical diagnosis the demand exist on development direct, simple and low cost method of IgE detection. For the clinical detection of IgE the ELISA test based on antibodies against IgE is typical [3]. In this case the anti-IgE should be labeled by enzyme. The alternative route for IgE detection is those using DNA aptamers [4]. Aptamers are short single-stranded nucleic acids (15-60 nucleotides), specifically generated by SELEX method against a wide variety of targets ranging from small molecules to macromolecules [5]. Aptamers bind their targets with high specificity comparable to those of antibodies. This peculiarity make them valuable tool for molecular recognition. The effectivity of the ligand detection by aptamer depends on the method of aptamer immobilization [6,7]. It is also important to use the method of immobilization that could provide sufficient stability of the sensor and possibility of its regeneration.

The dendrimers are a new class of polymers and their specific structure makes them suitable for the variety of bioanalytical applications [8,9]. They can be synthesized of various dimensions and with various chemical modifications. For example, the first generation (G1) PAMAM dendrimer (2.2 nm in diameter) possesses 8 terminal amine groups, whereas fourth generation (G4) PAMAM dendrimer contains 64 terminal amine groups. G4 has almost globular shape with a diameter of about 4.5 nm. Furthermore, functional groups found at the surface of dendrimers have remarkably higher chemical reactivity in comparison to their activity when present in other macromolecules. Due to a large number of available active groups on dendrimers it is possible to immobilize on their surface larger number of biomolecules in comparison with a flat surface.

We developed a quartz crystal biosensor using model system with human IgE as the analyte and DNA aptamer as immobilized receptor. The poly(amidoamine) (PAMAM) dendrimers of fourth generation (G4) and 1-hexadecanethiol (HDT) has been used for formation of self assembled monolayers on a gold surface for preparation of aptamer-based QCM biosensor. We combined the special properties of dendrimers with the SAMs concept to prepare the highly sensitive sensing surface on a gold-coated chip. Dendrimer terminated with the amino groups was used to anchor receptor, while the thiol chains serve as the stabilizing components. The advantage of this architecture in comparison to SAMs is higher local concentration of the terminal groups near the sensor surface, which can be functionalized. The biotinylated DNA aptamer was anchored on a surface of G4-HDT layers covered by neutravidin molecules. Neutravidin was crosslinked with PAMAM dendrimers via glutaraldehyde. The most important step in the immobilization procedure was reducing the Shiff base. The detection limit was of 100 ng/ml IgE. In addition, the aptamer receptors tolerated repeated layer regeneration after analyte binding and recycling of the biosensor with little loss of sensitivity [10].

In conclusion, we could show the suitability of DNA aptamer receptor on biosensor for sensitive and specific IgE detection. The determination of IgE alone will not predict an allergic state, since genetic and environmental factors also play an important role in the expressions of clinical symptoms.

Acknowledgements
This work was supported by European Commission 6 FP program NoE NeuroPrion (Contract No. FOOD-CT-2004-506579), by Agency for Promotion Research and Development under the contract No. APVV-20-P01705 and by the Slovak Grant Agency (Projects No. 2/7134/7 and 1/4016/07). We are grateful to Prof. M. Thompson for generous gift of flow cell.

References
[1] K. Ishizaka, H. Tomioka, T. Ishizaka, *J. Immunol* 105 (1970) 1459-1466.
[2] A.S. Gouni, B. Lamkhioued, K. Ochiai, Y. Tanaka, E. Delaporte, *Nature* 367 (1994) 183-186.
[3] M.P. Kreuzer, P.O´ Sullivan, M. Pravda, G.G. Guilbault, *Anal. Chem. Acta* 442 (2001) 45-53.
[4] M. Liss, B. Petersen, H. Wolf, E. Prohaska, *Anal. Chem*. 74 (2002) 4488-4495.
[5] S.D. Jayasena, *Clinical Chemistry* 45 (1999) 1628-1650.
[6] T. Hianik, V. Ostatná V, M. Sonlajtnerova, I. Grman, *Bioelectrochemistry* 70 (2007) 127-133.
[7] A. Bini, M. Minunni, S. Tombelli, C. Centi, M. Mascini, *Ana.l Chem.* 79 (2007) 3016-3019.
[8] D.A .Tomalia, A. Naylor, W.A. Goddard III, *Angew. Chem. Int. Engl*. 29 (1990) 138-175.
[9] L. Svobodová, M. Šnejdárková, T. Hianik, *Anal. Bioanal. Chem* .373 (2002) 735-741.
[10] M. Šnejdárková, L. Svobodová, V. Polohová, T. Hianik, *Anal. Bioanal. Chem* .390 (2008) 1087-1091.

P21

Biosensor based on aptabodies and carbon nanotubes – new tool for detection proteins

T. Hianik[1], A. Porfireva[1,2], I. Grman[1], G. Evtugyn[2]

[1] Department of Nuclear Physics and Biophysics, FMFI UK, Mlynská dolina F1, 842 48 Bratislava, Slovakia, e-mail: igor.grman@gmail.com

[2] Department of Analytical Chemistry, Kazan State University, 18 Kremlevskaya Street, Kazan, 42008, Russian Federation

DNA/RNA aptamers are in vitro synthesized single stranded nucleic acids with high affinity to proteins or to other low and macromolecular compounds, which is comparable with affinity of antibodies. So far used aptamers were based on single stranded DNA, thus had only one binding site for the ligand. Here we report simple method of molecular engineering based on known properties of DNA to hybridize in solution with complementary strand. We designed so-called aptabodies that in contrast with traditional aptamers contains two binding sites.

We used novel thickness shear mode acoustic methods (TSM) for characterization of the properties of the aptamers at the surface. This method has been recently applied for detection IgE aptamer interaction [1]. The electrochemical quartz crystal microbalance (EQCM) was used for preparation of carbon nanotube layers (MWNTs) by electropolymerisation and for detection thrombin – aptamer interactions [2]. We prepared also neutravidin layers chemisorbed at gold for immobilisation of biotinylated aptamers. We used known aptamer that bind thrombin in its fibrinogen binding site: 5'- GGT TGG TGT GGT TGG TTT TTT TTT TTT TTT 3'-BIOTIN. Hybridization of this aptamer with complementary supporting part: 3'- GGT TGG TGT GGT TGG AAA AAA AAA AAA AAA 5' resulted in formation of aptabody.

The layers with immobilized aptabody were thicker due to different conformation of single and double stranded aptamers. This suggests that aptabodies are oriented normally to the surface while single stranded aptamers had no preferred orientation. Addition of thrombin resulted in decrease of resonance frequency, which saturated at larger thrombin concentrations (100 nM). These changes were higher for aptabody in comparison with single stranded aptamer. Using Hill plot we determined the binding constant for aptabody: $(2.7\pm 0.4)\times10^{-4}$ and for single stranded aptamer: $(5.8\pm1.3)\times10^{-3}$, which suggest stronger binding of thrombin to aptabodies. The limit of detection (LOD) of thrombin for aptabody was 0.3 nM, while 0.9 nM for single stranded aptamer. The LOD for aptamers immobilized on neutravidin layer was much higher: 4 nM [3].

The nanofabricated sensors based on aptabody and MWNTs allowed us to detect thrombin with detection limit 3 times better in comparison with conventional single stranded aptamer. The results obtained by TSM method confirmed assumption on different configuration of single stranded aptamers and aptabodies at the surface.

Acknowledgement

This work was supported by European Commission under FP6 (DVT-IMP, IST-034256), by the Slovak Grant Agency (Project No. 1/4016/07) and by Russian Foundation for Basic Research (grant 06-03-32217).

References

[1] A. Porfirieva, G. Evtugyn, T. Hianik, *Electroanalysis* 19 (2007) 1915 – 1920.

[2] M. Šnejdárková, L. Svobodová, V. Polohová, T. Hianik, *Anal. Bioanal. Chem* .390 (2008) 1087-1091.

P22

Effect of acetylsalicylic acid on platelet aggregation in condition of in vitro induced hypercholesterolemia

Z. Kaderjáková[1], P.Grešner[2], C.Watala[2], L. Šikurová[1], I. Waczulíková[1]

[1] Department of Nuclear Physics and Biophysics, FMFI UK, Mlynská dolina F1, 842 48 Bratislava, Slovakia, e-mail: zuzana.kaderjakova@gmail.com,

[2] Department of Haemostasis and Haemostatic Disorders, Medical University of Lodz, Medical University Hospital No. 2, 113 Zeromskiego Street, 90-549 Lodz, Poland

Introduction

Several studies have confirmed relationship between hypercholesterolemia and increased platelet responsiveness to aggregation stimuli [1, 2]. The most common drug used to avoid potential complications resulting from platelet hyper-reactivity is Aspirin® (acetylsalicylic acid, ASA). However, it was observed that non-negligible part of patients with hypercholesterolemia shows reduced sensitivity to Aspirin® - a phenomenon called aspirin resistance [3]. The aim of this study was to investigate 1) the effect of enriching or depleting human platelets with cholesterol on their aggregation and 2) the responsiveness of these platelets to ASA. Since the ways of evaluation of aggregation curves vary considerably between different institutions [4], another goal of this study was to define which parameters of aggregation curves are affected in this kind of experiments and so need to be evaluated.

Materials and methods

Blood from healthy donors was withdrawn from peripheral vein into plastic syringes containing CTAD anticoagulant at 9:1 ratio. Isolated platelets were dissolved in Thyrode`s buffer up to a concentration of 3.10^8 ml^{-1}. Change in the cholesterol membrane content in platelets was induced by their incubation with Large Unilamellar Liposomes prepared by Extrusion Technique (LUVET) with 10% and 70% cholesterol to phospholipids mole ratio, for up to 2 hours [5]. Platelet function tests were performed on optical aggregometer Chronolog 490-2D, using two aggregation agents: collagen (2 µg/ml) and arachidonic acid (0.5 mmol/ml). ASA was added at final concentration of 7.5 and 15 µg/ml. Following 6 parameters, which characterise the shape of aggregation curve, were analyzed: lag phase, maximal aggregation, slope, time to achieve 10% of maximal aggregation, time to achieve 90% of maximal aggregation and time between 10 and 90% of maximal aggregation.

Results

We found out that maximal aggregation of the cholesterol-depleted platelets when stimulated by collagen was decreased compared with cholesterol-enriched platelets and control. Friedman statistical test yields significant differences in 4 of the 6 curve parameters: lag phase, maximal aggregation, slope and time to achieve 10% of maximal aggregation ($p < 0.05$, $n = 5$). apparent. Friedman statistical test showed significant differences only in 2 curve parameters: time to achieve 90% of maximal aggregation and time between 10 and 90% of maximal aggregation ($p < 0.05$, $n = 4$).

After incubation with ASA we observed that the cholesterol-enriched platelets were more resistant to inhibitory effect of ASA than the cholesterol-depleted ones. Statistically significant differences were found for these 3 parameters: maximal aggregation, time to achieve 90% of maximal aggregation and time between 10 and 90% of maximal aggregation ($p < 0.05$, $n = 5$). The same results were obtained also with final ASA concentration of 15µg/ml. Nevertheless, when we used arachidonic acid to induce the aggregation, results were not reproduced. The same experiment was performed with arachidonic acid as

aggregation agent instead of collagen, but differences between maximal aggregation of the cholesterol-enriched and cholesterol-depleted platelets were less

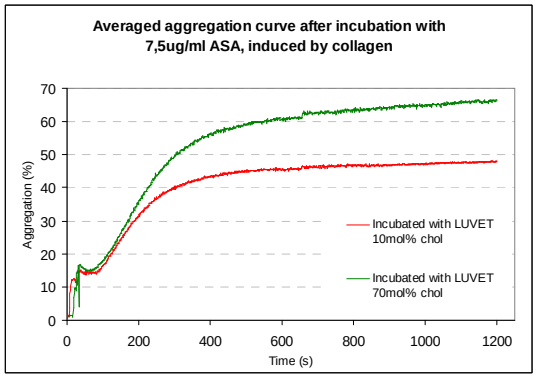

Figure 1 Collagen-stimulated aggregation of the cholesterol-enriched and cholesterol-depleted platelets

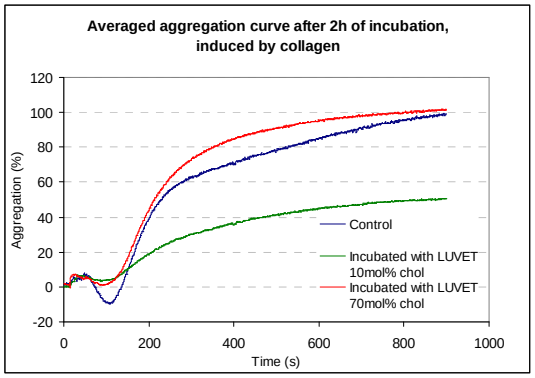

Figure 2. Aggregation curves of cholesterol-enriched and cholesterol-depleted platelets after 10 minutes of incubation with ASA

Discussion

Our results obtained with collagen as aggregation agent in the condition of LUVET-induced hypercholesterolemia are consistent with the findings reported in other studies dealing with membrane-cholesterol influence on the platelet aggregation process [5]. Reduced cholesterol influence on the platelet aggregation when induced by arachidonic acid may be explained by the fact that this kind of activation is not triggered by a receptor –ligand interaction [6] thus, it is not directly affected by the cholesterol content in the platelet membrane. Regarding experiments with ASA, our results support the works reporting potential association between hypercholesterolemia and reduced sensitivity of platelets to this drug [7].

Acknowledgement

This work was supported by the NATO Cooperative Linkage Grant CBP.NUKR.CLG 981884, the Slovak Grant Agency VEGA, project No. 1/3037/06, and by Grant UK Bratislava.

References

[1] D. Baldassarre, N. Mores, S. Colli, F. Pazzucconi, C.R. Sirtori, E. Tremoli, *J. Clinical Pharmacology and Therapeutics* 61 (1997) 684-691
[2] A.B. Sobol, C. Watala, *Diabetes Research and Clinical Practice*, 50 (2000) 1-16.
[3] M. Friend, I. Vucenik, M. Miller, *BMJ*, 326 (2003) 82-83.
[4] K.A. Moffat, M.R. Ledford-Kraemer, W.L. Nichols, C.P.M. Hayward, *J.Thromb. Haemost*. 93 (2005) 549-553
[5] S.J. Shattil, R. Anaya-Calindo, J. Bennett, R.W. Colman, R.A. Cooper, *J. Clinical Investigation*, 55 (1975) 636-643.
[6] D.A. Yardumian, I.J. Mackie, S.J. Machin, *J. Clin. Pathol*. 39 (1986) 701-712
[7] M. Boncler, P. Gresner, M. Nocun, J. Rywaniak, M. Dolnik, J. Rysz, R. Wilk, M. Czyz, K. Markuszewski, M. Banach, C. Watala, *Biochim. Biophys. Acta*, 1770 (2007) 1651-1659

P23

Spectroscopic method in the testing of pharmacologically active compounds on mitochondrial function.

M. Kardošová[1], O. Uličná[2], O. Vančová[2], B. Klajnert[3], L. Šikurová[1], I. Waczulíková[1]

[1] Department of Nuclear Physics and Biophysics, Division of Biomedical Physics, Faculty of Mathematics, Physics, and Informatics, Comenius University, Bratislava, Slovakia, , e-mail: mirkakardosova@gmail.com
[2] Pharmacobiochemical Laboratory Department of Internal Medicine, Faculty of Medicine, Comenius University, Bratislava, Slovakia
[3] Department of General Biophysics, University of Lodz, Banacha 12/16, 90-237 Lodz, Poland

Introduction:

Mitochondria play an important role in cellular metabolism, respiration and production of ATP essential for the normal function of all human organ system. Their membranes, like all biomembranes, are constituted by a lipid bilayer whose components exhibit a certain degree of static order and a variety of motional dynamics. The physical state of the membrane components is crucial for optimal function of mitochondrial membranes and it is also known that some important biophysical parameters can be evaluated by spectroscopic methods [1, 2]. Since mitochondrial membranes can be directly or indirectly influenced by the action of various compounds and since they contain several endogenous fluorophores, spectroscopy can be a useful tool to study biocompatibility of artificially synthesized compounds.

In our study we focused on dendrimers which represent a new class of highly branched treelike polymers whose interior cavities and multiple end groups make them suitable for targeting and delivery of pharmaceutical ingredients [3,4]. Our aim was to investigate an *in vitro* interaction between poly(amidoamine) (PAMAM) dendrimers, generations 4 (G4) and 2 (G2), and mitochondrial membranes isolated from liver of rats. To characterize the investigated system, we measured absorption and fluorescence spectra as well as fluorescence anisotropy of a fluorescent dye 1,6-diphenyl-1,3,5-hexatriene (DPH) in the suspension of mitochondrial membranes and the dendrimers.

Materials and methods:

We used 13 male Wistar rats weighing 220 – 270g. Rat livers were removed after decapitation and subsequently the mitochondrial membranes were isolated. To adjust the concentration and evaluate autofluorescence of the mitochondrial membranes, we measured emission spectra at several excitation wavelengths. Fluorescence anisotropy measurements were performed with a PerkinElmer spectrofluorimeter LS45 using DPH at a final concetration of 0.25 µmol/l. The mitochondrial suspensions were mixed with dendrimers dissolved in an isolation medium at the concentrations: c_1 = 0.5 µmol/l, c_2 = 2 µmol/l for G4, and c_1 = 5 µmol/l, c_2 = 10 µmol/l for G2. After addition of DPH the samples were incubated at 21 ± 1ºC for 30 minutes to allow complete incorporation of the probe into the membranes. DPH as a hydrophobic molecule incorporated into the hydrocarbon inside of the membranes in approximately 20 minutes. Upon illumination at 360 nm excited DPH molecules subsequently decay and the extent to which the total emitted light (detected at 425 nm) is polarized depends on the extent of molecular reorientation during the lifetime of the excited state, which in turn depends on the size, shape, and environment of the reorienting DPH molecule. A high degree of fluorescence anisotropy is assumed to indicate a high degree of structural order of the membrane. The steady-state fluorescence anisotropy is expressed as follows:

$$r = \frac{I_{\parallel} - I_{\perp} \cdot G}{I_{\parallel} - 2I_{\perp} \cdot G}$$

where G is an instrumental correction factor, $I_{\parallel}$ and $I_{\perp}$ are respectively the emission intensities with polarizers parallel and perpendicular to the direction of the polarized exciting light. Data were statistically evaluated with two way analysis of variance. Multiple comparisons were made by Tukey test.

Results and Discussion

The data in all groups were approximately normally distributed (Fig. 1).

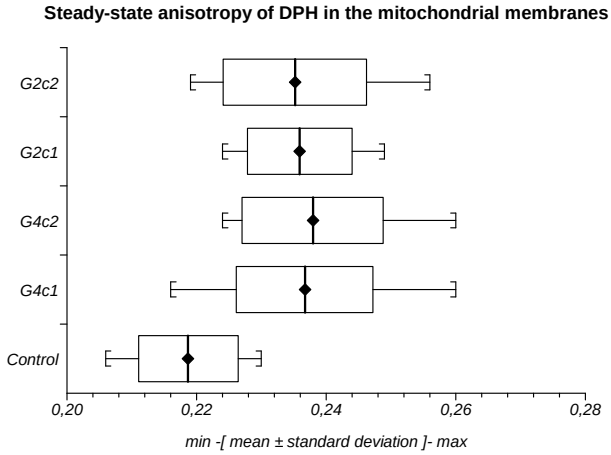

Fig.1.

We found that DPH fluorescence anisotropy values corrected for the effects of background noise were significantly increased in all the samples of mitochondria incubated with G4 or G2 dendrimers when compared to the non-incubated control membranes ($p<0.001$). The effect of dendrimer concentration was not observed ($p>0.05$). Analysis of the excitation and emission spectra pointed to a complex character of the signal recorded from DPH. Besides structural order of the influenced membranes also other parameters, such as membrane curvature, surface charge, as well as membrane-protein availability and movement, might be altered. Although we cannot ascribe the changes in fluorescence anisotropy of DPH purely to the changes in the order of membrane components, we could expect a direct interaction of PAMAM dendrimers with the polar head groups of membrane phospholipids, since molecular interaction typically leads to an increase in the polarization signal. This interaction occurred without deranging membrane integrity, however, mitochondrial function was already compromised (data not shown).

In conclusion, spectroscopy can be a valuable additional method to commonly used tests for assessing biocompatibility of various pharmacologically interesting compounds.

Acknowledgement

This work was supported by the Slovak Grant Agency VEGA, projects No. 1/3037/06, No. 1/3442/06, and by grant APVT 51-027404.

References

[1] I. Waczulikova, D. Habodaszova, M. Cagalinec, M. Ferko, O. Ulicna, A. Mateasik, L. Sikurova, A. Ziegelhoffer, *Can J Physiol Pharmaco*, 85 (2007) 372-381.
[2] B.A. Scalettar, J.R. Abney, Ch.R Hackenbrock, *PNAS USA*, 88 (1991) 8057-8061.
[3] B. Klajnert, M. Bryszewska, *Acta Biochimica Polonica* 48 (2001) 199-208.
[4] S. Svenson, D.A. Tomalia, *Drug Delivery Reviews*. 57 (2005) 2106-2129.

P24

Polarographic method in the testing of the effect of pharmacologically active compounds on mitochondrial function

Z. Garaiová[1], O. Uličná[2], O. Vančová[2], M. Labieniec[3], C.Watala[4], I.Waczulíková[1]

[1] Department of Nuclear Physics and Biophysics, Division of Biomedical Physics, Faculty of Mathematics, Physics, and Informatics, Comenius University, Mlynská dolina F1, 842 48 Bratislava, Slovakia, e-mail: garaiova.zuzana7@gmail.com
[2] Pharmacobiochemical Laboratory 3rd Department of Internal Medicine, Faculty of Medicine, Comenius University, Bratislava, Slovakia
[3] Department of General Biophysics, University of Lodz, Banacha 12/16, 90-237 Lodz, Poland
[4] Department of Haemostasis and Haemostatic Disorders, Medical University of Lodz, University Hospital No. 2, Lodz, Poland

Introduction:

Intracellular delivery of many pharmacologically active compounds, therapeutic agents, vaccines and genes is one of the new areas of research in the pharmaceutical and medical field. These compounds act by specifically interfering with cellular sites or biochemical processes, often called 'targets'. Mitochondria can be such site of expected action, but also the site of undesirable side effects of these compounds. Since mitochondria participate in a variety of physiological processes, including supplying energy to the cell, calcium distribution, maintaining the redox potential, generation of heat, free radicals and participating in apoptosis, any disturbance of these functions can have detrimental consequences for the cell [1, 2]. Early identification of mitochondria as undesirable primary or secondary targets of new chemical entities has a significant importance in avoiding or reducing the attrition rate in later stages of drug development. Inhibition of individual components of electron transport chain, uncoupling proteins, opening of the mitochondrial permeability transitions pore are pathways, which can contribute to altered oxygen consumption [3]. Measuring of mitochondrial oxygen consumption using polarographic method is one of the most informative ways of assessing mitochondrial dysfunction.

The aim of our study was to investigate the influence of dendrimers, compounds intensively studied for drug delivery and gene therapy, on the respiration of isolated rat liver mitochondria. Dendrimers are a class of macromolecules, having a highly branched architecture with very low polydispersity and high functionality [4]. We focused on *in vitro* effect of poly(amidoamine) (PAMAM) dendrimers G4, G2 (which possess 64 and 16 amino groups on their surfaces, respectively) and G3.5 (with 64 carboxylic groups terminating the chain ends) on the mitochondria.

Material and methods

We used 15 male Wistar rats weighing 220 – 270g. Rat livers were removed after decapitation. We tested three dendrimers, each at two concentrations: G4: 0.5 and 2 μM; G2: 5 and 10 μM, G3.5: 30 and 60 μM. Mitochondria oxidative phosphorylation was measured with an oxygraph Gilson 5/6H using a Clark oxygen electrode. We measured following parameters (Fig. 1): oxygen consumption by mitochondria stimulated by ADP - state 3 (QO_2S_3), basal uptake of

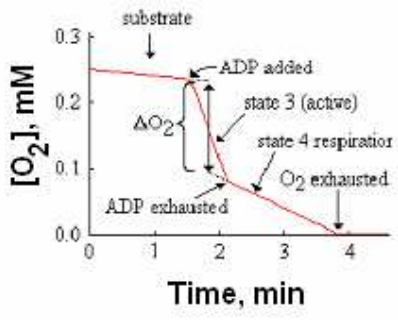

Fig.1 Oxygen consumption measure polarographic approach (www.bmb.leeds.ac.uk)

oxygen by mitochondria - state 4 (QO_2S_4), respiratory control index (RCI), coefficient of oxidative phosphorylation (ADP:O) and oxidative phosphorylation rate (OPR). Changes in the parameters of mitochondrial oxidative phosphorylation upon the addition of dendrimers were compared with control (no dendrimer) and statistically analyzed using the Friedman test.

Results:

We observed that RCI was significantly decreased when compared to controls for both oncentrations of all the investigated PAMAM dendrimers (Fig. 2). The decrease was concentration-dependent. ADP:O was reduced for G4 at both the concentrations and for G2 only at the higher concentration. For dendrimers G2 at the lower concentration and G3.5 at both the concentrations the parameter ADP: O was not significantly changed.

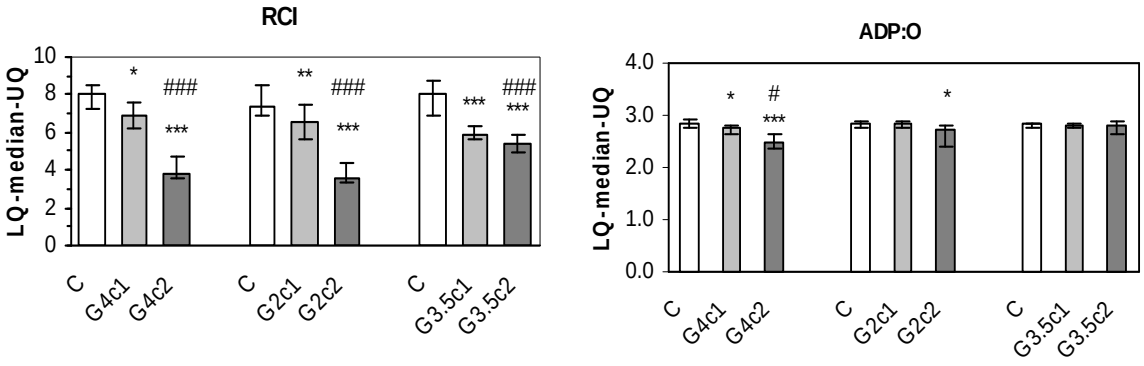

Fig.2 Effect of dendrimers on two parameters (RCI, ADP: O) of oxidative phosphorylation**.** The symbol * indicates significance of differences between control and dendrimers, and symbol # between the two concentrations of dendrimer (* $p<0.05$, ** $p<0.01$, ***$p<0.001$; #$p<0.05$, ## $p<0.01$, ###$p<0.001$).

Discussion:

RCI index calculated from QO_2S_3 and QO_2S_4 is a measure of the integrity of mitochondrial membranes. The decrease in the index upon the application of the dendrimers G4, G2 and G3.5 suggests that some kind of membrane perturbation occurred. Reduction in the coefficient of oxidative phosphorylation ADP:O points to a worsened phosphorylation. We found out that the inhibitory effect of a dendrimer depends not only on the used concentration of a dendrimer, but also on the number and charge of the end groups that means on the generation of the dendrimer. We can conclude that mitochondria are an appropriate model not only for *in vitro* testing the efficacy of pharmacologically active compounds, but also for testing their possible adverse effects. Measurement of mitochondria oxidative phosphorylation can be recommended each time when a possibility exists that the investigating compound enters the cell.

Acknowledgement

This work was supported by the Slovak Grant Agency VEGA, projects No. 1/3037/06, No. 1/3442/06, by the Ministry of Scientific Research and Information Technology grant PBZ-KBN-101/T09/2003/9, and by the NATO Cooperative Linkage Grant CBP.NUKR.CLG 981884.

References

[1] D.E. Amacher, *Current Medicinal Chemistry*, 12 (2005) 1829-1839.
[2] B.A. Scalettar, J.R. Abney, Ch.R Hackenbrock, *PNAS USA*, 88 (1991) 8057-8061.
[3] J. Hynes, L.D. Marroquin, V.I. Ogurtsov, K.N. Christiansen, G.J. Stevens, D.B. Papkovsky, Y. Will, *Technological Sciences*, 92 (2006) 186-200
[4] S. Svenson, D.A. Tomalia, *Drug Delivery Reviews*. 57 (2005) 2106-2129.

P25

Phylogenetic analysis of influenza A virus – neuraminidase active site

I. K. Haverlik, G. Ruttkay-Nedecký, I. Kinclová

Department of Nuclear Physics and Biophysics, FMFI UK, Mlynská dolina F1, 842 48 Bratislava, Slovakia, e-mail: kinclova@fmph.uniba.sk

Neuraminidase (NA) is an integral membrane glycoprotein of influenza A virus. Together with hemagglutinin(HA), it is one of the two integral membrane glycoproteins – these are the major determinants that undergo antigenic variation. Approximately 100 neuramidase molecules radiate from the surface of the virion. NA is important mainly in removing sialic acid from glycoproteins, including the sialic-acid-containing glycoprotein-receptors on the cell surface [1]. This biological activity is important for transport of the virus through the mucin layer to the target epithelial cells and in the later stage of infection it allows separation of new virions from the host cell and it prevents aggregation [2]. Antibodies to NA are not neutralizing the virus but they inhibit plaque size enlargement and mitigate the infection [3]. At present nine subtypes of influenza A virus neuraminidase (N1 – N9) are known [4].

Neuraminidase active site has been described by Colman et al. [5]. Eight amino acids which are in the direct contact with the substrate are considered to be functional (numbering according to N2 subtype): R-118, D-151, R-152, R-224, E-276, R-292, R-371 and Y-406. Another 10 amino acids are considered to be the "framework", and they seem to be important especially for stabilization of the 3-D structure of neuraminidase active site and they are: E-119, R-156, W-178, S-179, D-198, I-222, E-227, E-277, N-294 and E-425.

The aim of the present work was to find the degree of conservation of neuraminidase active site among 611 influenza A virus isolates compared.

Material and methods

The total number of 611 complete amino acid sequences of influenza A virus neuraminidase were compared, the sequences were obtained from the GenBank database [6]. For a particular virus subtype (various combinations of HA and NA subtypes, e.g. H1N1, H2N1, etc.), one neuraminidase isolate was always chosen for a particular year. Clustal [7] was used to align the sequences, with gap opening 10.00, gap extension 0.20.

Results and discussion

As it can be see from Table 1, all functional amino acid residues are conserved in all the subtypes but for one exception, which was found in arginine-224, which was replaced by threonine in one N1 isolate. Among the framework amino acids, several differences from the conserved amino acids were found. Replacement of aspartic acid-198 for asparagine was found in all isolates of subtypes N7 and N9 as previously described [5], and also in all isolates of N6 subtype. It was also found in some isolates of N2 subtype (A/Buenos Aires/4057/95 (H3N2) and A/Swine/Ontario/00130/97 (H3N2)) and in one N1 isolate (A/Taiwan/117/96 (H1N1)). In A/chicken/New York/13142-5/94 (H7N2), aspartic acid-198 was replaced for valine. N1 subtype comprised differences on two more sites. In A/Hong Kong/488/97 (H5N1) and A/Hong Kong/97/98 (H5N1), threonine was found instead of isoleucine-222. In the N1 isolate A/duck/Hong Kong/380.5/2001 (H5N1), asparagine-294 was replaced by serine.

Sequence analysis of neuraminidase showed that the amino acid residues in the enzyme active site are well conserved, as published elsewhere [5]. Several studies show that there exist exceptions in the active site of some isolates [8, 9]. Differently, in this study, out of 611 sequences analysed, one or more changes in the functional or framework residues were observed within 138 sequences, in four active sites (see Table 1). Nevertheless, it was

confirmed by this study that the replacement of Asp-198 by Asn is common to all N6, N7 and N9 isolates.

Table 1. Comparison of amino acid residues in the enzyme active site of neuraminidase. The upper number denotes the position in the neuraminidase sequence, N2 numbering. The number of occurrences of a given amino acid at the position is given in the parenthesis, and the neuraminidase subtypes are given for isolates containing the change (square parenthesis).

Functional	118	151	152	224	276	292	371	406
	R(611)	D(611)	R(611)	R(610) T(1)[N1]	E(611)	R(611)	R(611)	Y(611)

Framework	119	156	178	179	198	222	227	277	294	425
	E(611)	R(611)	W(611)	S(611)	D(477) N(133)* V(1)[N2]	I(609) T(2)[N1]	E(611)	E(611)	N(610) S(1)[N1]	E(611)

* [N1 (1)], [N2 (2)], [N6 (52)], [N7 (27)], [N9 (51)]

Acknowledgement
This work was partially supported by the Slovak Grant Agency VEGA, project No. 1/3037/06.

References

[1] A. Gottschalk, *Biochem. Biophys. Acta* 23 (1957) 645-646.
[2] P. Palese, K. Tobita, M. Ueda, and R. W. Compans, *Virology* 61 (1974) 397-410.
[3] R. G. Webster, P. A. Reay, and W. G. Laver, *Virology* 164 (1988) 230-237.
[4] R. A. M. Fouchier, V. Munster, A. Wallensten, T. M. Bestebroer, S. Herfst, D. Smith, G. F. Rimmelzwaan, B. Olsen, and A. D. M. E. Osterhaus, *J. Virol.* 79 (2005) 2814-2822.
[5] P. M. Colman, P. A. Hoyne, and M. C. Lawrence, *J. Virol.* 67 (1993) 2972-2980.
[6] D. A. Benson, I. Karsch-Mizrachi, D. J. Lipman, J. Ostell, B. A. Rapp, and D. L. Wheeler, *Nucl. Acids Res.* 28 (2000) 15-18.
[7] J. D. Thompson, D. G. Higgins, and T. J. Gibson, *Nucl. Acids Res*. 22 (1994) 4673-4680.
[8] E. T. Plakokefalos, P. Markoulatos, N. Spyrou, T.A. Bei, and N. C. Vamvakopoulos, *Arch. Virol.* 146 (2001) 1899-1918.
[9] S. E. Lindstrom, Y. Hiromoto, R. Nerome, K. Omoe, S. Sugita, Y. Yamazaki, T. Takahashi, and K. Nerome, *J. Virol.* 72 (1998) 8021-8031.

P26

Spectra calculation of β-cyclodextrin - coumarine complexes

A. Holúbeková[1], P. Mach[2], J. Urban[2]

[1] Faculty of Mathematics, Physics and Informatics, Comenius University, Mlynska dolina, 84248 Bratislava, Slovakia, e-mail: holubekova@fmph.uniba.sk
[2] Faculty of Mathematics, Physics and Informatics, Comenius University, Mlynska dolina, 84248 Bratislava, Slovakia

Cyclodextrins (CDs) are cyclic oligosaccharides composed of several d-glucose units bonded by α(1,4) linkages. The most common natural CDs are α-, β- and γ-CDs consisting of six, seven and eight D-glucopyranose residues, respectively. From a topological point of view, Beta-cyclodextrin (β-CD) can be described as a truncated cone, in which the narrow rim (6.4 Å) bears the primary hydroxyl group whereas the wide rim (15.4 Å) bears the secondary OH groups. Since no hydroxyl group is present within the toroidal cavity of β-CD, this zone of the molecule has a pronounced hydrophobic character. The unique shape and physical–chemical properties of the cavity, together with van der Waals forces and hydrogen bonding allows the formation of inclusion complexes with a wide range of compounds, where the extent of the complex formation depends on the polarity of the absorbed molecules.

The derivatives of coumarin (coumarins) usually occur as secondary metabolites present in seeds, root, and leaves of many plant species, although their presence has also been detected in microorganisms and animal sources. Because of the structural diversity found in this family of compounds they are used in many areas, as additives to food and cosmetics, optical brightening agents, dispersed fluorescent, laser dyes and for medical purposes as blood thinner to keep blood flowing smoothly and prevent the formation of blood clots, as anti-fungicidal and anti-tumors. Coumarins are very convenient also for the study of molecular complexes because of their spectroscopic activities. If coumarin enters the cavity of β-CD its spectra changes due to bonding with β-CD.

Our contribution presents quantum chemical calculations of the structures of inclusion complexes of β-CD with coumarins, (coumarin-6, coumarin-30, coumarin-47, and coumarin-522). On the basis of semiempirical PM3 method and DFT theory the optimal geometries have been found. Spectra of uncomplexed coumarin molecules and of complexes in vacuo were calculated using the TDDFT method and CIS method. Molecular dynamics study has been applied in the case of the β-CD coumarin-522 inclusion complex. Results show that coumarin molecules are inserted completely into the cavity and that inclusion of coumarins into βCD forms new H-bonds inside of the complex which stabilize the complex. The insertion of coumarin into host molecule changes its spectra.

P27

Simulations of unfolding of polypeptide chains in confinement

P. Palenčár, P. Cifra, T. Bleha

Polymer Institute, Slovak Academy od Sciences, 842 36 Bratislava, Slovakia, e-mail: upolppal@savba.sk

Stability and reactions of proteins inside a cell are affected by the presence of impenetrable boundaries (confinement effects) and by the presence of other soluble macromolecules (macromolecular crowding). In both cases the free space that a protein molecule can move around is limited. In former case the volume accessible to protein is confined within a single cage, in the latter case the accessible volume is dispersed throughout the space of a cell. The simple theories were presented [1,2] to provide qualitative estimates of the magnitude of macromolecular crowding and spatial confinement on equilibrium and rate of protein folding. Theories [1,2] predict that confining a protein into a small inert cage should stabilize the protein against the reversible unfolding.

In modeling of confinement effects on protein folding, the Monte Carlo and/or Molecular Dynamics (MD) simulations are used to compute structure and properties of native (ordered) and unfolded (denaturated) states in the cages of simple geometry [3]. In an effort to expand our confinement effect studies [4] by an MD atomistic modeling we have examined as an initial step the thermal refolding of single polypeptide chain of 56 alanine residues in cylindrical confinements by the MD method. The MD trajectories of 20 ns provided sufficiently equilibrated final structures of studied polyalanine. By performing series of MD simulations, the optimal temperature (T) range to observe the polypeptide refolding process was established. At high T (~ 950K) the disordered (random-coil) state is formed whereas at low T (~ 450K) polymer assumes the α-helical structure. In between, at T around 570 K, both structures are in equilibrium. The mean end-to-end distances and distribution functions of end-to-end distance P(R) were computed for a free and a confined polypeptide at these temperatures. Additionally, the polypeptide structure was characterized by a distribution of four secondary structure types, α-helix, β-sheet, random-coil and turn. The differences found between the quantities calculated for a free and a confined polymer represent the main outcome of this preliminary report.

Acknowledgement
This work was supported by the VEGA grants 2/6116/26 and 2/6014/26 and in part by the Centre of Excellence COMCHEM.

References

[1] H. X. Zhou and K. A. Dill, *Biochemistry* **2001**, *40*, 11289.
[2] A. P. Minton, *Biophys. J.* **2005,** *88*, 971.
[3] D.K. Klimov, D. Newfield and D. Thirumalai, *PNAS*, **2002,** *99*, 8019.
[4] P. Cifra, Z. Benkova and T. Bleha, J. *Phys. Chem. B*, **2007**, *112*, 1367.

P28

Theoretical study of structural changes caused by applying mechanical strain on peptide L_{24}

M. Krajčí, J. Urban, P. Mach

Department of Nuclear Physics and Biophysics, FMFI UK, Mlynská dolina F1, 842 48 Bratislava, Slovakia, e-mail: mkrajci@tex.dbp.fmph.uniba.sk

Our goal was to observe structural changes that take place when mechanical force is applied to single molecule L_{24} – artificial transmembrane peptide (Lyz_2-Leu_{24}-Lyz_2), also to observe how surrounding environment affects some basic properties of molecule.

Beacuse of high number of atoms in our simulation we were forced to use one of the fastest method that is available today, called molecular mechanics (MM), which is based on empirical parametrization of forces and energy. Our basic dynamics engine was program GROMACS [1] with enhanced forcefield ffgmx [2] for protein-lipid interactions. As every emepiric method, limitation are tight and interpretation of results must be very well thought. The ffgmx forcefield was designed for protein calculations and method was used many times before, yielding reasonable results [2]. Our method of implying force on molecule consisted of 2 steps. At first we did homogenous stretch or press of coordinates of all atoms in Z direction. Then we equilibrated sysem at zero temperaure in vacuum with endings of molecule fixed to its coordinates. One stretch or press step was 0.002 nm. We repeated same procedure with free DPPC molecules organised to bilayer as environment and also with DPPC fixed in Z direction. Here are some results we obtained:

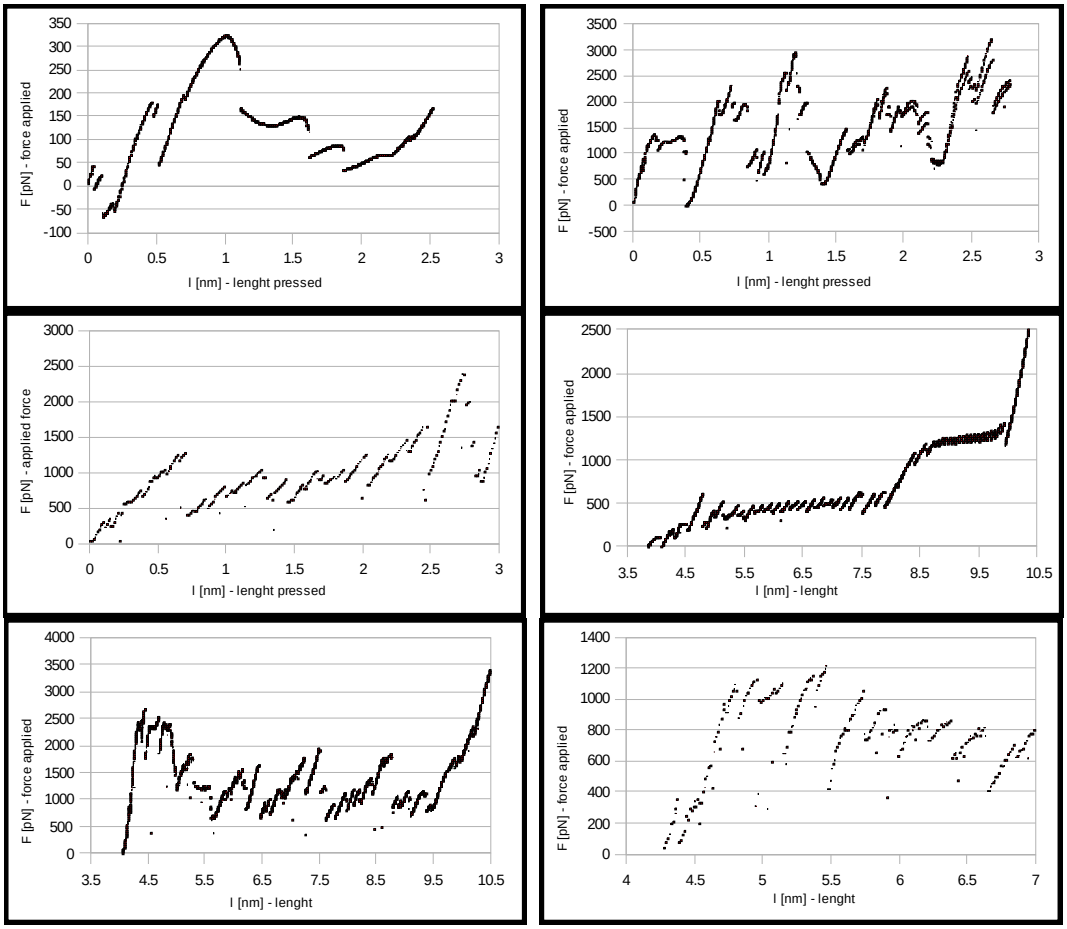

From top left to right: 1. pressing in vacuum, 2. pressing with surrounding DPPC (fixed), 3. pressing with DPPC (free), 4. stretching in vacuum, 5. stretching with surrounding DPPC (fixed), 6. stretching with DPPC (free)

Graphs show that the force applied is not continuous. Each jump on graphs is caused by sudden conformation change due to applied force. Here is example of such change observed in simulation of stretching without DPPC:

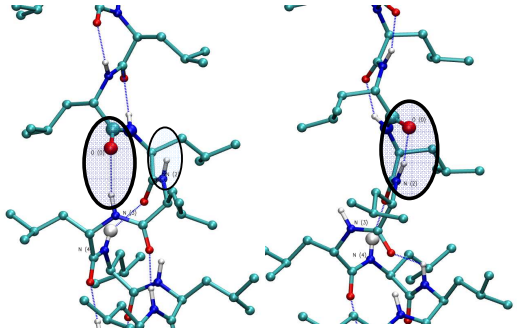

As we can see stabilisating H-bond is broken, new one is formed and system changes conformation. This change can not be normally undone. After releasing ends of the helix, it stays in this new conformation. This is prime reason why stretching and pressing isnt elastic acoording to Hook's law and why there are so many irregular jumps on the graphs. When conformation change occurs, there is drop in force required for further stretching, as can be seen from graphs.

Observing L_{24} stretched alone we could distinguish several stages of conformational changes, in which different types of H-bonds jumps occured. The type shown on pictures above is 1-3 to 1-2 jump. This type is responsible for periodical force jumps in (graph 4.) in stage 5.5nm-7.5nm. Untwisting and H-bond jumping happens from N-end of the peptide. This end is probably less stabile due to inherent assymetry of peptide chain of the molecule. According to some our other results MM method is not suitable for stretching more than 10.5nm or in our case for applying force bigger than ~2500pN, since atoms are not in their equilibium geometry any more and normaly covalent bond breaking would occur.

Pressing L_{24} alone was also very interesting, molecule was firstly elasticly bent. After shortened to size 2.8nm (1nm press from original size) it broke in middle into two parts (see graph 1.). Force required for pressing is much smaller than for stretching, this is due to fact that molecule was actually not pressed like string, but rather bent like a stick and then broken. H-bonds have stabilisating efect not only when stretching. They maintain certain helix size and they make the molecule rather rigid than flexible.

Generally surrounding DPPC put high degree of irregularity to the problem. It discarded stage-look of the stretch process and diferent types of structure changes happen in apparent random order, depending on starting position of DPPC molecules. Simulating with DPPC fixed caused huge increase of force required for stretching (graph 5.), this was due to the fact that big force was required for pulling the polar ends out of membrane. With DPPC free the increase isn't that markant (graph 6.), but this behaviour is rather strange, since the surrounding DPPC were atached to ends of L_{24} and moved with them as L_{24} was stretching.

Pressing of L_{24} when DPPC was fixed in Z direction gave also very interesting results. Environment had stabilisating effect, what can be read form the (graph 2.). Force required for pressing is almost 5 times bigger than without DPPC. L_{24} didnt broke into 2 rigid parts like in (graph 1.), rather one rigid part was very unwilingly untwisting and untwisted part behaved very much like free thread. Anomalous behaviour can be seen on (graph 2.) in stage 2.0-2.5nm showing limits of method. Pressing with free DPPC caused all DPPC molecules to follow polar ends just like in free stretching and big lipid globule around the bended-broken L_{24} was formed.

Acknowledgment
This work was partly supported by the Slovak Grant Agency VEGA, project No. 1/3040/06

References

[1] E. Lindahl, B. Hess, D. van der Spoel, *J. Mol. Mod.* 7 (2001) 306-317.
[2] S.J. Marrink, O. Berger, D. P. Tieleman, F. Jaehnig. *Biophys. J.* 74 (1998) 931943.

P29

Vicsometric detection of lysozyme and poly-L-lysine amyloid aggregation

D. Fedunová[1], M. Bánó[1], A. Bellová[2], J. Bágeľová[1], Z. Gažová[1,2], M. Antalík[1,2]

1 Institute of Experimental Physics, Slovak Academy of Sciences, Watsonova 47, 040 01 Košice, Slovakia

2 Department of Biochemistry, PF UPJŠ, Moyzesova 11, 040 01 Košice, Slovakia, email:fedunova@saske.sk

Aggregation and precipitation of proteins from aqueous solution is an omnipresent problem in biotechnology and medicine. Protein aggregates gain diverse structures from amorphous assemblies to highly ordered fibers. Highly organized protein fibrous structures containing intermolecular β-sheets in a distinctive orientation – amyloid fibrils – have been recognized as an accompanying feature of several neurodegenerative diseases (e.g. Alzheimer's disease, type II diabetes, spongiform encephalopathies) [1]. Recently, numerous peptides and proteins without connection to any known disease have been shown to be capable of forming amyloid fibrils *in vitro* under appropriate conditions [2]. Amyloid structure is based on unique form of polypeptide configuration, cross-β structure, but it does not require presence of specific side chain interaction or sequence patterns, which leads to the suggestion that the ability to form fibrils is generic property of polypeptide chain [2]. The study of processes leading to the amyloid formation is limited for example due to the low solubility of aggregated proteins and lack of high-resolution 3D structures. This suggests the use of simple models and introduction of new techniques for study the mechanism of amyloid fibrillation.

In this work we have used viscometric method for characterization of lysozyme and poly-L-lysine aggregation. The viscometry is useful method for study of the protein aggregation, providing information about conformation and rearrangement of macromolecules in solution. The viscosity was measured by unique Couette-type non-contact rotation viscometer developed in our laboratory [3]. The important advantage of this device against commercial ones is that data are collected without errors caused by the surface shear viscosity.

Hen egg white lysozyme has been recently found to form amyloid fibrils *in vitro* [4]. We have measured the kinetics of its fibrillation manifested by increase of reduced viscosity in 3 M guanidine hydrochloride solution, pH 6.3 and 50^{o}C with intensive stirring during 24 hours. The sigmoidal increase of reduced viscosity indicating the formation of aggregates is followed by slight decrease of this parameter during 7 hours of incubation. These finding suggest that after initial expansion of partially denatured and assembled protein molecules the formation of tightly packed structures occurs. Fluorescent dye thioflavine T is widely used as indicator of amyloid formation due to its specific binding directly with amyloid fibrils [5]. The parallel measurement of lysozyme fibrillation by this fluorescence probe shows that lysozyme amyloid fibrils are formed already after 2 hours of incubation.

Poly-L-lysine is also frequently used as model polypeptide for study of the mechanism of the protein aggregation. It undergoes thermal transition, the hallmark of protein aggregation, depending on pH, temperature or chain length [6]. We have observed thermal transition of poly-L-lysine in the region of pH from 9.7 to 11.8. Transition temperature is slightly shifted to the low pH with increasing chain length (Fig. 1). The thermal transition of longer chain occurs at lower temperature. This finding has been recently linked to the presence of distorted or solvated helices with turns in elongating chain facilitating the transition to β-sheet [6]. For each used poly-L-lysine chain (differing in chain length) we have found narrow pH interval (0.4 in range) in which the thermal transition is fully reversible. These results suggest that polypeptide conformation is sensitive on subtle changes in charge on its side chains. In addition, the interesting fact was observed that for given chain length the transition temperature increases with pH decrease and reversible

transition occurred at higher temperatures.

Another frequently used dye for amyloid staining is Congo red. However, this dye must be used with caution, because it can bind also to the native and partially folded protein conformations [7]. We have observed that Congo red induced the α-helix to β-sheet transition of poly-L-lysine at room temperature. This simple conformational transition from the α-helix to β-sheet is accompanied only by slight increase of reduced viscosity.

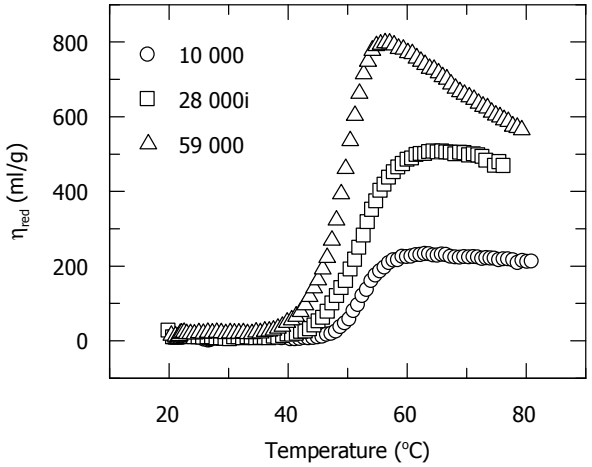

Fig. 1: Temperature dependence of reduced viscosity of poly-L-lysine with different molecular weight depicted inside. 0.5 mg/ml poly-L-lysine, 10 mM Gly, pH 11.3.

However, the thermal transition of poly-L-lysine is manifested by significant increase of reduced viscosity, which indicates the formation of large assemblies in solution. The formation of amyloid aggregates was confirmed by electron microscopy.

In summary, although the theoretical background for quantitative interpretation of viscometric data measured for such complicated objects as aggregates is not yet developed, they can provide qualitative characteristic about conformation and spatial arrangement of proteins into high ordered structures and about the kinetics of aggregation process.

Acknowledgement
This work was supported by the Slovak Grant Agency VEGA, projects No. 2/7055, 2/0056 a 2/6167.

References

[1] C. M. Dobson, *Trends. biochem. Sci.* 19 (1999) 31-37.
[2] M. Fändrich, C.M. Dobson, *EMBO J.* 21, (2002) 5682-5690.
[3] M. Bánó, I. Strhársky, I. Hrmo, *Rev. Sci. Instrum.* 74, (1998) 4788-4793.
[4] M. R. H. Krebs, D. K. Wilkins, E. W. Chung, M. C. Pitkeathly, A. K. Chamberlain, J. Zurdo, C. V. Robinson, M. C. Dobson, *J. Mol. Biol.* 300, (2000) 541-549.
[5] D. Allop, L. Swanson, S. Moore, Y. Davies, A. York, O. M. El-Agnaf, I. Soutar, *Biochem. Biophys. Res. Commun.* 285, (2001) 58-63.
[6] W. Dzwolak, T. Muraki, M. Kato, Y. Taniguchi, *Biopolymers.* 73, (2004) 463-469.
[7] R. Khurana, V. N. Uversky, M. Kato, Y. Taniguchi, *Biopolymers.* 73, (2004) 463-469.

P30

Effect of $HClO_4$ on conformational transitions of ferricytochrome *c*

J. Bágeľová[1] , D. Fedunová[1] , Z. Gažová[1,2], M. Antalík[1,2]

[1]Department of Biophysics, Institute of Experimental Physics SAS, 040 01 Kosice, Slovakia
[2] Faculty of Science University of P. J. Safarik, Moyzesova 11, 040 01 Kosice, Slovakia
e-mail: fedunova@saske.sk

The influence of various salts on the structure of denatured proteins is very complex and not completely understood yet [1-3]. The presence of heme groups in hemoproteins makes possible a very sensitive analysis of the changes caused by various denaturing solvents in the protein environment. Cytochrome *c* (cyt *c*) is a particularly useful model, because its heme group is covalently attached to the polypeptide chain, which supports the reversibility as well as rapid kinetics of the observed conformational transitions. In spite of the fact that there are numerous studies devoted to the conformational transition of ferricyt *c* at acid pH, it is not clear under which conditions the axial ligands, His18 and Met80, are released from heme iron, and what the differences are between high-spin penta- and hexacoordinated states of this protein [4-7]. The salt induced collapse of acid-denatured cyt c leads to a number of equilibria between high-spin and low-spin heme states and between two types of low-spin states. The equilibrium between these states is dependent on the concentration and/or size of the anions [8,9].

Conformational transitions of horse heart ferricytochrome *c* (ferricyt *c*) have been investigated in the presence of $HClO_4$ by optical absorption spectroscopy, magnetic circular dichroism (MCD) and circular dichroism (CD). In the presence of $HClO_4$ or 1 M $NaClO_4$ pH 2, 25 ^oC, the three ligation states of ferricyt *c* heme were identified. One is the high-spin state: His18-Fe-H_2O (40 – 50 %), and two are the low-spin states: His18-Fe-Met80 (30 - 25 %) and His18-Fe-His (30 - 25 %). Under these conditions low temperatures facilitate native heme coordination of ferricyt *c*. Transition from low-spin to high-spin heme coordination of ferricyt *c* is complete in 1 M $HClO_4$.

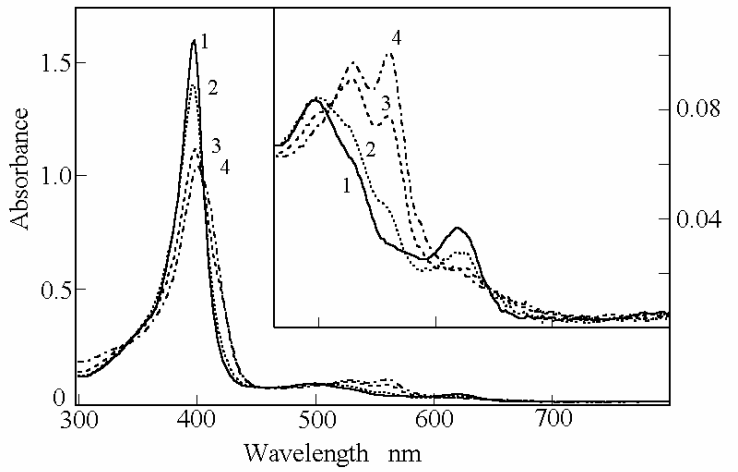

UV-vis absorption spectra of ferricyt *c* (9.5 μM) at various concentrations of $HClO_4$ recorded for 1 minute after mixing at 25 °C: in (1) 3 M; (2) 5.7 M; (3) 8.5 M; (4) 10 M $HClO_4$.

An increase in $HClO_4$ concentration above 3 M causes a decrease in the Soret band intensity of ferricyt *c*, β band is shifted to higher wavelengths, an intensive α band is formed at 556

nm and the intensity of the band at 620 nm is significantly lowered. The configuration around heme at high concentrations of $HClO_4$ differs from that observed in H_2SO_4.
As we know, the conformer with these spectral characteristics has not been observed up to now. Whereas ferricyt *c* spectra in $HClO_4$ (< 3 M, 25 ^oC) are stable and the reversibility of the transition to the native form due to increasing pH to 7 is preserved the higher concentration of $HClO_4$ (>3 M) partially destroys the heme region of cyt *c*. The part of presented results was published in [10].

Acknowledgement
This work was supported by the Slovak Grant Agency VEGA, projects No. 2/7055, 2/0056 a 2/6167.

References
[1] Y. Goto, N. Takahashi, A. L. Fink, *Biochemistry* 29 (1990) 3480-3488.
[2] A. Dong, T. Lam, *Arch. Biochem. Biophys.* 436 (2005**)** 154-160.A. A. Bhattacharya, T. Grüne, S. Curry, *J. Mol. Biol.* 303 (2000) 721-732.
[3] Y. Goto, L. J. Calciano, A. Fink, *Proc. Natl. Acad. Sci. USA* 87 (1990) 573-577.
[4] C. Indiani, G. de Sanctis, F. Neri, H. Santos, G. Smulevich, M. Coletta, *Biochemistry* 39 (2000) 8234-8242.
[5] S. Oellerich, H. Wackerbarth, P. Hildebrandt, *J. Phys. Chem. B.* 106 (2002) 6566-6580.
[6] M. Fedurco, J. Augustynski, C. Indiani, G. Smulevich, M. Antalik, M. Bano, E. Sedlak M., M.C. Lamczyk, J. H. Dawson, *Biochim. Biophys. Acta* 1703 (2004) 31-41.
[7] R. Varhac, M. Antalik, *Biochemistry* 43 (2004) 3564-3569.
[8] F. Sinibaldi, B. D. Howes, G. Smulevich, C. Ciaccio, M. Coletta, R. Santucci, *J. Biol. Inorg. Chem.* 8 (2003) 663-670.
[9] R. Santucci, C. Bongiovanni, G. Mei, T. Ferri, F. Polizio, A. Desideri, *Biochemistry* 39 (2000) 12632-12638.
[10] M. Stupák, J. Bágeľová, D. Fedunová, M. Antalík, *CCCC* 71 (2006) 1627-1641.

P31

Anti-amyloidogenic activity of acridines

Z. Gažová[1,2], A. Bellová[2] , J. Imrich[2] , P. Kristián[2], Z. Daxnerová[2], M. Antalík[1,2]

[1] Department of Biophysics, Institute of Experimental Physics SAS, 040 01 Kosice, Slovakia
[2] Faculty of Science University of P. J. Safarik, Moyzesova 11, 040 01 Kosice, Slovakia
e-mail:gazova@saske.sk

In the last decade the study of the protein amyloid aggregation is in the center of the research interest, when it was recognized that amyloid structures play important role in more than 20 human diseases, including Alzheimer's, Parkinson's and Huntington's diseases, type II diabetes, prion-related transmissible spongiform encephalopathies, and hereditary amyloidosis [1,2]. The amyloid diseases are, in terms of incidence, one of the most important groups of pathologies in the developed world. The protein deposits can be found in the brain, in skeletal tissue or in other organs with a single predominant protein component that is characteristic of each disease [2].

Numerous proteins have been identified as forming amyloid in vivo [3,4]. Although the proteins differ in their primary and tertiary structures, as well as their size and function, the amyloid structures formed from these proteins share common morphological and histochemical staining properties suggesting the hypothesis that different proteins follow similar fibril formation pathways [1]. There is a growing support that soluble oligomers rather than mature amyloid fibrils may be the main toxic species in amyloid related disorders. More recently, it has been found that amyloid polymerization is not only possible with disease-associated proteins, but also with proteins that are not associated with any known amyloid disease under certain conditions in vitro supporting the generic nature of the amyloid aggregation [1,2].

Currently, there are no effective cures for amyloid diseases, but experiments from various cell and animal models suggest that the reduction of amyloid aggregation is beneficial [5]. A great number of diverse small molecule compounds have been found to inhibit or reduce the aggregation of various proteins [6,7]. Despite these findings, clinical candidates have not yet been identified, and further screening is needed.

We concern our study to investigate the anti-amyloidogenic ability of low molecular weight compounds, acridines. We tested their ability to inhibit CEW lysozyme (chicken egg white) amyloid aggregation in vitro. Lysozyme is the main component of the massive amyloid deposits in the liver and kidney of individuals affected by hereditary systemic amyloidosis. We synthesized a variety of acridines (Fig.1) characterized by planar tricyclic core and aliphatic side chain with various length and terminal groups in C-9. The process of amyloid aggregation and inhibiting activity of acridines were followed by an assay based on the dye Thioflavin T whose fluorescence significantly increased in the presence of amyloid aggregates. We found that synthesized acridine derivatives are able to prevent formation of lysozyme fibrillization in dependence on the structure of aliphatic side chain. The most effective acridines showed clear dose-dependent inhibition of lysozyme fibrils. We determined concentration of half-maximal inhibition IC_{50} as well as half-maximal depolymerization DC_{50}. We found that these values corresponds micromolar concentrations in the case of the most effective acridine derivatives.

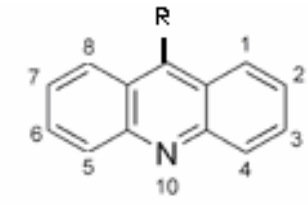

Fig.1. chemical structure of acridine

Anti-aggregating activity of the two most effective compounds was confirmed by electron microscopy. In the absence of acridines (Fig. 2A), long needle-like fibrils were observed (the thicker fibrils appeared to arise from interaction of

the thinner ones). In the presence of effective acridine compound (Fig. 2B) the amount of fibrils was reduced. Moreover, the fibrils that were produced in the presence of this most effective acridine appear thinner and shorter than those formed in the absence of compound.

We identified very effective inhibitor of CEW lysozyme fibrillization, characterized by inhibiting activity at low micromolar concentration [8]. This fact is important for a potential therapeutic use of these compounds in prevention of the human lysozyme amyloidoses. It is interesting that other type of acridine derivatives had capability to inhibit amyloid aggregation of different, unrelated proteins. Namely, Quinacrine and Quinacrine mustard inhibited formation of amyloid fibrils of tau and Aβ peptide [9]. The anti-scrapie activity probably through inhibition of the formation of protease-resistant prion protein has been found also for some other acridine derivatives [10]. These evidences could mean that anti-amyloid acridine may have relevance not only to lysozyme-related hereditary amyloidosis but also to amyloid diseases in general.

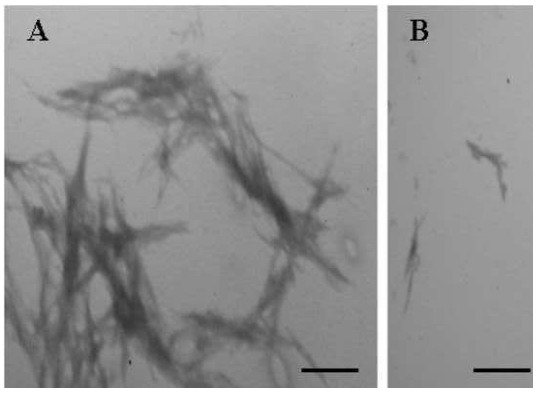

Fig.2. TEM images of lysozyme solution after process inducing protein amyloid aggregation in absence (A) and in presence of 100 μM effective acridine derivative Ac6 (B). The bars represent 500 nm.

Acknowledgement
This work was supported by the Slovak Grant Agency VEGA, projects No. 2/7055, 2/0056, 2/6167, 2471 and VVGS grant PF8/2007/CH

References

[1] C. M. Dobson, *Trends Biochem. Sci.* 24 (1999) 329-332.
[2] J. D. Sipe, in *Amyloid Proteins,* Wiley-VCH Verlag GmbH and Co. KgaA, Weinheim, Germany, 2005.
[3] M. C. Bennett, *Pharmacology & Therapeutics* 105 (2005) 311-331.
[4] V. M. Lee, M. Goedert, J. Q. Trojanowski, *Ann. Rev. Neurosci.* 24 (2001) 1121-1159.
[5] E. D. Roberson, K. Scearce-Levie, J. J. Palop, F. Yan, I. H. Cheng. T. Wu, H. Gerstein, G. Q. Yu, L. Mucke, *Science* 316 (2007) 750-754.
[6] C. Korth, B. C. May, F. E. Cohen, S. B. Prusiner, *Proc. Natl. Acad. Sci. U S A.* 98 (2001) 9836-9841.
[7] K. Doh-Ura, T. Iwaki, B. Caughey, *J. Virol.* 74 (2000) 4894-4897.
[8] Z. Gazova, A. Bellova, Z. Daxnerova, J. Imrich, P. Kristian, J. Tomascikova, J. Bagelova, D. Fedunova, M. Antalik, *Eur. Biophys. J.* (2008), in press
[9] S. Taniguchi, N. Suzuki, M. Masuda, S. Hisanaga, T. Iwatsubo, M. Goedert, M. Hasegawa, *J. Biol. Chem.* 280 (2005) 7614-7623.
[10] S. A. Priola, A. Raines, B. Caughey, *Science* 287 (2000) 1503-1506.

P32

Acridine derivatives as potent inhibitors of lysozyme aggregation

A. Bellová[1], Z. Gažová[2], J. Imrich[1], P. Kristian[1], Z. Daxnerová[1], M. Antalík[1, 2]

[1] Faculty of Science University of P. J. Safarik, Moyzesova 11, 040 01 Kosice, Slovakia
[2] Department of Biophysics, Institute of Experimental Physics SAS, 040 01 Kosice, Slovakia
e-mail: gazova@saske.sk

Amyloidosis are protein misfolding disorders in which soluble proteins aggregate in soluble oligomers and insoluble fibrils, accumulation of which has been found in several diseases, such as Alzheimer´s disease, Parkinson´s disease, transmissible spongiform encephalopathy, Huntington´s disease and diabetes type 2. Numerous *in vitro* studies have supported the thesis that partially folded protein molecules are the precursors of the nucleation and growth of amyloid fibrils [1], even though the detailed molecular mechanism underlying fibril formation is not well defined [2]. The proteins associated with amyloid diseases are not related to each other in sequence or in structure, however the amyloid fibrils share common characteristics in their morphology, tinctorial properties, and their core structures showing characteristic cross-β structure [3]. Currently, there are no clinical treatments available to prevent or reverse formation of such amyloid deposits [4].

We turned our attention on lysozyme amyloid fibrils as it has been shown that human lysozyme variants formed massive amyloid deposits in the liver and kidney of individuals affected by hereditary systemic amyloidosis. A promising strategy to achieve prevention of protein deposition diseases is an identification of low molecular compounds, which are able to inhibit protein polymerization or disaggregate protein deposits [5].

We aimed at acridines, small heterocyclic compounds known as anticancer drugs [6]. It was of interest if these compounds could be effective also as inhibitors of protein amyloid aggregation. We screened a small library of structurally distinct acridine derivatives (25 compounds) with various bulky side groups for their ability to inhibit lysozyme fibril formation *in vitro*. The lysozyme aggregation was detected by Thioflavin T fluorescence assay in the presence of studied compounds. We observed that ability of acridines to inhibit formation of fibrils and/or disrupt preformed amyloid fibrils from hen egg white lysozyme was different and strongly depended on the structure of the acridine side chains. Compounds belonging to the spiroacridines and tetrahydro-acridines had no disaggregation effect. Moreover, the lysozyme fibril formation was promoted in the presence of some tetrahydro-acridines (Fig. 1). We identified also a group of acridine derivatives able to inhibit the lysozyme fibril formation or destroy pre-formed fibrils at low

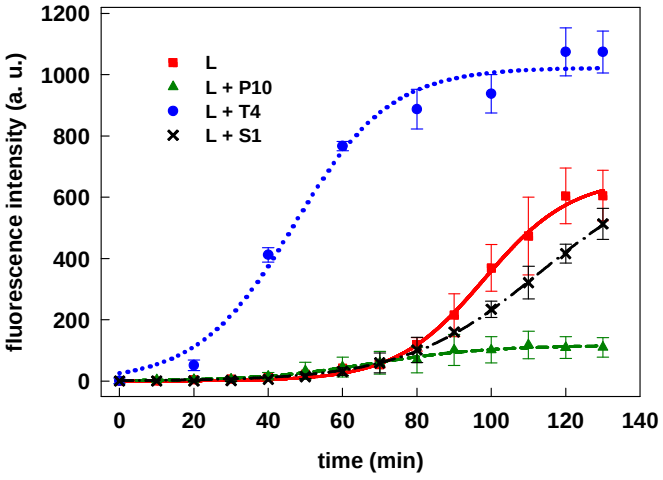

Fig. 1. The time-dependence of lysozyme aggregation determined in the absence (■) and in the presence of acridine derivates T4 (●), P10 (▼) and S1 (×). The error bars represent the average deviation for repeated measurements of three separate samples. The curves were obtained by fitting of the average values by non-linear least-square method.

micromolar concentrations (IC_{50} and DC_{50} values were between 5-50 μM). This activity was confirmed by electron microscopy and Congo red assay.

We found out that disaggregation activity of acridines was affected by a planar template and the composition and structure of side chains. These results suggest that acridine compounds may serve as prototypes for the development of drugs for the prevention or treatment of different types of amyloidoses.

Acknowledgement
This work was supported by the Slovak Grant Agency VEGA, projects No. 2/7055, 2/0056, 2/6167, 2471 and VVGS grant PF8/2007/CH.

References
[1] J. W. Kelly, *Curr. Opin. Struct. Biol.* 6 (1996) 11-17.
[2] Y. Kim, J. S. Wall, J. Meyer, C. Murphy, T. W. Randolph, M. C. Manning, A. Solomon, J. F. Carpenter, *J. Biol. Chem.* 275 (2000) 1570-1574.
[3] A. C. Ross, M. A. Poirier, M. C. Bennett, *Nature Rev. Mol. Cell Biol*. 6 (2005) 891-898.
[4] M. N. Vieira, J. D. Figueroa-Villar, M. N. L. Meirelles, S. T. Ferreira, F. G. De Felice, *Cell Biochem. Biophys*. 44 (2006) 549-553.
[5] M. Pickhardt, Z. Gazova, M. von Bergen, I. Khlistunova, Y. Wang, A. Hascher, E. M. Mandelkow, J. Biernat, E. Mandelkow, *J. Biol. Chem.* 280 (2005) 3628-3635.
[6] J. B. Hansen, E. Langvad, F. Frandsen, O. Buchardt, *J. Chem.* 26 (1983) 1510-1514.

AFM/SPM mikroskopy Agilent Technologies

Technologie AFM/SPM mikroskopů umožňuje zobrazování v atomárním měřítku s rozlišením až na desetiny nanometrů. Zásadní výhodou těchto mikroskopů je, že vzorky lze zobrazovat v libovolných podmínkách. Je možné měřit při různých teplotách dle potřeb aplikace nebo dokonce i přímo v kapalinách.

AFM/SPM systémy Agilent jsou používány v celé řadě oborů, jako jsou například:

- **výzkum a vývoj materiálů**
- **mikroelektronika**
- **nanolitografie**
- **aplikace s polymery**
- **biotechnologie**
- **medicína**

Nová demonstrační laboratoř

Společnost H TEST, a. s., otevřela v lednu 2008 ve své pražské kanceláři novou demonstrační laboratoř AFM (Atomic Force Microscopy) mikroskopie. Laboratoř je vybavena špičkovým AFM mikroskopem Agilent Technologies 5500. V rámci této nové demonstrační laboratoře mají potenciální zákazníci možnost podrobně se seznámit s technologií AFM a s mikroskopy z produkce firmy Agilent Technologies. Rovněž tak je možné ověřit vhodnost zobrazování pomocí AFM technologie v konkrétní aplikaci.

Kontaktní informace:

H TEST, a. s.
Na okraji 44B
16200 Praha 6
Tel.: 235 365 207, 204
Fax: 235 363 893
E-mail: info@htest.cz
www.htest.cz
www.agilent.com/find/nano

Agilent Technologies
Authorized Distributor

Přehled AFM/SPM mikroskopů Agilent:

Série 5100 AFM/SPM

AFM mikroskop Agilent 5100 je vhodný pro uživatele, kteří nepotřebují plnou funkčnost vrcholného modelu Agilent 5500, a přesto vyžadují možnost plné kontroly prostředí, ve kterém se nachází měřený vzorek. Pro plnou kontrolu prostředí, ve kterém se nachází měřený vzorek, je k dispozici volitelná hermeticky uzavřená komora a teplotně regulovaný adaptér pro uchycení vzorků.

- Velikost vzorku 20 x 20 mm
- Kontrola teploty a prostředí

Série 5400 AFM/SPM

Nový AFM mikroskop Agilent 5400 AFM/SPM je velmi přesný, univerzální přístroj za dostupnou cenu, určený zejména pro oblast vzdělávání a výzkumu a představuje tak ideální možnost zpřístupnění AFM technologie širokému spektru potenciálních uživatelů. Mikroskop je dodáván s podklady pro výuku AFM včetně vzorků pro experimenty.

- Velikost vzorku 20 x 20 mm
- Kontrola teploty

Série 5500 AFM/SPM

AFM mikroskop Agilent 5500 je vrcholný víceúčelový výzkumný mikroskopický systém pro AFM a SPM. Modulární koncepce této série dovoluje jednoduchou integraci stojanu pro velké vzorky až 150 x 200 mm (LS), invertovaného mikroskopu (ILM), skenerů pro malé i velké zobrazované plochy, adaptérů pro uchycení vzorků, soupravy pro elektrochemii nebo videomikroskopu.


Internet: www.shimadzu.de
Email: shimadzu@shimadzu.de
Shimadzu Europa GmbH
Albert-Hahn-Str. 6-10
47269 Duisburg, Germany
Phone +49 - 203 - 7687-0
Fax +49 - 203 - 766625
Austria
Benelux
Croatia
Czech Republic
Denmark
Finland
France
Germany
Greece
Hungary
Ireland
Israel
Italy
Norway
Poland
Portugal
Russia
Slovakia
Spain
Sweden
Switzerland
United Kingdom
MS^n capability
High mass accuracy
Fastest analysis
Discovery channel
The outstanding LCMS-IT-TOF is the perfect tool for the identification and characterization of unknown molecules, e.g. in biomarker discovery, proteomics or impurity analysis.
MS^n capability
providing an unsurpassed wealth of qualitative information and increased confidence in the results
High mass accuracy and high resolution
delivering information of formula composition on eluting components and fragments
Fastest analysis
Fast cycle times including polarity switching, allowing the identification of molecules in complex samples with narrow LC peaks
Additional software packages
supporting applications in metabolomics, proteomics and formula prediction
Hybrid mass analyzer combining ion trap and TOF: the LCMS-IT-TOF
www.shimadzu.de
SHIMADZU
Solutions for Science
since 1875


Internet: www.shimadzu.de
Email: shimadzu@shimadzu.de
Shimadzu Deutschland GmbH
Marketing & Customer Support Center
Albert-Hahn-Str. 6-10
47269 Duisburg, Germany
Phone +49 - 203 - 7687-0
Fax +49 - 203 - 766625
Austria
Benelux
Croatia
Czech Republic
Denmark
Finland
France
Germany
Greece
Hungary
Ireland
Israel
Italy
Norway
Poland
Portugal
Russia
Slovakia
Spain
Sweden
Switzerland
United Kingdom
Tri-Light Zone
As one of the market leaders, Shimadzu is proud to present a milestone in spectroscopy: the SolidSpec-3700DUV.
Highest sensitivity for the entire wavelength range with three detectors covering the full spectrum from deep UV to NIR (165 nm to 3,300 nm)
Non-destructive measurements using an exceptionally large sample compartment
For advanced applications, including quality control in semiconductor or electronics industry
Leading edge technology completed by the widest range of UV-VIS/NIR spectrophotometers for all applications - from basic use to advanced research
First ever UV-VIS-NIR system with three detectors: the SolidSpec-3700DUV
SHIMADZU
Solutions for Science
since 1875

List of Participants

Antalík Marián, prof. Ing., DrSc.
Department of Biophysics
Institute of Experimental Physics, SAS
Watsonova 47
040 01 Košice, Slovakia,
e-mail: antalik@saske.sk

Balgavý Pavol, prof., PhD.
Department of Physical Chemistry of Drugs
FAF UK
Odbojárov 10
832 32 Bratislava
e-mail: balgavy@fpharm.uniba.sk

Bleha Tomáš, prof. Ing..DrSc
Polymer Institute
Slovak Academy od Sciences
Dúbravská cesta 9
842 36 Bratislava, Slovakia
e-mail: bleha@savba.sk

Bryndzová Lenka, Mgr.
Department of Biophysics
UPJŠ
Jesenna 5
040 01 Košice, Slovakia
e-mail: lenka.bryndzova@yahoo.com

Caro Anton, DVM
Institute of Molecular Physiology and Genetics
Slovak Academy of Sciences
Vlárska 5
833 34 Bratislava, Slovakia,
e-mail: anton.caro@hotmail.com

Cocherová Elena, Ing., PhD
Institute of Molecular Physiology and Genetics
Slovak Academy of Sciences
Vlárska 5
833 34 Bratislava, Slovakia
e-mail: elena.cocherova@savba.sk

Drigeľová Mária, Mgr.
Institute of Molecular Physiology and Genetics
Slovak Academy of Sciences
Vlárska 5
833 34 Bratislava, Slovakia
e-mail: maria.drigelova@savba.sk

Fabriciová Gabriela, RNDr., PhD.
Department of Biophysics
PF UPJŠ
Jesenná 5
040 01 Košice, Slovakia
e-mail: gabriela.fabriciova@upjs.sk

Fedunová Diana, RNDr., PhD.
Institute of Experimental Physics
Slovak Academy of Sciences
Watsonova 47
040 01 Košice, Slovakia
email: fedunova@saske.sk

Fojta Miroslav, Doc. RNDr., PhD.
Institute of Biophysics
Academy of Sciences of the Czech Republic
Kralovopolska 135
CZ-612 65 Brno, Czech Republic
e-mail: fojta@ibp.cz

Gaburjáková Marta, RNDr., PhD.
Institute of Molecular Physiology and Genetics
Slovak Academy of Sciences
Vlárska 5
833 34 Bratislava, Slovakia
e-mail: marta.gaburjakova@savba

Gallová Jana, RNDr., PhD.
Department of Physical Chemistry of Drugs
FAF UK
Odbojárov 10
832 32 Bratislava, Slovakia
e-mail: gallova@fpharm.uniba.sk

Garaiová Zuzana, Bc.
Department of Nuclear Physics and Biophysics
FMFI UK
Mlynská dolina F1
842 48 Bratislava, Slovakia
e-mail: garaiova.zuzana7@gmail.com

Gažová Zuzana, RNDr., PhD.
Department of Biophysics
Institute of Experimental Physics
SAS
040 01 Košice, Slovakia
e-mail:gazova@saske.sk

Grman Igor, Mgr.
Department of Nuclear Physics and Biophysics
FMFI UK
Mlynská dolina F1
842 48 Bratislava, Slovakia
e-mail: igor.grman@gmail.com

Haasz Václav, Ing.
H Test a.s.
Na okraji 44B
162 00 Praha 6, Czech Republic
e-mail: haasz@htest.cz

Hianik Tibor, Prof. RNDr., DrSc.
Department of Nuclear Physics and Biophysics
FMFI UK
Mlynská dolina F1
842 48 Bratislava, Slovakia
e-mail: tibor.hianik@fmph.uniba.sk

Holúbeková Alžbeta, Mgr.
FMFI UK
Mlynska dolina F1
84248 Bratislava, Slovakia
e-mail: holubekova@fmph.uniba.sk

Chorvát Dušan, RNDr., PhD.
International Laser Center
Ilkovičova 3
812 19 Bratislava, Slovakia
e-mail: dusan@ilc.sk

Jakuš Ján, Prof. MUDr., DrSc.
Institute of Medical Biophysics
JLF UK
Malá Hora 4
037 54 Martin, Slovakia,
e-mail: jakus@jfmed.uniba.sk

Jancura Daniel, RNDr., PhD.
Department of Biophysics
UPJŠ
Jesenná 5
041 54 Košice, Slovakia
e-mail: jancura@upjs.sk

Jasem Pavol, Doc.RNDr.PhD
Department of Medical Biophysics
LF UPJŠ
Tr. SNP1
040 66 Košice, Slovakia
e-mail: Pavol.Jasem@upjs.sk

Kaderjáková Zuzana, Mgr.
Department of Nuclear Physics and Biophysics
FMFI UK
Mlynská dolina F1
842 48 Bratislava, Slovakia
e-mail: zuzana.kaderjakova@gmail.com

Karabaliev Miroslav, Dr., PhD.
Department of Physics and Biophysics
Faculty of Medicine Trakia University
11 Armeiska
Stara Zagora 6000, Bulgaria
e-mail: mi_karabaliev@abv.bg

Kardošová Miroslava, Bc.
Department of Nuclear Physics and Biophysics
FMFI UK
Mlynská dolina F1
84248 Bratislava, Slovakia
e-mail: mirkakardosova@gmail.com

Kienberger Ferry, Dr., PhD.
Agilent Technologies Austria
Aubrunnerweg 11
4040 Linz, Austria
e-mail: ferry_kienberger@agilent.com

Kinclová Ivana, Mgr.
Department of Nuclear Physics and Biophysics
FMFI UK
Mlynská dolina F1
842 48 Bratislava, Slovakia
e-mail: kinclova@fmph.uniba.sk

Kirchnerová Jana, Mgr.
Department of Nuclear Physics and Biophysics
FMFI UK
Mlynská dolina F1
842 48 Bratislava, Slovakia
e-mail: kirchnerova@fmph.uniba.sk

Kohuš Zsolt, Bc.
Department of Animal Physiology and Ethology
Faculty of Natural Sciences
Comenius University
Mlynská dolina B2
842 15 Bratislava, Slovakia
e-mail: zsolt.kohus@gmail.com

Kopáni Martin, RNDr., PhD
Department of Pathology
LFUK
Sasinkova 4
811 08 Bratislava, Slovakia
e-mail: martin.kopani@fmed.uniba.sk

Kotalová Mária, Mgr.
Department of Nuclear Physics and Biophysics
FMFI UK
Mlynská dolina F1
842 48 Bratislava, Slovakia
e-mail: kotalova@fmph.uniba.sk

Krajčí Miroslav, Mgr.
Department of Nuclear Physics and Biophysics
FMFI UK
Mlynská dolina F1
842 48 Bratislava, Slovakia
e-mail: mkrajci@tex.dbp.fmph.uniba.sk

Kriváne k Roland, RNDr., PhD.
Dortmund University of Technology
Department of Chemistry
Physical Chemistry I – Biophysical Chemistry
Otto-Hahn-Straße 6
D-44227 Dortmund, Germany
e-mail: roland.krivanek@tu-dortmund.de

Labuda Ján, Prof. Ing., DrSc.
Institute of Analytical Chemistry
Faculty of Chemical and Food Technology
Slovak University of Technology
812 37 Bratislava, Slovakia
e-mail: jan.labuda@stuba.sk

Lacinová Ľubica, RNDr., DrSc.
Institute of Molecular Physiology and Genetics
Slovak Academy of Sciences
Vlárska 5
833 34 Bratislava, Slovakia
e-mail: lubica.lacinova@savba.sk

Miškovský Pavol, Prof. RNDr., DrSc.
Department of Biophysics
PF UPJŠ
Jesenná 5
040 01 Košice, Slovakia
e-mail: misko@kosice.upjs.sk

Mlynár Jaromír, Ing.
Schimadzu Slovakia
Ul. Dr. V. Clementisa 10
821 02 Bratislava, Slovakia
e-mail: jaromir.mlynar@shimadzu.eu.com

Ondriaš Karol, RNDr., DrSc.
Institute of Molecular Physiology and Genetics
Slovak Academy of Sciences
Vlárska 5
833 34 Bratislava, Slovakia
e-mail: karol.ondrias@savba.sk

Palenčár Peter, Mgr., PhD.
Polymer Institute
Slovak Academy od Sciences
842 36 Bratislava, Slovakia
e-mail: upolppal@savba.sk

Poliaček Ivan, Mgr., PhD.
Institute of Medical Biophysics
JLF UK
Malá Hora 4
037 54 Martin, Slovakia
e-mail: poliacek@jfmed.uniba.sk

Poniková Slavomíra, Mgr.
Department of Nuclear Physics and Biophysics
FMFI UK
Mlynská dolina F1
842 48 Bratislava, Slovakia
e-mail: slavomira.ponikova@gmail.com

Pulmanová Petra, Mgr.
Department of Physical Chemistry of Drugs
FAF UK
Odbojárov 10
832 32 Bratislava, Slovakia
e-mail: pullmanova@fpharm.uniba.sk

Rybár Peter, RNDr., PhD.
Department of Nuclear Physics and Biophysics
FMFI UK
Mlynská dolina F1
842 48 Bratislava, Slovakia
e-mail: peter.rybar@fmph.uniba.sk

Šimera Michal, Bc.
FMFI UK
Mlynská dolina F1
842 48 Bratislava, Slovakia
e-mail:msimera@gmail.com

Slezák Peter, Bc.
Department of Nuclear Physics and Biophysics
FMFI UK
Mlynská dolina F1
842 48 Bratislava, Slovakia
e-mail: peter.slezak5@gmail.com

Staničová Jana, doc. RNDr., PhD.
Institute of Biophysics and Biomathematics
UVM
Komenského 73
041 81 Košice, Slovakia
e-mail: stanicova@uvm.sk

Suchánek Jaromír, RNDr.
Department of Informatics
University of Trenčín
Študentská 2
91150 Trenčín, Slovakia
e-mail: suchanek@tnuni.sk

Šnejdárková Maja, Ing., PhD**.**
Institute of Animal Biochemistry and Genetics
SAS
900 28 Ivanka pri Dunaji, Slovakia
e-mail: Maja.Snejdarkova@savba.sk

Tencerová Barbora, Mgr.
Institute of Molecular Physiology and Genetics
Slovak Academy of Sciences
Vlárska 5
833 34 Bratislava, Slovakia
e-mail: barbora.tencerova@savba.sk

Tomášková Zuzana, Mgr.
Institute of Molecular Physiology and Genetics
Slovak Academy of Sciences
Vlárska 5
833 34 Bratislava, Slovakia
e-mail: zuzana.vareckova@savba.sk

Topor Peter, Mgr.
Department of Nuclear Physics and Biophysics
FMFI UK
Mlynská dolina F1
842 48 Bratislava, Slovakia
e-mail: peter.topor@fmph.uniba.sk

Zahradník Ivan, RNDr., PhD.
Institute of Molecular Physiology and Genetics
Slovak Academy of Sciences
Vlárska 5
833 34 Bratislava, Slovakia
e-mail: ivan.zahradnik@savba.sk

Zahradníková Alexandra, Ing., PhD.
Institute of Molecular Physiology and Genetics
Slovak Academy of Sciences
Vlárska 5
833 34 Bratislava, Slovakia
e-mail: alexandra.zahradnikova@savba.sk

Zvarík Milan, Mgr.
Department of Nuclear Physics and Biophysics
FMFI UK
Mlynská dolina F1
842 48 Bratislava, Slovakia
e-mail: zvarikmilan@gmail.com

Author Index

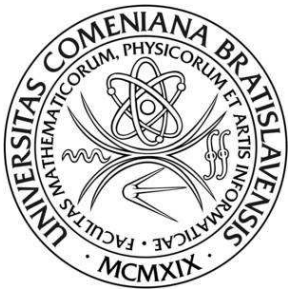

Faculty of Mathematics, Physics and Informatics, Comenius University, Bratislava
Slovak Biophysical Society

III. Slovak Biophysical Symposium – Proceedings of the III. Slovak Biophysical Symposium

Edited by: prof. RNDr. Tibor Hianik, DrSc.
For printing prepared by: Mgr. Peter Topor

Printed by: Copycentrum PACI, FMFI UK, Mlynská dolina, 842 48 Bratislava

Published by: Library and publishing centre FMFI UK, Bratislava, 65 pieces

First edition, Bratislava, April 2008.